Phosphodiesterases as Crucial Regulators of Cardiomyocyte cAMP in Health and Disease

Doctoral Thesis

In partial fulfillment of the requirements for the degree
"Doctor rerum naturalium (Dr. rer. nat.)"
in the Molecular Medicine Study Program
at the Georg-August University Göttingen

Submitted by

Ruwan K. Perera

born in Düsseldorf

Göttingen, 2014

Thesis Committee Members:

1. Thesis Committee Member / Supervisor

Dr. Viacheslav O. Nikolaev

Molecular Imaging of the Heart, Research Group

Heart Research Center Göttingen, University of Göttingen

2. Thesis Committee Member

Prof. Dr. Blanche Schwappach

Department of Biochemistry I

University Medical Center, University of Göttingen

3. Thesis Committee Member

Prof. Dr. Stefan Luther

Biomedical Physics, Research Group

Max Planck Institute for Dynamics and Self-Organization

Date of Disputation: September 9, 2014

AFFIDAVIT

Here I declare that my doctoral thesis entitled

“Phosphodiesterases as Crucial Regulators of Cardiomyocyte cAMP in Health and Disease”

has been written independently with no other sources and aids than quoted.

Ruwan K. Perera

Göttingen, July 2014

List of Publications

Peer Review Publications and Submitted Manuscripts

- **Perera R.K., Sprenger J.U., Steinbrecher J.H., Hübscher D., Lehnart S.E., El-Armouche A., Nikolaev V.O.** (2014). Microdomain switch of cGMP-regulated phosphodiesterases leads to ANP-induced augmentation of β-adrenoceptor-stimulated contractility in early cardiac hypertrophy. ***European Heart Journal***. In revision.

- **Perera R.K., Fischer T.H., Maier L.S., Hasenfuss G., Nikolaev V.O.** (2014). Atropine augments cardiac contractility by inhibiting phosphodiesterases. Submitted.

- **Gotz, K., Sprenger, JU., Perera, R.K., Steinbrecher, J.H., Lehnart, S.E., Kuhn, M., Gorelik, J., Balligand, J .L., and Nikolaev, V.O.** (2014). Transgenic Mice for Real Time Visualization of cGMP in Intact Adult Cardiomyocytes. ***Circulation Research***. *114*, 1235-1245

- **Perera, R.K., and Nikolaev, V.O.** (2013). Compartmentation of cAMP signalling in cardiomyocytes in health and disease. ***Acta Physiologica*** *207*, 650-662.

- **Sprenger J.U., Perera R.K., Gotz KR, Nikolaev VO.** (2012). FRET microscopy for real-time monitoring of signaling events in live cells using unimolecular biosensors**. J Vis Exp.** 20;(66):e4081.

Conference Abstracts

- **Perera R.K., Steinbrecher J.H., Hübscher D., Lehnart S.E., Nikolaev V.O.** (2014). ANP potentiates catecholaminergic stress in early cardiac disease. ***Cardiovascular Research*** *(2014) 103 (suppl 1):* S110

- **Perera R.K. and Nikolaev, V.O.** (2013). Roles of Phosphodiesterases 2 and 3 at the T-tubules of Adult Mouse Cardiomyocytes. ***Circulation Research.****2013;* 113: A192

- **Perera, R.K., and Nikolaev, V.O.** (2013) FRET measurements of local cAMP signaling in the sarcolemmal / T- tubular compartment of cardiomyocytes. ***European Journal of Heart Failure*** *(2013) 15 (S1),* S

Contents

Abstract

Cyclic nucleotides are ubiquitous second messengers, which regulate cellular functions by acting in discrete subcellular microdomains. Cardiac phosphodiesterases (PDEs) are indispensable for β-adrenoceptor signaling regulation by restricting and maintaining distinct cAMP microdomains. In the mammalian myocardium, at least five PDE families (PDE1, 2, 3, 4, 8) contribute to cAMP breakdown, each with unique binding affinities and regulatory properties. Moreover, different PDE families and isoforms localize to distinct functional cAMP microdomains, making them promising targets to modulate cell function. However, the use of selective PDE inhibitors to treat heart failure is problematic due to a high risk of tachyarrhythmias and sudden cardiac death. Furthermore, progressive heart failure is accompanied by severely altered PDE expression patterns. Despite considerable insights into cardiac cAMP handling in general, exact mechanisms of cAMP regulation by PDEs inside functionally relevant microdomains are still poorly understood.

This work firstly describes compartmentalized functions of cardiac cAMP and uncovers that atrial natriuretic peptide can augment catecholamine-stimulated contractility in order to increase heart function in early cardiac hypertrophy. Real-time cAMP analysis of distinct β_1- and β_2-adrenoceptor-associated sarcolemmal cAMP microdomains using a novel targeted Förster resonance energy transfer (FRET)-based biosensor, pmEpac1, reveals that this effect is brought about by spatial redistribution of cGMP-sensitive phosphodiesterases 2 and 3 between β-adrenoceptor subtype-specific cAMP microdomains. While whole-cell PDE protein levels and activities are still unaffected at this early disease stage, differential subcellular PDE localization leads to altered cGMP/cAMP-crosstalk, which shifts the balance between β_1- and β_2-adrenoreceptor-mediated effects on cardiac function. These findings point towards a novel functionally relevant adaptation mechanism, which occurs early during disease and might compensate for a loss of heart function by redistribution of cGMP-regulated PDEs between distinct membrane microdomains, thereby modulating the functionally relevant ANP-cGMP / β-adrenoceptor-cAMP crosstalk at the sarcolemma of adult cardiomyocytes.

Secondly, a previously unappreciated PDE4 inhibitory side effect of atropine, a clinically relevant muscarinic receptor blocker, was uncovered in this work. This mechanism can, at least in part, explain incidences of tachycardia, which are frequently observed upon atropine administration and have been attributed solely to the antagonism at cardiac muscarinic M_2-receptors. However, in isolated mouse cardiomyocytes expressing the FRET-based cAMP biosensor Epac1-camps, even upon G_i-protein inactivation with pertussis toxin or in M_2-receptor knockout cells, atropine increases isoproterenol pre-stimulated cAMP levels, similar to the effects of PDE inhibitors. Furthermore, in intact wild type and M_2-receptor deficient hearts, it leads to increased beating frequency. Detailed analysis of atropine-mediated changes in cAMP handling using FRET approaches and *in vitro* assays show that atropine indeed inhibits PDE4 activity. Therefore, inhibition of PDE4 by atropine may be responsible at least for some of its multiple side effects.

Figure List

Abbreviations

5’-AMP	adenosine-5’-monophosphate
8-Br-cAMP-AM	8-Bromoadenosine-3',5'-cyclicmonophosphate,acetoxymethyl ester
ACh	acetylcholine
AC	adenylyl cyclase
AKAP	A kinase anchoring protein
ANP	atrial natriuretic peptide
Atr	atropine
AWThd	anterior wall thickness in diastole
bpm	beats per minute
β-AR	beta-adrenoceptor
β_1-AR	beta-1-adrenoceptor
β_2-AR	beta-2-adrenoceptor
βArr	beta-arrestin
BAY	BAY 60-7550
BNP	B-type natriuretic peptide
b.p.	base pairs
BSA	albumin bovine serum
BW	body weight
Ca^{2+}	calcium
CaMKII	Ca^{2+}/Calmodulin-dependent Kinase II
cAMP	3‘-5‘-cyclic adenosine monophosphate
CFP	cyan fluorescent protein
cGMP	3’-5’-cyclic guanosine monophosphate
CGP	CGP-20-712A
Cilo	cilostamide
CNBD	cyclic nucleotide-binding domain
CNGC	cyclic nucleotide gated channel
COPD	chronic obstructive pulmonary disease
dNTPs	desoxyribonucleotide triphosphates
EC	excitation-contraction
ECG	electrocardiogram
EF	ejection fraction
Epac	exchange protein directly activated by cAMP
FAS	fractional area shortening
FRET	Förster resonance energy transfer
FS	fractional shortening
$G\alpha_i$	alpha subunit of inhibitory G-proteins
GAPDH	glyceraldehyde 3-phosphate dehydrogenase
$G\alpha_s$	alpha subunit of stimulatory G-proteins
Gβγ	-beta-gamma subunit of GPCRs
GFP	green fluorescent protein
GPCR	G-protein coupled receptors
HCN2	hyperpolarization-activated cyclic nucleotide-gated channel 2
HW	heart weight
ICI	ICI 118,551

ISO	isoproterenol / isoprenaline
IBMX	3-Isobutyl-1-methylxanthine
LTCC	L-type calcium channel
LVEDD	left ventricular end diastolic diameter
LVESD	left ventricular end systolic diameter
mAChR	muscarinic acetylcholine receptor
o.n.	over night
PDE	phosphodiesterase
PKA	protein kinase A
PI3Kγ	phosphoinositide-3 kinase gamma
PLN	phospholamban
P_i	monophosphate
pPLN	phospho-phospholamban
PP_i	pyrophosphate
pTnI	phospho-troponin I
Roli	rolipram
RyR2	ryanodine receptor 2
Ser	serine
SERCA2a	sarcoplasmic/endoplasmic reticulum Ca2+ ATPase 2a
SR	Sarcoplasmic reticulum
TnI	troponin I
YFP	yellow fluorescent protein

1 Introduction

1.1 The Role of cAMP in the Heart

The second messenger 3',5'-cyclic adenosine monophosphate (cAMP) is a key signaling molecule important for a plethora of physiological functions. In general, cAMP signaling pathways start with the activation of G-protein-coupled receptors (GPCRs) associated to either stimulatory or inhibitory G-proteins (G_s, G_i), which in turn modulate the activity of the cAMP-synthesizing enzymes adenylyl cyclases. However, diverse effects attributed to cAMP strongly depend on the particular cell type with differential expression of various GPCR subsets and downstream targets of cAMP, leading to highly versatile, sometimes even opposing functional outcomes. For example, elevated cAMP leads to increased heart muscle contraction, at the same time decreased smooth muscle cell contractility[1]. Other important processes regulated by cAMP include metabolism and gene expression[2], insulin secretion[3,4] vascular tone immune reactions[5,6] and memory formation[7].

In the mammalian heart, cAMP primarily controls beating frequency, force of contraction and relaxation, referred to as chronotropic, inotropic and lusitropic effects, respectively. This is achieved through the β-adrenergic signaling pathway, which starts with catecholamine-induced activation of G_s-coupled β-adrenergic receptors (β-ARs) and results in cAMP-dependent protein kinase (PKA)-mediated phosphorylation of functional components of the excitation-contraction (EC) coupling system in cardiomyocytes. Calcium-handling proteins such as voltage-gated L-type calcium channels (LTCCs), calcium release units formed by ryanodine receptor 2 (RyR2), the negative regulator of the sarcoplasmic/endoplasmic reticular calcium ATPase (SERCA), phospholamban (PLN) and contractile proteins such as troponin I (TnI) have been shown to be functionally modulated through PKA-dependent phosphorylation[8,9]. This regulation is important for the beneficial effects of catecholamines on cardiac contractility during the classical 'fight-or-flight' response. However, chronic β-adrenergic stimulation affects the heart in a more detrimental way, i.e. causing down-regulation of β_1-adrenergic receptor (β_1-AR) expression, cardiomyocyte apoptosis, hypertrophy and loss of pump function, leading to decompensated heart failure[10-14]. In sharp contrast to β_1-AR-driven effects, selective stimulation or transgenic overexpression of β_2-ARs, does not lead to cardiomyocyte apoptosis, cardiac hypertrophy and failure[15,16]. Instead, β_2-ARs might protect against these abnormalities unless the receptor is overexpressed at extremely high levels (>300-fold) or a chronic heart failure phenotype is established[17]. Other receptors coupled to cAMP are represented by prostaglandin and glucagon receptors. Despite triggering intracellular cAMP increase their activation does not stimulate contractility, probably due to their association with cAMP pools which are spatially separated from those that elicit a positive inotropic response[18-20]. Apart from PKA, another important effector of cAMP is expressed in cardiomyocytes, which is called exchange protein directly activated by cAMP (Epac). It acts as a guanine nucleotide exchange factor for some small G-proteins such as Rap1 and mediates many PKA-independent effects of cAMP in various tissues[21]. In the heart, Epac1 is the predominant isoform expressed[22] and shows relatively minor effects on cardiac function at the basal state[23]. Instead, Epac seems to be one of the key factors downstream of chronic β_1-AR stimulation and cAMP, which promote the

development of cardiac hypertrophy[24,25]. It is supposed to do so via the activation of pro-hypertrophic genes and calcium/calmodulin-dependent protein kinase type II (CaMKII). The role of Epac-mediated pathways was further addressed in a recent study, in which transgenic mice with myocardial expression of the PKA inhibitory peptide no longer showed β-AR-agonist-induced hypertrophy, SR calcium overload and CaMKII activation but were rather protected against Epac/Rap1/ERK-mediated cardiomyocyte apoptosis[26]. Interestingly, one report demonstrated that stimulated β_1-AR but not β_2-AR can activate CaMKII via the recruitment of β-arrestin, which serves as a scaffold for both, CaMKII and Epac1 in cardiomyocytes[27]. This β-arrestin-dependent mechanism explains the link between β_1-AR- and CaMKII-dependent phosphorylation of PLN as well as CaMKII-dependent induction of pro-hypertrophic fetal gene expression and apoptotic pathways by β_1-AR. Especially when considering the disease-associated upregulation of CaMKII activity, its synergistic action on promiscuous substrates such as LTCC, RyR2 and PLN may not only stimulate PKA-mediated contractility but also the incidence of arrhythmias[28].

1.2 FRET-based Methods to Measure cAMP in living cells

Cyclic AMP content in any given cell type or tissue can be traditionally measured by standard antibody-based techniques such as radioimmunoassays and enzyme-linked immunoassays[29,30]. These methods allow quantification of total cAMP content (free cytosolic cAMP plus cAMP bound to various proteins) after lysis or mechanical disruption of thousands of cells or of the tissue. However, such methods have no spatial resolution and do not allow measurements of physiologically relevant free cAMP concentrations in intact living cells or in various subcellular locations within one cell. To overcome these difficulties, several live cell imaging techniques have been developed over the past two decades, which shed light into subcellular cAMP signaling in a more native context[31,32].

The majority of these findings relies on cAMP biosensors, which monitor intracellular dynamics of this second messenger based on Förster resonance energy transfer (FRET). In 1948, the German physicist Theodor Förster first described how two fluorescent molecules exchange energy in a nonradiative way[33]. The underlying physical principles are demonstrated in the Jablonski-Diagram (Figure 1A) according to which photon absorption by a donor fluorophore promotes it from its singlet ground sate, S_0 to a higher excitation level, S_1. In order to return to its ground state the excited donor releases lower-energy photons (fluorescence), which can be absorbed by an adjacent acceptor fluorophore within the a distance of 10 nm, known as the Förster radius. The acceptor is thereby lifted to its S_1 level and subsequently emits energy in form of fluorescence to return the S_0. A FRET pair consists of two fluorophores with incompletely separated absorption-emission spectra. The limited overlap in donor-emission and acceptor-absorption spectra is the basis on which FRET can occur between these two fluorophores.

About two decades ago, Adams et al.[34] created the first FRET-based cAMP probe, called FlCRhR. This pioneer-sensor consisted of a PKA holoenzyme with two fluorescent dyes chemically fused to the R- and C-subunits, and needed to be microinjected into living cells to monitor PKA dissociation upon elevation of intracellular cAMP and its re-association when cAMP is decreased. Since then, a series of more compact and 'easy-to-use' genetically encoded FRET biosensors has been generated, which are easily introduced into cells by transfection of the DNA construct to monitor cAMP with high resolution in space and time[35-39]. To achieve effective FRET pairs, such biosensors consist of green fluorescent protein (GFP) mutants, flanking a single cyclic nucleotide-binding domain (CNBD) (Figure1B). In cardiomyocytes, transient expression of such biosensors is commonly achieved via transfection of neonatal cardiomyocytes or adenoviral gene transfer in adult cardiomyocytes[40]. Adult rat ventricular myocytes are preferred for latter approach due to their relatively high stability in cell culture. However, significantly less stable mouse and human cardiomyocytes can be also successfully transduced with such adenoviruses[41-44] Expression of a functional FRET biosensor via adenovirus in adult myocytes requires at least 40–48 hours during which dedifferentiation and remodeling of normal cell physiology are likely to occur[45]. To address this problem and to enable cAMP measurements in freshly isolated cells, transgenic mice were generated expressing biosensors in adult heart muscle. In these mice, unimolecular sensors based on a single cAMP-binding site (from Epac1 or from hyperpolarization-activated cyclic nucleotide-gated channel 2 (HCN2) called Epac1-camps or HCN2-camps, respectively) sandwiched between a pair of fluorescent proteins could be expressed without any physiological abnormalities[37,46]. An additional advantage of such models is that they can be easily combined with various genetic and experimental heart disease models. So far, the sensors expressed in such transgenic mice were not targeted to any subcellular microdomain and were solely capable of monitoring changes in free cytosolic cAMP levels. Recently, various targeted versions of Epac1-camps have been cloned, which are can measure cAMP in various subcellular compartments or microdomains; however, they have mostly been used in transfected or transduced neonatal cardiomyocytes[19,47-49].

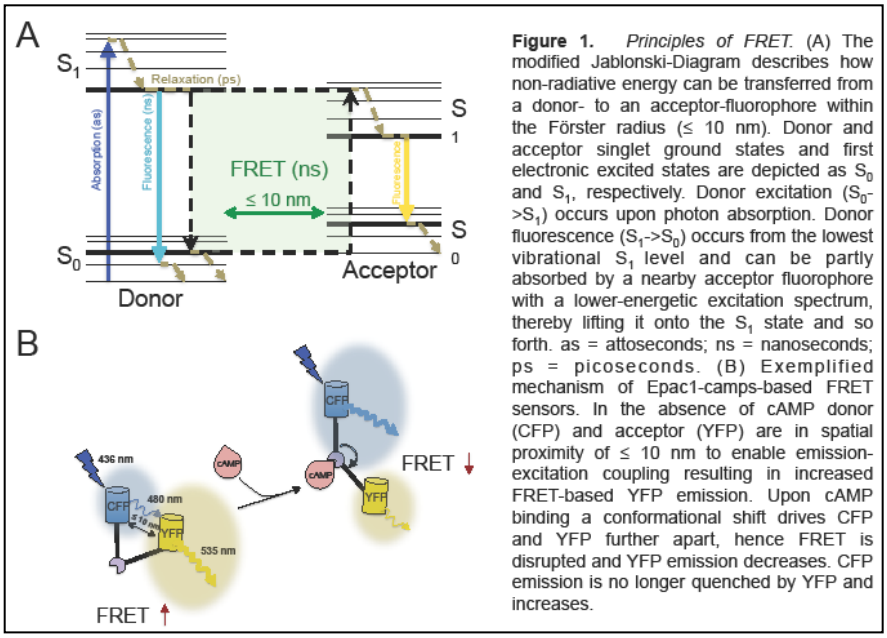

Figure 1. *Principles of FRET.* (A) The modified Jablonski-Diagram describes how non-radiative energy can be transferred from a donor- to an acceptor-fluorophore within the Förster radius (≤ 10 nm). Donor and acceptor singlet ground states and first electronic excited states are depicted as S_0 and S_1, respectively. Donor excitation (S_0->S_1) occurs upon photon absorption. Donor fluorescence (S_1->S_0) occurs from the lowest vibrational S_1 level and can be partly absorbed by a nearby acceptor fluorophore with a lower-energetic excitation spectrum, thereby lifting it onto the S_1 state and so forth. as = attoseconds; ns = nanoseconds; ps = picoseconds. (B) Exemplified mechanism of Epac1-camps-based FRET sensors. In the absence of cAMP donor (CFP) and acceptor (YFP) are in spatial proximity of ≤ 10 nm to enable emission-excitation coupling resulting in increased FRET-based YFP emission. Upon cAMP binding a conformational shift drives CFP and YFP further apart, hence FRET is disrupted and YFP emission decreases. CFP emission is no longer quenched by YFP and increases.

1.3 Key Factors for cAMP Compartmentation

The theory of cAMP compartmentation emerged about three decades ago from the observation that cAMP and PKA activities are differentially stimulated in 'membrane' and 'cytosolic' rabbit cardiomyocyte fractions by β-adrenergic and prostaglandin receptor agonists. The β-adrenergic agonist isoproterenol stimulated cAMP in both fractions, while prostaglandin increased cAMP exclusively in the cytosolic fraction, which is not coupled to positive inotropic response[18,50]. A later study combined whole-cell patch-clamp recordings of LTCC currents (hence indirectly reporting cAMP/PKA activity – at least at the membrane) in long frog ventricular myocytes, with simultaneous local application of β-AR agonists through a double-barreled micropipette to either half of the cell. Comparing the change in current upon close and distant agonist application revealed that cAMP activated by β_2-AR expressed in these cells is not diffusing over long distances inside the cell unless the cAMP-hydrolyzing enzymes phosphodiesterases (PDEs) are inhibited, which was in contrast to the global adenylyl cyclase stimulation by forskolin, associated with more diffuse signals[51]. Though indirectly, this finding further indicated the presence of discrete subcellular pools cAMP associated with various types of stimulation. To date, cAMP compartmentation has developed from an elegant hypothesis into a well-appreciated paradigm. Key regulators for cAMP compartmentation in the myocardium include scaffolding proteins that recruit macromolecular PKA-signaling complexes, differential subtype-specific β–AR localization to particular membrane structures and especially PDEs as enzymes responsible for localized cAMP degradation hence shaping subcellular cAMP gradients. Exemplar cardiac cAMP microdomains are summarized in Figure 2.

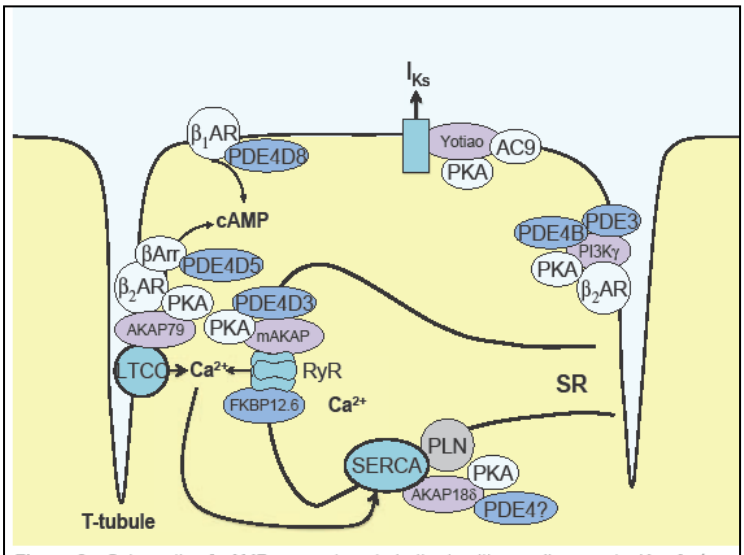

Figure 2. *Schematic of cAMP compartments in the healthy cardiomyocyte.* Key factors that contribute to 3′,5′-cyclic adenosine monophosphate (cAMP) compartmentation in healthy cardiomyocytes (*Perera et al., Acta Phys 2012*[52]).

1.3.1 Scaffolding Proteins

A-kinase anchoring proteins (AKAPs)

One important factor in regulating compartmentalized cAMP signaling is represented by scaffolding proteins such as those belonging to the AKAP family, which recruit PKA to its effector proteins. Furthermore, PDEs, other kinases, protein phosphatases (PPs) or even different GPCRs bind to certain AKAPs to form functionally relevant signaling complexes[53-58]. To date, a considerable number of cardiac AKAPs has been described (mAKAP, AKAP15/18δ, AKAP79/150, D-AKAP1/2, AKAP95, AKAP220, AKAP-Lbc, gravin, ezrin, yotiao)[58,59]. Some of these AKAPs and their role in heart function were studied in detail.

As such, mAKAP anchors PKA and PDE4D3 to the RyR2 complex, close to the sites of interaction with protein phosphatases PP1/PP2 and FKBP12.6 (calstabin), thereby forming a signaling unit to regulate the calcium

release from sarcoplasmic reticulum (SR)[60,61]. AKAP15/18δ facilitates PKA-dependent phosphorylation of PLN, the negative regulator of SERCA2a. AKAP79 (AKAP150 or AKAP6) mediates PKA-dependent phosphorylation of the cardiac LTCC and is critically involved in increased calcium influx in response to β–AR stimulation. A functional complex comprised of AKAP79, PKA, adenylyl cyclase type 5/6 and LTCC has been described in caveolin-3-rich membrane compartments of cardiomyocytes[62]. AKAP15/18α, another AKAP associated with cardiac LTCC modulates βAR effects on calcium transients and contractility, acting in concert with AKAP79[56,63]. In addition to AKAPs, other proteins can also serve as scaffolds for cAMP/PKA signaling units.

β-arrestins

β-arrestins (βArrs) comprise another important group of scaffolding proteins. βArr 1 and 2 are two highly homologous isoforms, which are expressed in the myocardium. Initially, their function in cardiomyocytes was thought to be limited to termination and desensitization mechanisms of β–AR signaling[64-66]. However, considerable evidence has been presented that βArrs can contribute to the molecular make-up of submembrane and β–AR-associated cAMP microdomains, especially through the recruitment of PDE4s[67-69]. Pioneering studies by Baillie et al.[68] and Perry et al.[69] established that βArrs bind PDE4D isoforms to promote the PKA-mediated switch from stimulatory to inhibitory G-protein coupling (G_s-to-G_i) of β_2-ARs. An elegant biochemical study by Richter et al. later on demonstrated that β_1- and β_2-AR are dynamically associated with different PDE4D isoforms. In particular, β_1-AR forms a complex with PDE4D8, which dissociates upon receptor activation, whereas β_2-AR recruits βArr and PDE4D5 upon stimulation[70]. This leads to different subcellular cAMP gradients, underpinning cAMP compartmentation and different functional effects induced by these two receptor isoforms.

Phosphoinositide 3-kinase gamma (PI3Kγ)

Very recently, PI3Kγ was added to the list of scaffolding proteins that are actively involved in cAMP compartmentation. As such, PI3Kγ has been shown to recruit PKA regulatory subunits type II (RII-subunits), PDE3 and PDE4 and form distinct functional signaling complexes at the membrane of cardiomyocytes. Importantly, this function of PI3Kγ is independent of its catalytic activity but crucial for establishing regulatory feedback loops via PDE3s and 4s and protecting the heart from catecholamine-induced ventricular arrhythmias[71].

1.3.2 Subtype-specific β-AR localization

Marked differences between β_1- and β_2-ARs in terms of their physiological and pathophysiological responses suggest that these receptors might trigger different downstream signaling pathways or affect different cAMP microdomains and associated functional responses. β_2-AR has been shown to switch from G_s to G_i upon prolonged agonist application in order to decrease the magnitude of the cAMP signal, which can explain why β_2-AR activation does not lead to phosphorylation of cytosolic substrates such as PLN or contractile proteins[72-74]. Instead, G_i–coupling has been shown to mediate cardioprotective effects of this receptor subtype by

activation of Akt (protein kinase B) and PI3 kinases[75,76]. Using a FRET-based approach with adult mouse cardiomyocytes transgenically expressing the HCN2-camps biosensor in heart muscle, it was established that local and selective stimulation of β_1-AR results in diffusive far-reaching cAMP signals, while β_2-AR cAMP signals are highly locally confined even upon G_i-protein inactivation[37], suggesting differences in cAMP compartmentalization between the two β-AR subtypes. However, the precise localization of both receptor subtypes in cardiomyocytes was unclear at that time, because the available antibodies could not reliably detect endogenously expressed amounts of the receptors in electron microscopy or immunofluorescence studies. The non-optical imaging technique, scanning ion conductance microscopy (SICM), allows non-contact imaging of living cell membrane with nanometer resolution[77]. Using a combined SICM/FRET approach together with local ligand application, it could be later on established that β_1- and β_2-ARs are differentially distributed on the sarcolemma of adult cardiomyocytes. Especially β_2-ARs showed to be exclusively localized in the transverse tubules that are crucial for LTCC function and EC coupling[78].

1.3.3 cAMP-hydrolyzing Phosphodiesterases

cAMP-hydrolyzing PDEs play a central role in cAMP compartmentalization by shaping, separating and modulating distinct subcellular cAMP microdomains. The PDE superfamily of enzymes is represented by 11 families with over 60 individual isoforms. In mammalian myocardium, five PDE families (PDE1, 2, 3, 4 and 8) hydrolyze cAMP[79-83]. PDE1, 2 and 3, are dual-specific PDEs that can hydrolyze both cAMP and cGMP, whereas PDE4 and 8 are specific for cAMP. Their high versatility in substrate specificities, regulatory properties as well as their systemic and isoform-specific subcellular distributions make PDEs an attractive target for pharmacotherapy. However, a lack of isoform-selective inhibitors has largely prevented a general breakthrough in clinical exploitation of PDE-dependent mechanisms.

PDE1

PDE1 is also referred to as the "Ca^{2+}/calmodulin-stimulated PDE". *In vitro* studies have shown that enzyme activity can be increased up to 10-fold by calcium/calmodulin binding[84]. This way, PDE1 is believed to establish a crosstalk between calcium and cyclic nucleotide signaling[85]. Three PDE1 isoforms, i.e. 1A, 1B, 1C are expressed in cardiomyocytes. All show dual specificity and hydrolyze both cAMP and cGMP. However, PDE1A and B prefer cGMP over cAMP as a substrate, whereas PDE1C binds both cyclic nucleotides with equal affinities[86-90]. Much less is known about the subcellular distribution of PDE1s and their contribution to cAMP compartmentation in cardiomyocytes. These questions should be further investigated in the light of the possible cardioprotective role of PDE1, supported by the fact that the PDE1 inhibitor IC86340 is able to protect the heart from pressure overload-induced hypertrophy[88]. However, the lack of truly selective inhibitors has so far hampered thorough functional investigations of myocardial PDE1 dependent functions and its role in modulating the cAMP dynamics.

PDE2

The second cardiac dual-specific PDE family is represented by PDE2. Members of this family are assembled as homodimers, each monomer bearing a pair of tandem regulatory GAF domains (GAF = cGMP-specific phosphodiesterases, adenylyl cyclases and FhlA) on their N-terminus. Binding of cGMP to one of these domains (GAF-B) stimulates the activity of catalytic domains by an allosteric mechanism[91]. Therefore, PDE2 is also referred to as the "cGMP-stimulated PDE" (Figure 3). Mammalian cardiomyocytes express several PDE2A isoforms (2A1, 2A2 and 2A3), which are associated with both, cytosolic compartment and sarcolemmal membrane[83]. Two studies performed either using a FRET biosensor in neonatal or cyclic nucleotide gated channel (CNGC) recordings in adult rat myocytes have shown an association of PDE2 activity with the subsarcolemmal microdomain[92,93]. The first study described a negative feedback mechanism involving the □$_3$AR and endothelial nitrite monoxide synthetase (eNOS)/ soluble guanylyl cyclase (sGC)/ 3',5'-cyclic guanosine monophosphate (cGMP) signaling pathway, which leads to PDE2 activation, thereby counteracting an increase in cAMP and positive inotropic response after β-adrenergic stimulation. The second study found that cGMP pools produced by both particulate guanylyl cyclase and soluble guanylyl cyclase are controlled by PDE2.

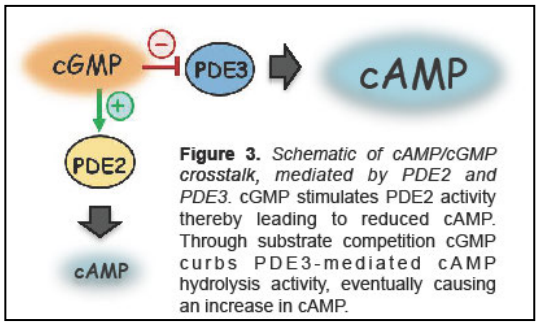

Figure 3. *Schematic of cAMP/cGMP crosstalk, mediated by PDE2 and PDE3.* cGMP stimulates PDE2 activity thereby leading to reduced cAMP. Through substrate competition cGMP curbs PDE3-mediated cAMP hydrolysis activity, eventually causing an increase in cAMP.

PDE3

Two PDE3 isoforms PDE3A and PDE3B have been described in cardiomyocytes[83,94], whereby PDE3A is considered as the predominant isoform in mammalian hearts[95-97]. The PDE3 family represents the third group of dual-specific PDEs. Furthermore, similar to PDE2, its activity can be modulated by cGMP. However, in contrast to PDE2, which is stimulated by cGMP, this second messenger inhibits PDE3 activity (Figure 3). Therefore, PDE3 is also known as the "cGMP-inhibited PDE". PDE3 is considered the second most important cAMP-degrading enzyme in rodent cardiomyocytes and the predominant cAMP-PDE in human cardiomyocytes[44]. In 2004, Patrucco and co-workers[94] showed that PDE3B co-precipitates with PI3Kγ. They postulated a complex of PI3Kγ and PDE3B, which regulates local cAMP pools at the sarcolemma and, at the same time, controls PLN phosphorylation, thereby participating in cAMP/PKA-mediated signaling. Recently, the same group identified PDE3A in the PI3Kγ-associated cAMP compartment[71].

PDE4

Type 4 PDEs are cAMP-specific. In mammalian systems, four genes (*pde4a-d*) encode about 20 isoforms. Each isoform contains a unique N-terminal region, which is responsible for subcellular localization[98], and PDE4A, PDE4B and PDE4D were shown to be expressed in rodent and the human hearts[99,100]. In the past few years, the hypothesis of different PDE4 isoforms each playing a unique role in cardiomyocyte cAMP compartmentalization has gained increasing interest. To date, several studies are available that report PDE4 subtypes and isoforms to be critical for the fine-tuning of different cAMP microdomains. For example, PDE4B associates with the LTCC

complex at the sarcolemma of adult mouse cardiomyocytes and represent the major isoform responsible for the regulation of PKA-mediated phosphorylation of this channel upon β-adrenergic stimulation[101]. PDE4D3 is part of the RyR2 signaling complex[43], whereas PDE4D5 and PDE4D8 were reported to form signaling complexes with either β_1- or β_2-ARs in a ligand-dependent manner[70]. A still not identified PDE4D isoform has been shown to co-immunoprecipitate with the SERCA2a signaling complex in mouse hearts. This PDE is responsible for the regulation of PLN phosphorylation and hence SERCA2a activity under basal conditions[102,103]. PDE4A and PDE4B but no D-isoforms were also found in the PI3Kγ-cAMP compartment[71].

PDE8

Phosphodiesterase 8 is another cAMP-specific PDE in mammalian myocardium. Two genes encode the PDE8A and B isoforms, of which PDE8A is expressed in human and mouse hearts[104]. Its most profound property is its insensitivity to the unselective PDE inhibitor 3-Isobutyl-1-methylxanthin (IBMX). Regarding cAMP compartmentalization in cardiomyocytes, PDE8 has long been neglected. In a recent study, it was demonstrated that cardiomyocytes isolated from PDE8A knockout mice show increased β-adrenergic-stimulated calcium transients, LTCC currents and calcium spark frequencies[105]. This indicates the involvement of PDE8A in the calcium homoeostasis. The authors also report a 'leaky' RyR2 phenotype, which is suggested to be the result of a compensatory increase in SR calcium re-uptake. Recently, it was shown that, similar to PDE4, this PDE can also be phosphorylated by PKA, which leads to an increase in its hydrolyzing activity[106]. This may represent an important negative feedback loop regulating cAMP dynamics in subcellular microdomains of cardiomyocytes. Further efforts are necessary to study the exact role of PDE8A for cAMP compartmentation.

1.4 Pathophysiology of Chronic Heart Disease

Chronic heart disease is often triggered by catecholamine-induced augmentation of cardiac output, which occurs as a result of increased afterload due to hypertension or aortic valve disease. In order to compensate the increased demand of oxygen, the secretion of natriuretic peptides, especially that of the atrial and B-type kind (ANP, BNP) is increased to achieve enhanced blood flow by cGMP-dependent vasodilatation mechanisms. However, chronic pressure overload ultimately causes exhaustion of this adaptive response, during which the heart undergoes different stages of progressive morphological and functional remodeling. These range from compensated hypertrophy to decompensated states of late- and end-stage heart failure (Figure 4). [107]

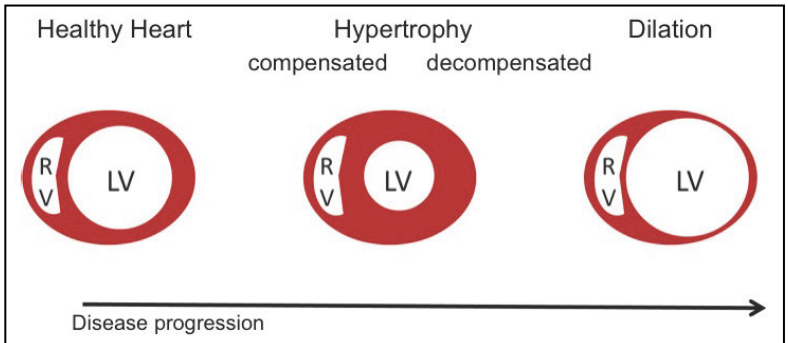

Figure 4. *Schematic of progressive chronic cardiac disease.* Hypertrophy is characterized by increased left-ventricular (LV) wall thickness, caused by enhanced incorporation of myofilaments in cardiomyocytes. In the compensated state, heart function is mostly preserved. Upon decompensation, increased cardiomyocyte apoptosis and fibrosis finally cause LV dilation. (*Ganau et al., JACC 1992*[106] modified).

During *compensated hypertrophy*, the heart muscle responds to the enhanced demand on cardiac contractility by a gain in left-ventricular size, achieved through increased wall thickness. Single cardiomyocytes incorporate additional sarcomeres, leading to increased cellular diameters. At this state, cardiac performance is largely preserved. In contrast, *decompensation* is morphologically characterized by progressive dilatation of the left ventricle due to myocyte apoptosis, which may be accompanied by increased fibrosis. Together, all these factors account for a dramatic drop in cardiac function. A molecular hallmark of heart failure is the desensitization of β-AR and ANP receptor signaling cascades. Dramatic reduction of β_1-AR density in failing myocytes[108,109] and desensitization of the ANP receptor NPR-A due to its dephosphorylation in cardiac hypertrophy[110,111] have been consistently documented. These molecular changes result in the reduction of catecholamine-stimulated cardiomyocyte force and ANP-mediated cGMP generation in late-stage cardiac disease, while disease-initiating alterations are still poorly defined. Despite the essential role of the second messenger pathways for normal heart function, little to nothing is known about alterations in microdomain-specific cAMP or cGMP signaling and about cGMP/cAMP cross-talk in diseased cardiomyocytes, especially not at disease onset, which is potentially relevant for therapeutic prevention strategies.

1.5 Changes in cAMP Compartmentation in Diseased Cardiomyocytes

Cardiac disease has been associated with changes in compartmentalized cAMP signaling. Today there is considerable evidence that remodeled subcellular signaling pathways promote or potentially cause chronic heart failure. Known alterations in compartmentalized cAMP signaling are illustrated in Figure 5.

Remodeling of AKAP-associated signaling complexes

Early studies by the group of Meredith Bond revealed that in human failing cardiomyocytes, the proper association of the PKA with AKAPs is dramatically decreased[112]. This was explained by the decrease in the basal RII (regulatory PKA subunit II) autophosphorylation, which normally increases PKA affinity for AKAPs. Disrupted interaction between AKAPs and PKA might result in the reduced phosphorylation of other PKA targets, including those associated with cardiomyocyte EC coupling. Disruption of the mAKAP/RyR2 signaling complex responsible for calcium release from SR has also been shown to cause severe

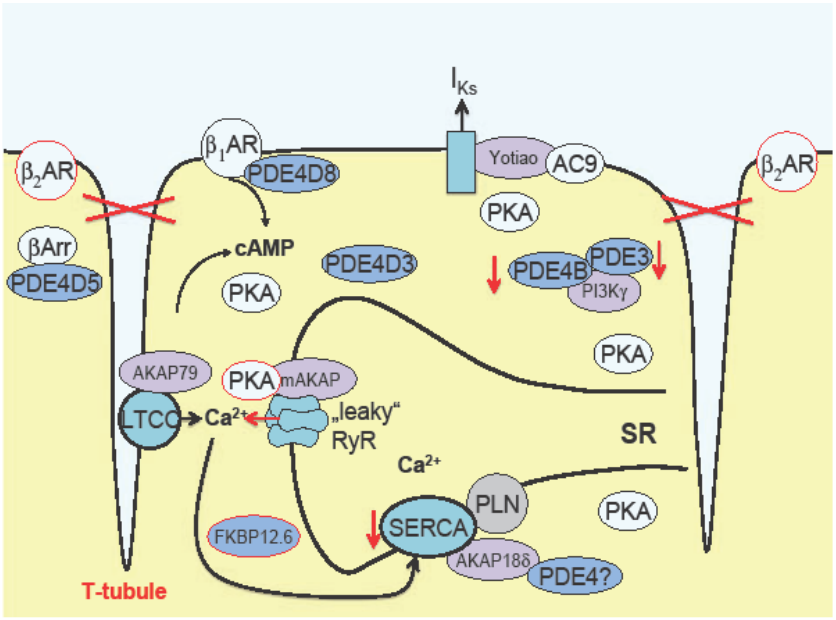

Figure 5. Schematic of disease-related alterations in cAMP compartmentation. Affected structures are marked in red, e.g. FKBP12.6 dissociates from the RyR_2, de-tubulation and β_2-AR re-distribution, down-regulation of multiple PDE isoforms. (*Perera et al., Acta Phys 2012*[52]).

impairment of heart function in experimental mouse models, which resemble human disorders such as age-related cardiomyopathy, exercise-induced arrhythmias and sudden cardiac death. In a series of elegant studies, the group of Andrew Marks could show that failing hearts display a destabilization of the RyR2 complex caused by the pronounced dissociation of FKBP12.6 (calstabin) from the signaling complex due to hyperphosphorylation of RyR2[61,113-115]. The same group later reported that deletion of FKBP12.6 leads to a cardiac phenotype similar to that of failing hearts with delayed afterdepolarizations, favoring severe arrhythmias and sudden cardiac death caused by spontaneous diastolic calcium release from the 'leaky' RyR2[115]. It was further demonstrated that the hyperphosphorylation of RyR2 by the local pools of PKA is involved in these processes due to depletion of PDE4D from the complex that occurs in failing cardiomyocytes under chronic β-adrenergic stimulation[43]. This phenotype could be recapitulated in PDE4D knockout mice, and such effects might be also linked to the adverse effects of the selective PDE4 inhibitors[116] that have been reported to promote arrhythmia in human heart muscle[44]. Recently, Beca et al.[102] showed that under basal conditions (which is in contrast to the β-adrenergic stimulation used in the studies mentioned above), PDE4 is not involved in the regulation of PKA-mediated RyR2 phosphorylation, but in this state, it rather maintains proper calcium handling via the SERCA2a–PLN complex. In addition to PKA, the increased activity of CaMKII can lead to hyperphosphorylation and leakiness of the RyR2[117,118]. A recent study by Kashimura et al. demonstrated that in a genetic mouse model of catecholaminergic polymorphic ventricular tachycardia, RyR2 leak after β-adrenergic stimulation does not result from a lowered threshold for calcium waves but rather from increased SR calcium content[119]. Therefore, it can be anticipated that for the leak mechanism to be effective, the SR calcium content must be maintained, a technical point frequently missed in studies that argue against the RyR2 hyperphosphorylation hypothesis.

Redistribution of β-AR subtypes

Nikolaev et al. combined FRET with scanning ion conductance microscopy (SICM/FRET) to analyze sarcolemmal distributions of β_1- and β_2-ARs in failing rat cardiomyocytes[78]. Here, widespread membrane β_1-AR localization was basically unchanged, while β_2-AR redistributed from the T-tubules onto the de-tubulated outer membrane areas. Interestingly, following the receptor redistribution, its subcellular cAMP gradients were also remodeled so that they were no longer confined but diffused throughout the entire cytosol, similar to the β_1-AR cAMP signals. These diffuse signals have been associated with increased PLN phosphorylation and arrhythmias, which occur in heart failure. They might be a result of the loss of receptor coupling to local PKA and PDE4 pools found in the T-tubules of healthy cardiomyocytes. In addition, proper localization of PKA was also shown to be disrupted, leading to a loss of the negative PKA-PDE4 feedback regulatory loop capable of restricting β_2-AR cAMP signals to the T-tubular compartment. Future work should more precisely analyze the composition and remodeling of such macromolecular complexes in heart failure. Probably, the regulation of β_2-AR cAMP is likely to be more complex than previously anticipated, because a recent study suggests that β_2-AR signaling is also dependent on PI3Kγ-mediated scaffolding, which is apparently important to protect the heart from arrhythmias[71]. Interestingly, the findings of this study suggest that PI3Kγ interaction with PDE4 might regulate β_2-AR cAMP signaling in the cytosol, whereas a PI3Kγ/PDE3 complex shapes those signals at the membrane.

More insights into the architecture of this cAMP compartment are definitely needed to fully understand the nature of β_2-AR cAMP signaling in healthy and failing myocytes.

Altered PDE expressions and activities

Cardiac hypertrophy has been associated with changes in PDE activity patterns. In 2009, Abi-Gerges et al. established that expressions and activities of PDE3A and PDE4s are dramatically reduced in cardiomyocytes isolated from rats that underwent transverse aortic constriction to induce cardiac hypertrophy[95]. By electrophysiological CNG channel-based measurements of subsarcolemmal cAMP, they showed that upon β-adrenergic stimulation, cAMP signals are significantly reduced in hypertrophied cardiomyocytes, which might be due to the above-mentioned receptor desensitization. However, the responses to PDE3 and PDE4 inhibitors were also shown to be markedly reduced in this compartment. Analyses of subtype-specific PDE expressions and activities revealed that the expression levels and activities of PDE3A and PDE4A, PDE4B but not PDE4D were reduced in hypertrophied cardiomyocytes. It was proposed that this decrease in cAMP-hydrolyzing PDE activity could be a potential short-term adaptation mechanism to counterbalance the reduction in cAMP production by desensitized βARs. In addition to PDE3 and PDE4 downregulation, some PDE amounts might conversely increase during disease progression. As such, PDE2 has recently been identified to be upregulated in heart failure models of rodents and dogs but importantly also in end-stage heart failure patients, thereby possibly contributing β−AR desenzitation[120]. However, little is known about how local PDE pools, associated with AKAPs and other subcellular signaling complexes are affected in heart disease. The work by Lehnart et al. (2005) vividly demonstrated that despite unchanged global PDE4D expression and activity in failing cardiomyocytes, the reduction in local PDE4D content inside the mAKAP/RyR2 signaling complex leads to PKA-mediated hyperphosphorylation of RyR2 in failing myocytes making them more susceptible to arrhythmias[43]. Nevertheless, more direct investigations of cAMP dynamics in various subcellular compartments are needed to fully understand the molecular mechanism of cardiac disease.

1.6 Autonomous Nervous Control of Heart Function

The autonomous nervous system regulates functions of various organs via the sympathetic and parasympathetic neurotransmitters norepinephrine and acetylcholine, which once released from nerve terminals, activate adrenergic and muscarinic G-protein coupled receptors on the membranes of target cells. In the heart, sympathetic innervation augments contractile force and beat frequency by β-AR-mediated increases in intracellular levels of cAMP. Conversely, parasympathetic control via the Vagus nerve is achieved through acetylcholine-mediated activation of type 2 muscarinic acetylcholine receptors (M_2) and leads to a decrease of cellular cAMP, resulting in lowered heart rate and less pronounced decrease in force of contraction (Figure 6).

1.7 Effects and Clinical Use of Atropine

Atropine is a plant secondary metabolite, tropane alkaloid extracted from the deadly nightshade (*Atropa belladonna*) and other species of the *Solanaceae* family. It is a potent competitive antagonist for muscarinic acetylcholine receptors (mAChRs) with an affinity (dissociation constant, K_D) of approximately 1nM[121,122]. In mammalian organisms, five different sub-types of mAChRs, M_1-M_5[123] are expressed, of which the M_1, M_3 and M_5 receptor subtypes are coupled to G_q, whereas M_2 and M_4 are G_i-coupled. As an unselective mAChR antagonist, atropine has been widely used for multiple purposes over the centuries. Presumably, the Egyptians already used *Solanaceae* plant extracts to alleviate respiratory complaints[124]. The Greeks and Romans knew about its poisonous potential and in medieval times, its effect to dilate the pupils was utilized by court ladies to achieve a brighter glance, hence its name *Belladonna*[125]. Its pharmacological properties are known since the early 20th century[122]. But as early as in the 1830s, L-atropine was first purified from plant extracts, which enabled further understanding of its effects as a potent modulator of the autonomic nervous system, eventually leading to the discovery of the neurotransmitter acetylcholine[125].

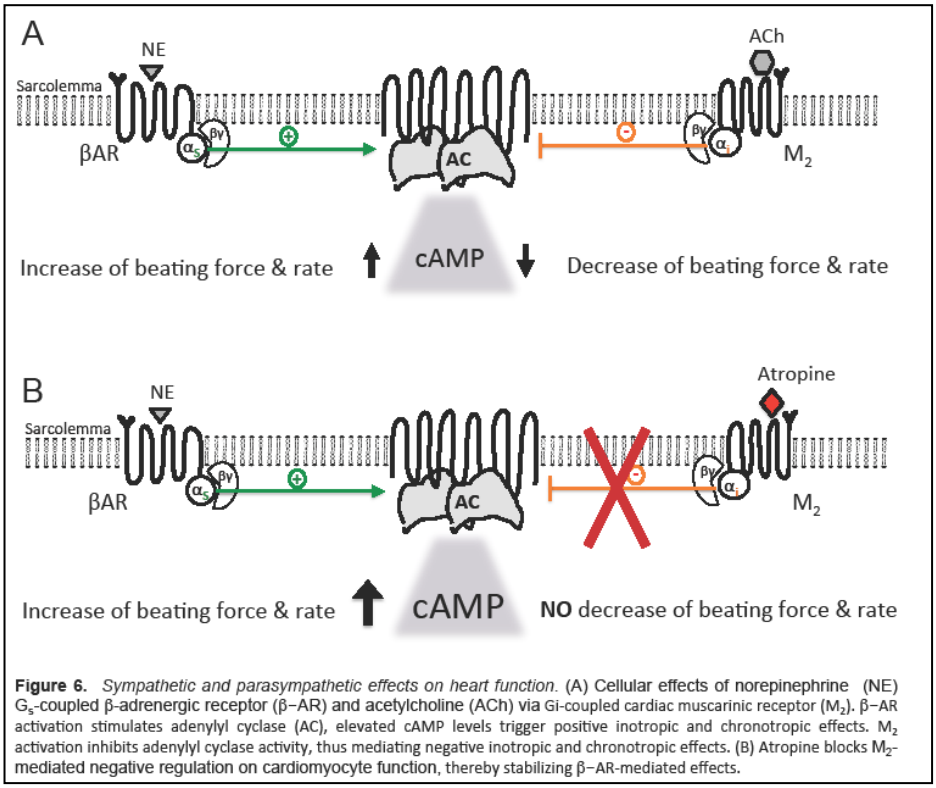

Figure 6. *Sympathetic and parasympathetic effects on heart function.* (A) Cellular effects of norepinephrine (NE) G_s-coupled β-adrenergic receptor (β−AR) and acetylcholine (ACh) via Gi-coupled cardiac muscarinic receptor (M_2). β−AR activation stimulates adenylyl cyclase (AC), elevated cAMP levels trigger positive inotropic and chronotropic effects. M_2 activation inhibits adenylyl cyclase activity, thus mediating negative inotropic and chronotropic effects. (B) Atropine blocks M_2-mediated negative regulation on cardiomyocyte function, thereby stabilizing β−AR-mediated effects.

Today, atropine and atropine-derived anticholinergics are used for multiple indications, such as to prevent hyper-salivation during anesthesia or as antidotes for organophosphate poisoning. They are used for pupil dilation during eye examinations or as bronchodilators for the therapeutic treatment of asthma and chronic obstructive pulmonary disease (COPD)[126-128]. In the heart, atropine blocks the inhibitory effect of acetylcholine on heart rate and contractility, and is used to reduce susceptibility to bradycardia and atrioventricular block or during stress echocardiography[129]. Furthermore, atropine is still a first-line drug for acute bradycardia treatment[130].

However, because of its broad range activity spectrum, atropine also shows multiple side effects such as blurred vision and dizziness, cottonmouth, nausea and emesis, urine retention and even severe arrhythmias. Moreover, lower doses of atropine (<0.5 mg) are known to trigger paradoxical bradycardia, whereas higher doses tend to elicit tachycardia[131,132]. It is subject of debate whether this is due to differential effects on the

central and the terminal parasympathetic nervous system[133,134]. Atropine-induced tachyarrhythmia has been attributed exclusively to the antagonism at cardiac G_i-coupled M_2-receptors and inhibition of parasympathetic events. However, exact molecular mechanisms behind these inadvertent phenomena remain elusive.

Redundancy in atropine and PDE4 inhibitor effects

Interestingly, a number of aforementioned atropine effects show similarities to those of PDE inhibitors, especially PDE4 inhibitors[135-137] used e.g. for treatment of airway diseases such as asthma and COPD [138-140] or bladder function disorders [141,142].

Conversely, PDE4 inhibitors are also associated with a plethora of adverse effects that are partly reminiscent of atropine-related side effects such as emesis or nausea, but importantly also tachycardia[116,135,136]. Furthermore certain PDE4 isoforms have been shown to prevent catecholamine-induced arrhythmias[43,44,71,101,143].

2 Aims

Local β-Adrenergic Signaling at the Sarcolemma of Adult Mouse Cardiomyocytes

Several publications have shed light onto molecular changes in the β-AR signaling cascade that accompany the failing heart phenotype, such as β-AR desenzitation and downregulation[12], β-AR redistribution[78] or changes in the activity of certain PDEs[120,144]. So far, however relatively little is known about alterations in β-AR signaling pathways that occur at the onset of cardiac disease, i.e. in early compensated cardiac hypertrophy, where subtle changes would first affect subcellular compartments, rather than the whole cell.

The purpose of this project was to establish a new transgenic mouse line expressing a localized FRET-based cAMP biosensor, which would allow analysis of local cAMP dynamics exclusively at the sarcolemma of freshly isolated adult cardiomyocytes. Using this mouse as a tool, investigations of subtype-specific β-AR-mediated cAMP signals, their regulation by PDEs and role in chronic cardiac disease were performed.

Atropine Modulates Phosphodiesterase Activity in the Heart

Atropine is an unspecific anticholinergic drug that inhibits all five mammalian muscarinic acetylcholine receptor subtypes. As such, atropine is linked to multiple side effects. Its pro-arrhythmic potential has long been acknowledged but not completely understood.

Importantly, a considerable number of atropine-associated side effects show similarities to effects evoked by PDE4 inhibition. The aim of this project was to analyze the molecular mechanisms by which atropine can affect cardiac function independently of the parasympathetic nervous system and M_2 receptors. In particular, the effects of atropine on PDE4 activity to promote tachycardia were investigated.

3 Materials and Methods

3.1 Materials

Description	*Company*

3.1.1 Stable cell lines

HEK293A	Invitrogen, #R705-07

3.1.2 Plasmids

pcDNA3.0	Invitrogen
-MHC-HCN2	*see Nikolaev et al., 2006*[37]

3.1.3 Bacteria strains

One Shot® TOP10 chemically competent *E. coli*	Invitrogen
One Shot® OmniMax2T1	Invitrogen

3.1.4 Animals

FVB/NRj animals were obtained from Janvier Labs (Saint Berthevin, France) and used for pronuclear injection with the pmEpac1construct by the Max-Planck-Institute of Experimental Medicine. All animal experiments were performed in accordance with institutional and governmental guidelines.

3.1.5 Oligonucleotides

Oligonucleotides were purchased from MWG Biotech GmbH, Ebersberg

MHCseqfor	5'-TGACAGACAGATCCCTCCTAT-3'
YFPrev	5'-CATGGCGGACTTGAAGAAGT-3'
pmYFPKpnIfor	5'-AAAGGTACCATGGGATGTATCAATAGCAAGC-3'
YFPEcoRIrev	5'-AAAGAATTCCTTGTACAGCTCGTCCATG-3'
PDE1ABamHIfor	5'-AAAGGATCCATGCCCTTGGTGGATTTCTTCTGCGGGTCTACTGATACGGAC-3'
PDE1AXhoIstoprev	5'-AAACTCGAGCTATGGACGTGTGTAAGCA-3'

3.1.6 Chemicals

AG 1-X8 Resin	Biorad, # 140-1441
Albumin Fraction V	Applichem, # A1391.0100
Ammonium persulfate	Sigma, # A3678
Ampilcillin	Roth, # K029.1
Ampuwa® water	Fresenius Kabi Deutschland GmbH
BAY 60-7550	Santa Cruz, # sc-205219
BES buffer grade	Applichem, A1062
β-Mercaptoethanol	Sigma, # M3148
Bromphenol Blue sodium salt	Applichem, # A1120
8-Bromoadenosine-3', 5'-cyclic monophosphate, acetoxymethyl ester	Biolog, # B028

Description	*Company*
2,3-Butanedione monoxime	Sigma, # B0753
Calcium chloride dihydrat	Merck, # 17257
cAMP	Sigma, # A9501
cAMP [5',8-^{3}H]	Hartmann Analytic GmbH, # 1790
Cesium chloride	Sigma, # C3032
CGP-20712A methanesulfonate salt	Sigma, # C231
Cilostamide	Sigma, # C7971
Crotalus atrox snake venom	Sigma, # V7000
di-8-ANEPPS	Molecular Probes®, # F1221
Dimethyl sulfoxide HYBRI-MAX®	Sigma, # D2650
DirectPCR-Tail	Peqlab, # 31-102-T
D(+) Sucrose	Roth, # 4621.2
dNTPs	Promega, # U1240
EDTA	Roth, # 8040.3
EGTA	Sigma, # E4378
Ethanol Rotipuran >99,8 %	Roth, # 9065.1
Ethidium bromide - Solution 1 %	Applichem, # A1152
Forskolin	Sigma, # F6886
Fura2-AM	Invitrogen, # F-1201
Glucose	Sigma, # G7021
Glycerol	Sigma, # G8773
Glycine	Roth, # 3908.3
Hematoxylin	Fluka # 51260
HEPES	Sigma, # H4034
Hydrochloride acid 37 %	Sigma, # 84422
^{125}I-cyanopindolol	Perkin Elmer, Inc. # NEX189100UC
ICI-118.551 hydrochloride	Sigma, # I127
Iron(III) chloride hexahydrate	Roth, # P742.1
3-Isobutyl-1-methylxanthin	Applichem, # A0695
Isoproterenol hydrochloride	Sigma, # I6504
Laminin	Sigma, # L2020
LB- Agar powder Miller	Applichem, # A0927
LB- Medium powder Miller	Applichem, # A0954
Lipofectamine® 2000 Reagent	Invitrogen, #11668-019
Loading buffer DNA IV (for Agarose gels)	Applichem, # A3481
Magnesium chloride hexahydrate	Applichem, # A1036
Magnesium sulfate heptahydrate	Sigma, # M2773
MDL-12,330A hydrochloride	Sigma, # M182
Methanol	Roth, # HN41.2

Description	*Company*
8-methoxymethyl-3-isobutyl-1-methylxanthine	Sigma, # M2547
Milk powder	Roth, # T145.1
N,*N*,*N*′ ,*N*′ -Tetramethylethylenediamine	Sigma, # T9281
peqGOLD Universal Agarose	Peqlab, # 35-1020
PhosStop	Roche, # 04906837001
Ponceau S	Sigma, # P3504
Potassium bicarbonate	Sigma, # P7682
Potassium chloride	Sigma, # P5405
Potassium dihydrogen phosphate	Merck, # 4873
RNAse free water	Ambion, # AM9937
Phenol red sodium salt	Sigma, # P5530
Protease Inhibitor Cocktail	Roche, # 11872580001
Protein Marker V	Peqlab, #27-2211
Quick-Load® 100bp DNA ladder	Biolabs, # NO467S
Quick load® 1 kb DNA ladder	Biolabs, # NO468S
Rolipram	Sigma, # R6520
Roticlear®	Roth, # A538.5
Roti-Histofix® 4%	Roth, # P087.5
Rotiphorese® Gel 30	Roth, # 3029.1
Sodium azide	Sigma, # S2002
Sodium bicarbonate	Sigma, # S5761
Sodium chloride	Sigma, # S5886
Sodium dodecyl sulfate solution 20%	Fluka, # 05030
Sodium hydroxide	Roth, # 6771.3
Sodium phosphate dibasic	Sigma, # 255793
Sodium phosphate dibasic dihydrate	Sigma, # 71643
Sucrose	Sigma, # S0389
TAE-buffer (50x)	Applichem, # A1691
Target Retrieval Solution, Citrate pH=6 (10x)	Dako, # S2369
Taurine	Sigma, # T8691
TRIS	Roth, # 4855.3
Triton-X® 100	Applichem, # A1287.0025
Tween-20®	Sigma, # P1379
Vectashield® Mounting Medium	Vector Laboratories, # H-1000
Lectin from Triticum vulgaris (wheat)	Sigma, # L5266

3.1.7 Cell culture

Description	*Company*
Antibiotic-Antimycotic, 100x	Gibco, # 15240062
DMEM, 4.5 % glucose	Biochrom, # F0445
FCS	Biochrom, # S0615
Glutamine	Biochrom, # K0283
Iscove Basal Medium	Biochrom, # FG 0465
OPTI-MEM®	Gibco, # 11058
PBS Phosphate Buffered Saline (Dulbecco)	Biochrom, # L1825
Penicillin/Streptomycin	Biochrom, # A2213
Plaque GP Agarose	Biozym, # 850110
Trypsin/EDTA solution	Biochrom, # L2143

3.1.8 Enzymes and Kits

BamHI	New England Biolabs, # R0136
EcoRI	New England Biolabs, # R0101
KpnI	New England Biolabs, # R0142
XbaI	New England Biolabs, # R0145
XhoI	New England Biolabs, # R0146
GoTaq DNA Polymerase, 500U	Promega, # M3175
KpnI	New England Biolabs, # R3142
Liberase DH	Roche, # 05401054001
NotI	New England Biolabs, # R3189
PacI	New England Biolabs, # R0547
Pfu DNA Polymerase	Promega, # M774B
Pierce BCA Protein Assay Kit	Thermo Scientific, # 23227
Plasmid Midi Kit	Qiagen, # 12945
Plasmid Mini Kit	Qiagen, # 12125
Proteinase K	Applichem, # A3830-0500
QIAquick Gel Extraction Kit	Qiagen, # 28704
QIAquick PCR purification Kit	Qiagen, # 28104
Qproteome Cell compartment Kit	Qiagen, # 37502
Sodiumacetate solution 3M	Applichem. # 3947
Super Signal West Pico Chemiluminescent Substrate	Thermo Scientific, # 34080
SYBR® Green Super Mix for iQ™	Quanta Biosciences, # 95053
T4 DNA Ligase	NEB, # M0202S
Trypsin 2.5 %	Gibco #15090
XbaI	New England Biolabs, # R0145
XhoI	New England Biolabs, # R0146

3.1.9 Primary Antibodies

Description	*Company*
anti-α-actinin	Sigma, # A7811
anti-β-arrestin 2	Santa Cruz, # sc-13140
anti-Calsequestrin	Thermo Scientific, # PA1-913
anti-GAPDH	HyTest Ltd, **#** 5G4
anti-PDE2A	Fabgennix, # 101AP
anti-PDE2A	Santa Cruz, # sc-17228
anti-PDE3A	Santa Cruz, # sc-11834
anti-PDE4D8	home made (Marco Conti)
anti-PDE8A	home made (George Baillie)
anti-pPLN (Phospho Serine 16)	Badrilla, # A010-12
anti-pTnI (Phospho Serine 23/24)	Cell Signaling, # 4004

3.1.10 Secondary Antibodies

Alexa Fluor® 488 Goat Anti-Mouse IgG	Invitrogen, # A11055
Alexa Fluor® 633 Goat Anti-Rabbit IgG	Invitrogen, # A21070
Immun-Star™ Goat Anti-Mouse (GAM)-HRP Conjugate	Biorad, # 170-5047
Immun-Star™ Goat Anti-Rabbit (GAR)-HRP Conjugate	Biorad, # 170-5046

3.1.11 Technical devices and software for fluorescence microscopy

Arduino I/O board	Sparkfun Electronics
Attofluor® cell chamber	Invitrogen
AxioObserver A1 epifluorescence microscope	Carl Zeiss MicroImaging
AxioCam ICc1	Carl Zeiss MicroImaging
Axiovert 200 microscope	Carl Zeiss MicroImaging
Axio Vision software	Carl Zeiss MicroImaging
CFP/YFP filter set	Chroma Technology
CoolLED 440 nm	CoolLED
CoolSNAP-HQ CCD-camera	Visitron Systems
DualView filter slider	Photometrics
DV2 DualView (505dcxr filter)	Photometrics
ImageJ Software	National Institutes of Health
Inverted fluorescent microscope	Nikon
710 NLO microscope	Carl Zeiss MicroImaging
Microsoft Office Picture Manager	Microsoft Corporation
Oil immersion 63x objective	Carl Zeiss MicroImaging
ORCA-03G camera	Hamamatsu Photonics
Polychrome V light source	TILLPhotonics
Stemi 2000-C microscope binocular	Carl Zeiss MicroImaging

Description	*Company*
ZEN 2010 Software	Carl Zeiss MicroImaging

3.1.12 Technical devices and software for cardiomyocyte contractility measurements

Fluorescence System Interface	IonOptix
IonWizard- Core and Analysis	IonOptix
MyoCam-S	IonOptix
MyoPacer Cell Stimulator	IonOptix
Sarcomere Length Acquisition Module	IonOptix

3.1.13 Other technical devices and software

AlphaImager® software	ProteinSimple
Binocular macroscope	Olympus
Biotek Reader (for BCA assay)	BIOTEK Instruments
Chart5™ Software	ADInstruments
Centrifuges	Thermo Scientific
iCycler	Biorad
MicroBeta^2	Perkin Elmer, Inc.
MicroBeta^2 Windows Workstation	Perkin Elmer, Inc.
Microtom Leica RM 2165	Leica
Mini-PROTEAN® Electrophoresis System	Biorad
MS-400 MicroScan Transducer	Linear Array Technology
MS-Excel™	Microsoft®
MS-PowerPoint™	Microsoft®
MS-Word™	Microsoft®
MultiImage Light Cabinet	Alpha Innotech Corporation
Mupid-One Gel Electrophoresis Unit	ADVANCE Co., Ltd.
NanoDrop 2000	Thermo Scientific
Origin 8.5G Software	OriginLab® Corporation
pH meter	Inolab
Powerpac HC	Biorad
Thermocycler	Sensoquest
ThermoMix compact	Eppendorf
Tracheal tube	Hugo Sachs Electronic
Ultracentrifuge L-70	Beckman
Ultra-Turrax MicraD-1	Art-Labortechnik
Vevo 2100	VisualSonics (Toronto, Canada)
Ventilator Minivent	Hugo Sachs Electronic

Description	*Company*
X-Ray Film processor SRX 101A	Konica

3.1.14 Other Materials

Elca®med	Asid Bonz GmbH
Eppendorf tubes	Eppendorf
Ethilon suture 9-0	Ethicon
Falcon tubes	BD Falcon
Fiber pads for Western blot	Bio Rad, #1703933
Filter Unit 0.2 RC Spartan 13 0.2 µm (DNA filtration)	Whatman, # 10463040
Forene®	Abbott
21-gauge needle	BD Microlane
26-gauge needle	BD Microlane
Gauze	Th Geyer, # 9.068291
Round Glass Cover Slides, ø 24 mm	Thermo Scientific, #004710781
Microscope Slides	Thermo Scientific, # J1800AMNZ
Medical X-Ray Film	Fujifilm, # 4014403
Prolene suture 6-0	Ethicon
Protran Nitrocellulose Transfer Membrane	Whatman, # 4018650
Quickseal Centrifuge Tubes (virus centrifugation)	Beckmann, # 342413
Scintilation Liquid Lumasafe Plus	Lumac LSC, # 3097
Serological pipettes	Sarstedt
Slide-A-Lyzer Dialysis Cassettes, 10K MWCO	Thermo Scientific, # 66383 0.5ml
Spacer Plates for Western blot	Bio Rad, #1653311
Steriflips	Millipore, # SCGP00525
Short Plates for Western blot	Bio Rad, #1653308
Temgesic®	Essex Pharma GmbH
U-40 Insulin 30Gx1/2	Braun, # 40012525
U-40 Insulin Omnifix Solo	Braun, # 9161309v
Water bath	Julabo
6 Well Plates	Starlab, # CC7682-7506
6-0 polyviolene suture	Harvard Apparatus
96 Well Plates	Nunc, # 167008
96 Well Plates for MicroBeta^2	Perkin Elmer, Inc. #1450-401

3.1.15 Buffers and solutions

All buffers were prepared in deionized H_2O, if not indicated otherwise

Description	*Composition*	
Plasmid dialysis		
TE Buffer	Tris, 1 M, pH 7.4	5 ml
	EDTA, 0.5 M, pH 8	0.2 ml
	Ampuwa®	1000 ml
***E.coli* transformation**		
5x KCM buffer	$CaCl_2$	150 mM
	$MgCl_2$	250 mM
	KCL	500 mM
LB medium	LB medium powder	25 g/l
	dH_2O ad 1000 ml	
	Autoclave, cool down to 50°C	
	add Ampicillin	100 µg/ml
LB plates	LB agar powder	40 g/l
	dH_2O ad 1000 ml	
	Autoclave, cool down to 50°C	
	add Ampicillin	100 µg/ml
HEK293A Cell Transfection		
2x BBS	Na_2HPO4	1.5 mM
	BES	50 mM
	NaCl	280 mM
	pH	6.95
$CaCl_2$	$CaCl_2$	2.5 M

Description	*Composition*	
Cardiomyocyte Isolation		
Stock Buffer 10x	NaCl	1.13 M
	KCL	47 mM
	KH_2PO_4	6 mM
	$Na_2HPO4x2H_2O$	6 mM
	$MgSO_4x7H_2O$	12 mM
	Phenol red	0.32 mM
	$NaHCO_3$	120 mM
	$KHCO_3$	100 mM
	HEPES	100 mM
	Taurine	300 mM
Perfusion Buffer 1x *sterile filtrate*	Stock Buffer 10x	10 ml
	BDM solution	2 ml
	Glucose	100 mg
	dH_2O	
BDM Solution	BDM	500 mM
BSA Solution	BSA	10 % (w/v)
$CaCl_2$ Solution 100mM	$CaCl_2$	100 mM
$CaCl_2$ Solution 10 mM	$CaCl_2$	10 mM
Liberase DH Solution	Liberase DH	50 mg
	dH_2O (injection grade)	12 ml
Digestion Buffer	Perfusion Buffer 1x	26 ml
	$CaCl_2$ solution, 100 mM	3.75 µl
	Trypsin 2.5 %	200 µl
	Liberase DH Solution	300 µl
Stopping Buffer 1	Perfusion Buffer 1x	2.25 ml
	BSA Solution	250 µl
	$CaCl_2$ Solution 100 mM	1.25 µl
Stopping Buffer 2	Perfusion Buffer 1x	9.5 ml
	BSA Solution	500 µl
	$CaCl_2$ Solution 100 mM	3.75 µl

Description	*Composition*	
Tyrodes		
FRET tyrode	NaCl	144 mM
	KCl	5.4 mM
	$MgCl_2$	1 mM
	$CaCl_2$	1 mM
	HEPES	10 mM
	pH	7.3
ION Optix tyrode	NaCl	149 mM
	KCl	1 mM
	$MgCl_2$	1 mM
	HEPES	5 mM
	Glucose	10 mM
	$CaCl_2$	1 mM
	pH	7.54
Langendorff tyrode	NaCl	118 mM
(Krebs-Henseleit buffer)	KCl	4.7 mM
	KH_2PO_4	1.2 mM
	$MgSO_4$	1.25 mM
	$NaHCO_3$	24 mM
	$CaCl_2$	1.25 mM
	glucose	11 mM
Immunoblot Solutions		
Homogenization Buffer	HEPES	10 mM
	Succrose	300 mM
	NaCl	150 mM
	EGTA	1 mM
	$CaCl_2$	2 mM
	Triton X 100	10 %
	pH	7.4
	10 ml + PhosStop and Protease Inhibitor Cocktail, 1 tablet each	
SDS Stop 3x	Tris	200 mM
	SDS	6 % (v/v)
	Glycerol	15 % (v/v)
	Bromphenol Blue	
	β-Mercapthoethanol	10 % (v/v)
	pH	6.7

Description	*Composition*	
4x Tris/SDS pH 6.8	Tris	500 mM
	SDS	0.4 % (v/v)
	pH	6.8
4x Tris/SDS pH 8.8	Tris	1.5 M
	SDS	0.4 % (v/v)
	pH	8.8
APS solution	APS	10 % (w/v)
10x SDS Running Buffer	Tris	250 mM
	Glycine	1.9 M
	SDS	1 % (v/v)
	pH	8.3
Stock Transfer Buffer 10x	Tris	325 mM
	Glycine	1.9 M
Transfer Buffer 1x	Stock Transfer Buffer 10x	10 % (v/v)
	Methanol	20 % (v/v)
Ponceau S Solution	Ponceau S in 10% acetic acid	0.5 % (w/v)
Stock TBS Buffer 10x	Tris	100 mM
	NaCl	1.5 M
	pH	7.5 (HCl)
TBS-Tween	Stock TBS Buffer 10x	10 % (v/v)
	Tween 20	0.1 % (v/v)
Stacking Gel (3.8 ml; 2Gels)	Acrylamide	500 µl
	4x Tris/SDS pH 6.8	940 µl
	dH_2O	2.31 ml
	10% APS	18.8 µl
	TEMED	7.5 µl
Separating Gel 10 % (12 ml; 2 Gels)	Acrylamide	4 ml
	4x Tris/SDS pH 8.8	3 ml
	dH_2O	5 ml
	10 % APS	48 µl
	TEMED	18 µL

Description	*Composition*	
Separating Gel 15 %	Acrylamide	6 ml
(12 ml; 2 Gels)	4x Tris/SDS pH 8.8	3 ml
	dH_2O	3 ml
	10 % APS	48 µl
	TEMED	18 µL
PDE Activity Assay		
Wash Buffer	Tris	40 mM
	pH	8.0 (HCl)
Homogenation Buffer	Wash Buffer	10 ml
	$MgCl_2$	10 mM
	PhosStop	1 tablet
	Protease Inhibitor Cocktail	1 tablet
cAMP Stock Solution	cAMP	1 mM
BSA Stock Solution	BSA	10 % (w/v)
[^{3}H]cAMP Stock Solution	[^{3}H]cAMP	1mCi/ml
Ready-To-Use Reaction Buffer	$MgCl_2$	10 mM
	β-Mercaptoethanol	10 mM
	cAMP	2 µM
	BSA	1.5 % (w/v)
	[^{3}H]cAMP in Wash Buffer	2.5 µl/ml
Stop Solution	EDTA	15 mM
	pH in Wash Buffer	8.0 (NaOH)
Venom	Snake Venom	1mg/ml
Immunostaining		
Blocking buffer	FCS	10 % (v/v)
	Triton-X® 100 in PBS	0.1 % (v/v)

3.2 Methods

3.2.1 Cloning and transgenic mouse generation

A. pmEpac1 cloning:

For generation of pmEpac1, the Epac1-CNBD (cyclic nucleotide-binding domain) sequence was excised out of the Epac1-camps plasmid[36] (pcDNA3.0) using EcoRI and XbaI. Same restriction sites were used to remove the Epac2-CNBD sequence from the pmEpac2 construct[145]. The Epac1-CNBD sequence was then ligated into the cut open pmEpac2-construct to achieve pmEpac1.

B. αMHC subcloning

1. pmYFP was excised out of the new pmEpac1 construct with KpnI and EcoRI and subsequently PCR amplified using *pmYFPKpnIfor* and *pmYFPKpnIfor* primers to achieve KpnI and EcoRI restriction sites at the same time increasing expression efficiency due to a loss of 11 b.p. upstream of pmYFP start codon. PCR products were digested with KpnI and EcoRI to achieve "sticky ends"
2. Epac1-CFP was cut out of the pmEpac1 construct by EcoRI and XhoI.
3. αMHC-HCN2 vector containing simian virus polyadenylation signal (SV40)[37] was cut with KpnI and XhoI to remove the HCN2 sensor construct.

pmYFP (KpnI/EcoRI), Epac1-CFP (EcoRI/XhoI) and αMHC vector (KpnI/XhoI) were then triple-ligated to achieve the αMHC-pmEpac1 construct.

C. πcDNA3.0 transcloning

For expression control in HEK293 cells, pmEpac1 was excised out of the αMHC vector using KpnI and XhoI and pasted into pcDNA3.0 vector using identical restriction sites.

D. Epac1-camps-PDE1A cloning

To generate Epac1-camps-PDE1A, the mouse PDE1A sequence was fused in frame to the C-terminus of Epac1-camps via BamHI restriction site and a helical linker MPLVDFFC.

Epac1-PDE4A1[146] construct served as vector:

1. PDE4A1 was excised with BamHI und XhoI.
2. Murine PDE1A Sequence was PCR amplified using *PDE1ABamHIfor* and *PDE1AXhoIstoprev* primers to achieve BamHI and XhoI restriction sites.
3. Thus amplified PDE1A sequence was then ligated into cut open Epac1-camps-PDE4A1 vector.

Cloning PCR reaction mix:

10x Pfu reaction buffer	10 µl
10 mM desoxyribonucleotide triphosphates mix (dNTPs)	2 µl
forward primer	2.5 µl 10 pmol/µl (final conc. 25 µM)
reverse primer	2.5 µl 10 pmol/µl (final conc. 25 µM)
template cDNA	100–300 ng
Pfu polymerase	1 µl
ddH_2O	ad 100 µL

Cloning-PCR reaction protocol:

94°C	5 min		
94°C	30 sec	⎫	
55°C	30 sec	⎬	30x
72°C	1 min	⎭	
72°C	7 min		

Digestion protocol:

Standard digestion was carried out overnight at 37°C:

7 µg plasmid DNA (or 49.5 µl of the Qiaquick purified PCR product)
2.5 µl Restriction Enzyme 1
2.5 µl Restriction Enzyme2
5 µl 10 x Buffer 4
0.5 µl 100x BSA
ddH_2O ad 50 µl

Ligation protocol

Ligation of the digested fragments and vector was performed in a reaction using T4 ligase over night (o.n.) at 14°C:

αMHC vector	(KpnI/XhoI-Fragment)	1 µl	(25 ng)
pmYFP	(EcoRI/KpnI-Fragment)	4.5 µl	(125 ng)
Epac-CFP	(EcoRI/XhoI-Fragment)	7 µl	(125 ng)
T4 Ligase buffer 10x		1.5 µl	
T4 Ligase		1 µl	

For plasmid amplification, E. coli TOP10 (competence 1x10^9 cfu/µg DNA) were transformed with ligation mix, using the following reaction mix:

E.coli TOP10	100 µl
Ligation Mix	15 µl
H_2O	65 µl
5x KCM Buffer	20 µl

For microinjections, the pmEpac1 construct was linearized using SpeI for overnight digestion at 37°C:

50 µg DNA
10 µl SpeI
20 µl Buffer 4
2 µl 100x BSA
H_2O ad 200 µl

The linearized construct was purified on a 1 % Agarose gel, extracted using the Qiaquick Gel extraction Kit and eluted with 100 µl of sterile TE buffer.

After filtration of the linearized and purified αMHC-pmEpac1 construct through a 2 µm filter under sterile conditions, the DNA was transferred into a sterile dialysis chamber (Slide-A-Lyzer). Dialysis was performed in 500 ml TE buffer which was exchanged every 4 hours (overall 2 l TE buffer). The dialysis chamber was unloaded under sterile conditions and DNA concentration was measured using a Nanodrop device. A concentration of 1-5 ng/µl was considered sufficient for pronuclear microinjection.

The pronuclear microinjection of FVB/N mice with the αMHC-pmEpac1 construct was performed as previously described[147]. Microinjections were carried out by Dr. Ursula Fünfschilling and co-workers (Transgenic Core Facility of the Max-Planck Institute for Experimental Medicine, Göttingen, Germany).

The resultant founder mice and their heterozygous offspring were genotyped by a standard PCR resulting in a ~365 bp fragment on a gel. In brief, tail biopsies were digested overnight in 200 µl DirectPCR-Tail supplemented with 500 µg/ ml Proteinase K at 55°C and 1000 rpm in a ThermoMixer. The reaction was terminated by boiling at 85°C for 45 min. After cooling down, tail lysates were directly used as a template for PCR amplification performed.

Genotyping-PCR reaction mix:

0.5	µl	Tail lysate
14.7	µl	H_2O
4.0	µl	5x GoTaq buffer
0.5	µl	dNTPs 10 mM
0.05	µl	MHCseqford primer, 100 pmol/µl
0.05	µl	YFPnewrev primer, 100 pmol/µl
0.2	µl	GoTaq Polymerase

Genotyping-PCR reaction protocol:

94°C	4 min	
94°C	30 sec	35x
62°C	30 sec	
72°C	50 sec	
72°C	7 min	

3.2.2 Cell culture and transfection

Day 0: HEK293A cells were cultured at 37°C and 5 % CO_2 in DMEM medium supplemented with 4.5 g/l glucose, 10 % FCS, 2 mM L-glutamine, 100 U/ml penicillin and 100 µg/ml streptomycin. For transfection with plasmid DNA, cells were plated onto 24 mm glass coverslips in 6-well plates.

Day 1: At about 60-70 % confluence, cells were transfected using the

Calcium-Phosphate method:

H_2O	440 µl
2.5 M $CaCl_2$	50 µl
Plasmid DNA (1 µg/µl)	10 µl
2x BBS	500 µl

After 10 min of incubation at RT, 166 µl of the reaction mix were added dropwise to each well.

To yield higher transfection efficiencies, e.g. for protein overexpression analyzes, cells were grown to 60-70% confluence in 15-cm cell culture dishes and transfected using the

Lipofection method:

1. Lipofectamine 2000® reagent:	Opti-Mem® Medium	455 µl
	Liopectamine 2000®	45 µl
2. DNA reagent:	Opti-Mem® Medium	490 µl
	DNA (1µl/µg)	10 µl

Lipofectamine 2000® and DNA reagents were mixed 1:1 and incubated at room temperature. After 20 minutes the reaction mix was dropwise pipetted onto the cells.

Day 2: 24-30 hours post transfection cells were e.g. subjected to FRET measurements.

3.2.3 Adult cardiomyocyte isolation

Mice were sacrificed by cervical dislocation. Hearts were rapidly explanted. In a petri dish with ice-cold PBS the aorta was mounted onto a blunted cannula (24-26-gauge) and subjected to retrograde perfusion (Langendorff perfusion). A constant flow rate of 3.5 ml was assessed using a peristaltic pump. The heart was perfused with *Perfusion Buffer 1x* for 3 minutes, followed by 8 minutes perfusion with *Digestion Buffer*.

Thereafter, the heart was removed from the perfusion apparatus and the ventricles were briefly cut into pieces. Digestion was slowed down by adding *Stopping Buffer 1* to the crude suspension, followed by homogenation with a 1ml-syringe without needle to detach single cardiomyocytes from the extra cellular matrix. The cell suspension was briefly filtered using gauze with a mesh diameter of 200 µm and left to settle for 10-15 minutes.

Sedimented cardiomyocytes were then transferred into *Stopping Buffer 2* and further subjected to re-calcification. Cellular calcium was increased in five steps to achieve a final concentration of 1mM, letting cells accommodate for 4 minutes, after each step.

Re-calcification protocol:

1.	50 µl *$CaCl_2$ Solution 10 mM*	=>	62 µM
2.	50 µl *$CaCl_2$ Solution 10 mM*	=>	112 µM
3.	100 µl *$CaCl_2$ Solution 10 mM*	=>	212 µM
4.	30 µl *$CaCl_2$ Solution 100 mM*	=>	500 µM
5.	50 µl *$CaCl_2$ Solution 100 mM*	=>	1000 µM

After recalcification, cardiomyocytes were either seeded onto laminated coverslides for functional studies, or subjected to e.g. *in vitro* stimulation prior to immunoblot analysis.

For immunoblot analysis cells were isolated as described, however re-calcification was carried out in BSA-free Stopping Buffer 2 to minimize excessive signal background due to unspecific antibody cross reactions with BSA. After re-calcification cells were quickly spun down (2.000 rpm for 2 minutes) and flash-frozen. For further sample preparation see *4.12 Immunoblot assay*.

3.2.4 FRET-based cAMP measurements in living cells

Freshly isolated cardiomyocytes were plated onto laminin-coated round glass cover slides. For FRET measurements, cover slides with adherent cells were mounted in an Attofluor microscopy chamber and maintained in FRET buffer. FRET recordings were performed using a homemade FRET microscopy system[148]. The donor fluorophore (CFP) was excited with a 440 nm blue-light beam at five-second intervals using a CoolLED single-wavelength light emitting diode. Simultaneously, the FRET emission was separated into CFP and YFP signals using a DualView beam splitter. Split emission signals were detected via a charge-coupled device (CCD) camera. Image acquisition was synchronized to the five-second light pulse intervals. After a stable baseline was reached, cells were challenged with different compounds e.g. ISO or PDE inhibitors diluted in the FRET buffer to stimulate cellular cAMP responses.

FRET recordings on HEK293A cells were performed in a similar way one-day post transfection.

Offline data analysis was carried out using Microsoft Excel and Origin 8.5G software.

Raw values of YFP and CFP emissions were fed into following equation:

FRET ratio = (YFP – 0.63 x CFP) / CFP

to correct for CFP bleedthrough into the YFP channel. 0.63 is the bleedthrough factor, which was assessed for the particular FRET microscopy setup used, prior to FRET measurements.

Changes in the FRET ratio were plotted against time in seconds to display the measured FRET traces, representing the time course of cellular/subcellular cAMP dynamics.

3.2.5 Single-cell contractility measurements

Freshly isolated cardiomyocytes were plated onto laminin-coated glass coverslides, mounted onto custom made measuring chambers. Contractile responses were evaluated by the optical sarcomere length measurement method (IonOptix) at 1 Hz pacing frequency using field stimulation of 20-40 V as previously described[149]. Similar to FRET recordings, cells were sequentially challenged with various compounds by pipetting, i.e. ISO and selective/unselective PDE inhibitors to stimulate contractility. Contractility recordings were offline analyzed using ION Wizard™ and Origin 8.5G software.

3.2.6 Heart rate measurements

Mice were sacrificed by cervical dislocation. Hearts were rapidly explanted and subjected to Langendorff perfusion (see *3.2.3 Adult cardiomyocyte isolation*) with the Krebs-Henseleit tyrode, oxygenated with 95% O_2 and 5% CO_2 at 37.5 °C with a constant flow rate of 3.5 ml/min. Hearts were placed in an organ bath with 37.5°C temperate Krebs-Henseleit tyrode and heart beats were detected using a custom made electrode. Heart rates

were amplified and online processed with Chart5™ Software. The perfusion setup consisted of a closed flow circuit (Figure 7). The tubing was insulated with double-walled glass pipes. The inner spaces of all pipes and containers (i.e. buffer container and organ bath) were filled with heating water and connected to a thermostated circulating water bath. The heating bath was set to 42°C to maintain a temperature of 37.5°C of the perfusate and at the organ bath. Stimulatory compounds were introduced sequentially. I.e. hearts were perfused for 3-5 minutes to reach stable heart rates and then stimulated with 10 nM ISO for 3-5 min. After reaching the plateau phase, 10 nM of atropine were additionally washed in for another 5 min. Electrocardiograms (ECGs) were offline analyzed using Chart5™ and Origin 8.5G software.

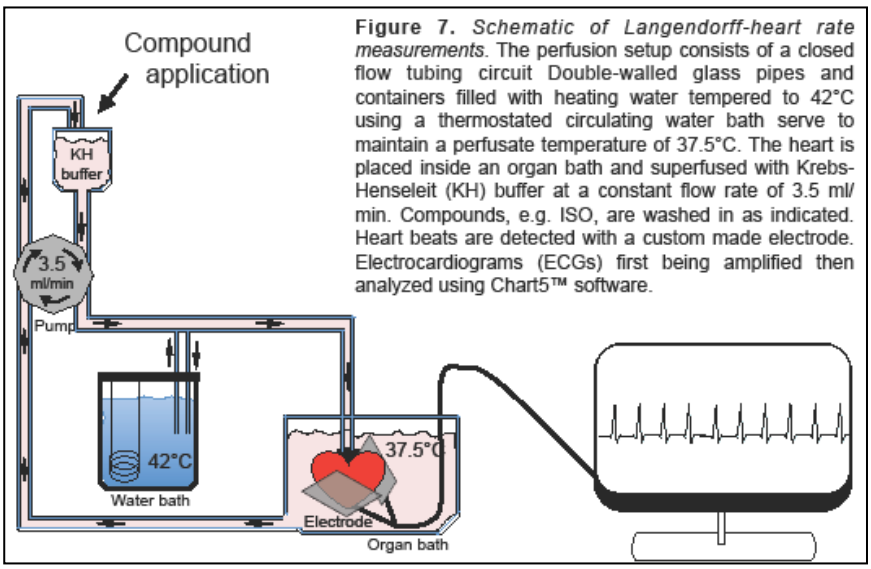

Figure 7. *Schematic of Langendorff-heart rate measurements.* The perfusion setup consists of a closed flow tubing circuit Double-walled glass pipes and containers filled with heating water tempered to 42°C using a thermostated circulating water bath serve to maintain a perfusate temperature of 37.5°C. The heart is placed inside an organ bath and superfused with Krebs-Henseleit (KH) buffer at a constant flow rate of 3.5 ml/ min. Compounds, e.g. ISO, are washed in as indicated. Heart beats are detected with a custom made electrode. Electrocardiograms (ECGs) first being amplified then analyzed using Chart5™ software.

3.2.7 Transverse aortic constriction (TAC)

9-13 week aged female mice were randomized into sham or TAC group. Mice were anesthetized using 1.5 - 2 % isoflurane in 100 % oxygen. A suprasternal incision was made, and the aortic arch was visualized using a binocular macroscope. TAC occurred by spacer defined (26-gauge) constriction using a 6-0 polyviolene suture between the first and second trunk of the aortic arch[150]. For sham, the aorta was exposed but not constricted. Doppler velocity was measured by a 20 MHz probe to quantify the pressure gradient across the TAC region or after sham procedure by transthoracic echocardiography. Mice were sacrificed 8 weeks after surgery for Langendorff heart rate recordings or ventricular cardiomyocyte isolation and subsequent single-cell measurements or biochemical assays. TAC surgeries and pressure gradient measurements were carried out by Dipl. Biol. Julia Steinbrecher (Department of Cardiology and Pulmonology, University Medical Centre Göttingen).

3.2.8 Histology, morphometric analysis and echocardiography

Histology

For histology and morphometric analysis, hearts were perfused with ice-cold PBS to remove blood and fixed in 4% Roti Histofix at 4°C overnight. The fixed hearts were paraffin embedded, and 5 µm heart cross sections were generated at a Microtome (Leica RM 2165). For the following applications, paraffin cross-sections were de-waxed in xylol (20 min twice) and rehydrated with 6 subsequent decreasing ethanol series (100 % - 25 %, 5 min each step) and with deionized dH_2O.

Hematoxylin-eosin staining

Hematoxylin-eosin (HE) staining of heart cross-sections was performed in the pathology department of the University Medical Center Göttingen using a standard HE staining protocol. In brief, cell nuclei were stained

thrice with hematoxylin (2 min each), and after 2 min washing the cytosol was stained twice using eosin (2 min each). After rehydration and mounting, heart cross-sections were analyzed using a Stemi 2000-C microscope binocular with associated AxioCam ICc1 and Axio Vision Software.

Wheat Germ Agglutinin staining

For cardiomyocyte dimension analysis, transverse heart sections were incubated with Wheat Germ Agglutinin (WGA, 75 µg/mL) for 30 min in the dark, washed thrice for 5 min with PBS, mounted and analyzed by microscopy. Images were analyzed with ImageJ software. The cell diameter was measured in 100 cells from 5 sections per heart.

Echocardiography

Prior to echocardiography, mouse weights were assessed. Echocardiography and analysis were performed in a double-blinded fashion by Kirsten Koschel, Sabrina Wollborn, Beate Knocke, Roland Blume and Marcel Zoremba (Department of Cardiology and Pulmonology, University Medical Centre Göttingen) as previously described[151,152]. Briefly, cardiac parameters, i.e. septum thickness, left ventricular enddiastolic diameter (LVEDD), left ventricular endsystolic diameter (LVESD), enddiastolic volume (EDV), endsystolic volume (ESV), heart frequency and heart weight were used to calculate functional values such as ejection fraction (EF) and fractional shortening (FS).

EF: blood volume the heart ejects per contraction (Calculations according to *Simpson et al., 1993*[152]).

$$EF = \frac{\quad}{\quad} \times 100$$

FS: pump function and shortening of the left ventricle during contraction.

$$FS = \frac{\quad}{\quad}$$

3.2.9 Confocal microscopy

Confocal microscopy was performed using Zeiss LSM 710 NLO microscope equipped with a Plan-Apochromat x63/1.40 oil-immersion objective.

Live staining: For live cell imaging, freshly isolated adult cardiomyocytes plated on class coverslides were incubated with the lipophilic fluorescent probe di-8-ANEPPS (50 µM, Molecular Probes®) for 10-15 minutes at room temperature in FRET buffer and subsequently subjected to confocal microscopy. Prior to microscopy, cells were washed once with FRET buffer at room temperature. Images were acquired for CFP/YFP (405 nm diode laser excitation), di-8-ANEPPS (488 nm argon ion laser excitation) and analyzed using ZEN 2010 software.

Immunostaining: For co-localization experiments, cells were fixed for 20 min with ice-cold ethanol at -20°C, washed and co-stained with mouse monoclonal anti-α-actinin antibody (Sigma) and either goat polyclonal anti-PDE2A (sc-17228, Santa Cruz) or goat polyclonal anti-PDE3A (sc-11834, Santa Cruz) antibodies, followed by the secondary anti-mouse Alexa 633 Fluor® and anti-goat Alexa 488 Fluor® antibodies (A-21063 and A-11055, respectively, Life Technologies). Images were taken and automatically analyzed using the ZEN 2010 software to calculate the Pearson's coefficient which shows the degree of co-localization. See below for antibody dilutions:

Antibody (source)	Dilution
Anti-α-actinin (mouse)	1: 300
Anti-PDE2A (goat)	1: 100

Anti-PDE3A (goat)	1: 100

3.2.10 Radioligand binding

Radioligand binding studies were performed by Christian Dees (Institute of Pharmacology and Toxicology, University Würzburg), as previously described[153]. Briefly, isolated cardiomyocyte cell membranes were incubated in the assay buffer containing 5 mM Tris, pH 7.4 for 1 h at 30°C with 60-100 pM ^{125}I-cyanopindolol and increasing concentrations of ICI118551. Thereafter, samples were filtered through GF/F glass fiber filters (Millipore, Schwalbach, Germany), washed twice, and the filter-bound radioactivity was quantified using a scintillation counter.

3.2.11 Phosphodiesterase activity assay

Freshly isolated cardiomyocytes were prepared for *in vitro* measurement of cAMP-PDE hydrolyzing activity following the two-step method by Thompson and Appleman[154,155].

Isolated cardiomyocytes were left to sediment in Stop buffer I (see *3.2.3 Adult cardiomyocyte isolation*), washed once with PDE-Assay Wash Buffer and sonicated in 500 µL of ice-cold PDE-Assay Homogenization Buffer. Protein concentrations were quantified using BCA Protein Assay. 30 µg of total protein were set to a total volume of 200 µl PDE-Assay Homogenation Buffer containing selective PDE inhibitors. Contributions of individual PDE families were calculated from the effects of 100 nM BAY (PDE2), 10 µM cilostamide (PDE3), 10 µM rolipram (PDE4), and 100 µM IBMX (unselective inhibitor).

Step I: cAMP -> 5'-AMP:

For cAMP breakdown, each sample was incubated with 200 µL PDE-Assay Ready-To-Use Reaction Buffer containing 1 µM cAMP and 2nM [^{3}H]cAMP (1:500 ratio) as a substrate, for 10 minutes at 33°C. Reaction was terminated by adding 200 µL Stop solution and boiling for 1 minute at 95°C.

Step II: 5'-AMP -> P_i + adenosine:

Heat inactivated samples were incubated with 50 µg of 5'-nucleotidase-containing snake venom (*Crotalus atrox*) for 20 minutes at 33°C to hydrolyze 5'-AMP. The samples were loaded onto self-made columns containing 50 mg AG1-X8 resin for anion exchange chromatography to bind non-hydrolyzed [^{3}H]cAMP, thereby separating it from cleaved [^{3}H]adenosine. Quantification of cleaved [^{3}H]adenosine was performed by scintillation counting (MicroBeta^2) in a 96 well format. Data were collected with the MicroBeta^2 Windows Workstation.

3.2.12 Immunoblot assay

For samples preparation, freshly isolated cardiomyocytes were shock frozen and homogenized using a 1ml-syringe with needle. Proteins were quantified using BCA Protein Assay. Samples were generally boiled at 70°C for 10 minutes or at 95°C for 5 minutes, respectively, if not indicated differently.

10-50 µg of total protein per lane were subjected to 10 or 15 % SDS-PAGE modified from Laemmli (1979)[156] followed by immunoblot analysis according to Towbin et al. (1979)[157].

Primary antibodies used, were prepared in TBS-Tween with 1, 3 or 5 % of either low fat milk or BSA,
as depicted below. If not indicated differently, incubation proceeded at 4°C o.n.:

Antibody (source)	Blocking reagent / dilution	Comments
Anti-beta-Arrestin 2 (goat)	5 % milk / 1:1000	-
Anti-Calsequestrin (rabbit)	3 % BSA / 1: 5000	-
Anti-GAPDH (mouse)	5 % milk / 1:80000	4°C, 1 hour
Anti-PDE2A (rabbit)	3 % BSA / 1:750	-
Anti-PDE4D8 (rabbit)	5 % BSA / 1:2000	Blocked in 5 % milk
Anti-PDE8 (rabbit)	3 % BSA / 1:1000	-
Anti-pPLN (Phospho-Ser16) (rabbit)	5 % milk / 1:5000	-
Anti-pTnI (Phospho-Ser23/24) (rabbit)	5 % BSA / 1:1000	-

Secondary antibodies (Immun-Star™ Goat Anti-Mouse or Anti-Rabbit (GAM)-HRP Conjugate) were diluted 1:5000 in the same blocking reagent as used for primary antibody incubation.

Blots were scanned and analyzed densitometrically by ImageJ software for uncalibrated optical density.

3.2.13 Statistical analysis

Normal distribution was tested by the Kolmogorov-Smirnov test. Differences between experimental groups were analyzed using Origin 8.5G software and one-way ANOVA (for normally distributed values) or Mann-Whitney (for nonparametric datasets) tests at the significance level of 0.05, followed by Bonferroni's post-hoc test. Data are presented as means ± SE from the indicated number of independent experiments (animals and cells) per condition.

4 Results

4.1 Local β-Adrenergic Signaling at the Sarcolemma of Adult Mouse Cardiomyocytes

4.1.1 N-terminal fusion of Epac1-camps to an acylation substrate sequence promotes plasma membrane targeted expression

In 2002, Zacharias et al. demonstrated that expression of GFP-mutants in MDCK cells could be restricted to plasma membrane lipid rafts by fusing it to a 10 amino acid long SH4 domain of Lyn kinase containing a myristoylation/palmitoylation motif, MyrPalm (see *Methods, subsection 3.2.1, Cloning and transgenic mouse*

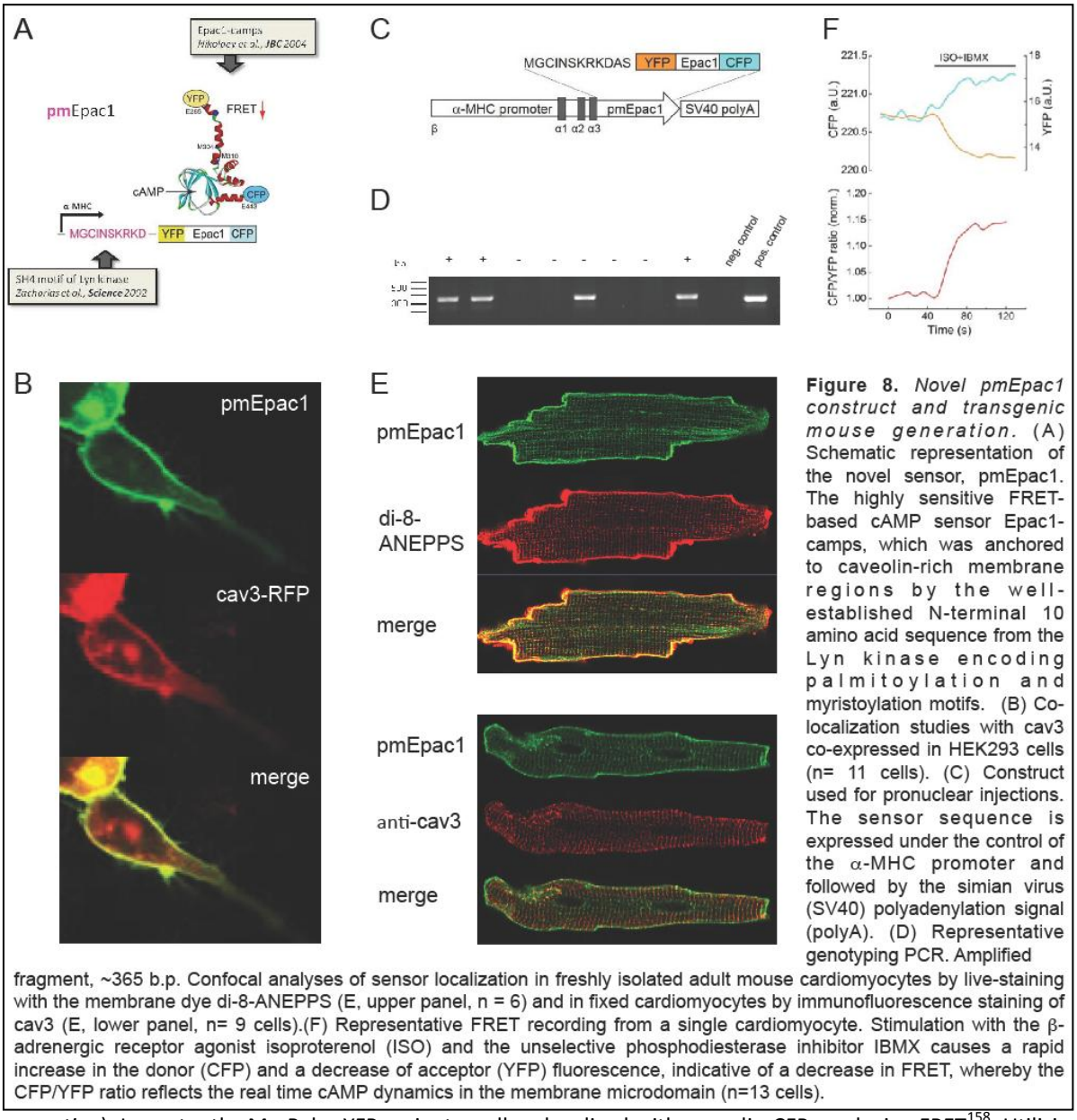

Figure 8. *Novel pmEpac1 construct and transgenic mouse generation.* (A) Schematic representation of the novel sensor, pmEpac1. The highly sensitive FRET-based cAMP sensor Epac1-camps, which was anchored to caveolin-rich membrane regions by the well-established N-terminal 10 amino acid sequence from the Lyn kinase encoding palmitoylation and myristoylation motifs. (B) Co-localization studies with cav3 co-expressed in HEK293 cells (n= 11 cells). (C) Construct used for pronuclear injections. The sensor sequence is expressed under the control of the α-MHC promoter and followed by the simian virus (SV40) polyadenylation signal (polyA). (D) Representative genotyping PCR. Amplified fragment, ~365 b.p. Confocal analyses of sensor localization in freshly isolated adult mouse cardiomyocytes by live-staining with the membrane dye di-8-ANEPPS (E, upper panel, n = 6) and in fixed cardiomyocytes by immunofluorescence staining of cav3 (E, lower panel, n= 9 cells).(F) Representative FRET recording from a single cardiomyocyte. Stimulation with the β-adrenergic receptor agonist isoproterenol (ISO) and the unselective phosphodiesterase inhibitor IBMX causes a rapid increase in the donor (CFP) and a decrease of acceptor (YFP) fluorescence, indicative of a decrease in FRET, whereby the CFP/YFP ratio reflects the real time cAMP dynamics in the membrane microdomain (n=13 cells).

generation). Importantly, MyrPalm-YFP variants well co-localized with caveolin-CFP producing FRET[158]. Utilizing

this strategy, Wachten et al.[145] later generated a MyrPalm-fused version of the Epac2-camps, thereby engineering the first membrane-targeted version of the cAMP FRET biosensor, pmEpac2 (pm = PalmMyr ⇔ plasma membrane). pmEpac1 was generated accordingly, using the pmEpac2 vector as a template and replacing the Epac2- by the Epac1-CNBD sequence. Transient co-expression of pmEpac1 with RFP-tagged cav3 in HEK293 cells confirmed their good co-localization at the plasma membrane (Figure 8A, B).

4.1.2 Heart-specific expression of pmEpac1 leads to localization at the sarcolemma of adult mouse cardiomyocytes (with T-tubular enrichment)

To drive transgene expression in a tissue-specific manner (in the myocardium), pmEpac1 was cloned into a construct containing the α-myosin heavy chain (αMHC) promoter[37]. For transgenic mouse generation, the linearized construct was purified, dialyzed and subjected to pronuclear injections into one-cell mouse embryos (Figure 8C).

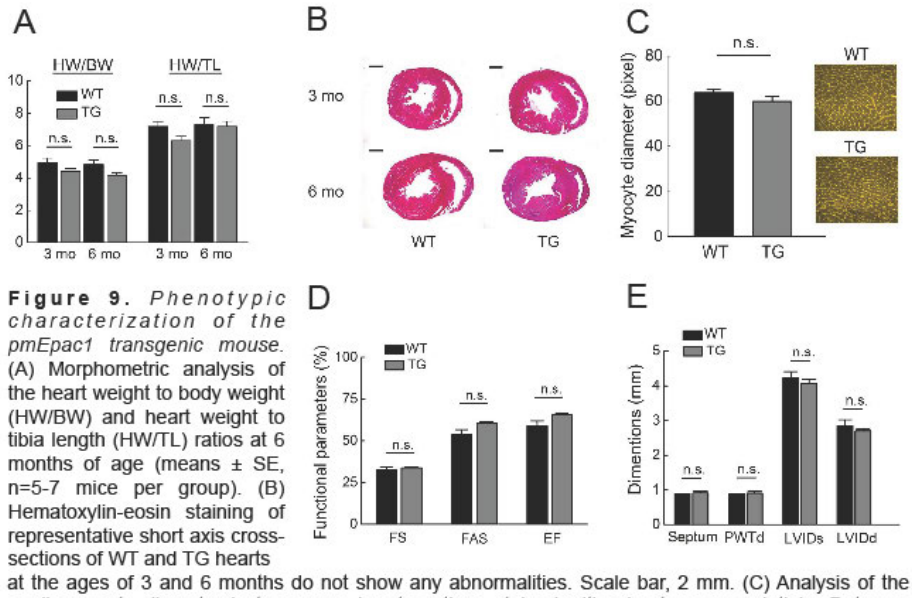

Figure 9. *Phenotypic characterization of the pmEpac1 transgenic mouse.* (A) Morphometric analysis of the heart weight to body weight (HW/BW) and heart weight to tibia length (HW/TL) ratios at 6 months of age (means ± SE, n=5-7 mice per group). (B) Hematoxylin-eosin staining of representative short axis cross-sections of WT and TG hearts at the ages of 3 and 6 months do not show any abnormalities. Scale bar, 2 mm. (C) Analysis of the cardiomyocyte diameter in transverse heart sections stained with wheat germ agglutinin. Data are means ± SE, from 4 WT and 5 TG hearts with 100 cells counted in each section. Functional parameters (D) and heart dimensions (E) measured at 6 months by echocardiography are not significantly different between wild type (WT) and transgenic (TG) littermates (n=5 mice). PWTd, posterior wall thickness in diastole; LVIDs, left ventricular inner dimension in systole; LVIDd, left ventricular inner dimension in diastole; FS, fractional shortening; FAS, fractional area shortening; EF, ejection fraction; n.s. – not significant.

Three injection rounds resulted in eight pmEpac1 positive heterozygous founder animals. However, only in the offspring from founder #113, over 95% of all isolated adult cardiomyocytes showed pmEpac1 expression, as determined by fluorescence microscopy. Therefore, the colony #113 was selected to generate a new pmEpac1 transgenic mouse line. Live stains of freshly isolated adult ventricular cardiomyocytes from line #113 with the unspecific lipophilic membrane dye di-8-ANEPPS and subsequent confocal imaging showed good co-localization of pmEpac1 with the sarcolemma, with local enrichment in T-tubular structures (Figure 8E, upper panel). Immunostaining of pmEpac1 cardiomyocytes with cav3-specific antibodies further indicated a preferable expression in caveolar structures (Figure 8E, lower panel). Importantly, stimulation of isolated cardiomyocytes with saturating concentrations of the beta-adrenergic agonist isoproterenol (ISO) together with the unspecific PDE inhibitor 3-Isobutyl-1-methylxanthin (IBMX) led to a clear change in FRET with good signal-to-noise ratio (Figure 8F).

4.1.3 Heart-specific expression of pmEpac1 does not affect normal cardiac function

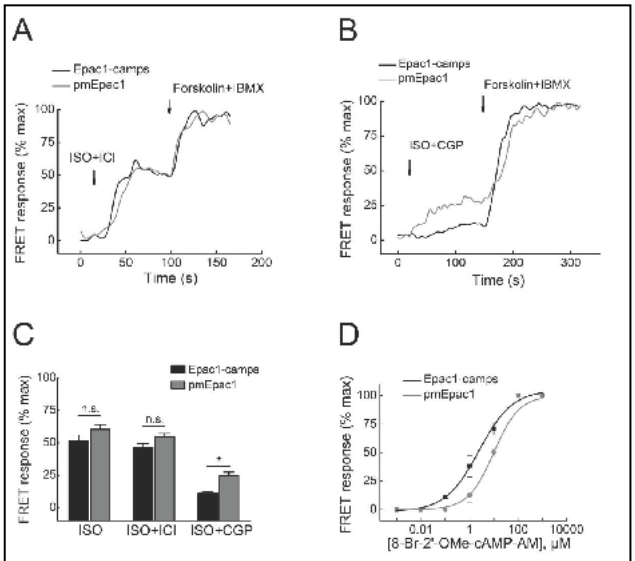

Figure 10. *pmEpac1 is particularly sensitive to the local β_2-AR-cAMP signals.* Representative single-cell FRET recordings with the cytosolic (Epac1-camps) and the membrane (pmEpac1) sensors. (A) Selective stimulation of β_1-AR with 100 nM of ISO plus 50 nM of the β_2-AR antagonist ICI118551 (ICI) leads to comparable cAMP signals from both sensors. Maximal stimulation was evoked by 10 µM forskolin plus 100 µM IBMX. (B) Selective β_2-AR stimulation with 100 nM ISO plus 100 nM of the β_1-AR blocker CGP20712A (CGP) induces a ~2-fold stronger response in the membrane microdomain. (C) Quantification of the FRET responses to ISO alone (stimulation of both β_1- and β_2-AR) and those shown in A and B, means ± SE, n = 10-12 cells isolated from 2 hearts per condition. * - significant difference at $p<0.05$, n.s. – not significant. The differences between ISO and β_1-AR responses are not significant. (D) Comparison of sensitivities between the two sensors using the previously established protocol. 13 Cells were pretreated with 100 µM MDL-12330A for 10 min to inhibit the basal adenylyl cyclase activity and titrated with increasing concentrations of the cell- permeable cAMP analogue 8-Br-2'-OMe-cAMP-AM. EC_{50} values were 3.0 ± 1.1 and 9.1 ± 1.1 µM for Epac1-camps and pmEpac1, respectively (means ± SE, n = 5-6 each). Similar to previously developed membrane-targeted version of the cAMP biosensor Epac2-camps, pmEpac1 shows 3-times lower affinity to cAMP than its parental cytosolic construct Epac1- camps. Epac1-camps myocytes were isolated from the previously developed transgenic mice.

To establish whether cardiac-specific pmEpac1-expression per se would affect normal heart function, pmEpac1 mice were compared to their wild type littermates in terms of heart and cardiomyocyte size, histology and *in vivo* cardiac contractility. For morphometric analysis, hearts explanted from mice aged three and six month, respectively were weighted and put into relation to either whole body weight or tibia length (Figure 9A). Further, cross-sections of transgenic and wild type hearts were subjected to hematoxylin and eosin staining to assess overall tissue morphology (Figure 9B). Last, diameter of isolated adult cardiomyocytes from pmEpac1-transgenic and wild type mice were determined after wheat-germ-agglutinin staining (Figure 9C). None of these parameters showed any difference between the transgenic mice and their wild type littermates, suggesting no alteration in heart morphology by transgene expression. To further investigate heart morphology and *in vivo* function, pmEpac1 transgenic mice and wild type littermates were subjected to echocardiography at the age of six months. Measured and calculated parameters included septum and diastolic posterior wall thickness (PWTd) as well as left-ventricular inner diameters in systole and diastole (LVIDs, LVIDd). In addition, functional parameters such as fractional shortening, fractional area shortening and ejection fraction (FS, FAS, EF) were also compared (Figure 9D,E). Changes in any of the above-mentioned parameters would indicate the presence of a pathological heart-phenotype. Importantly, none of these parameters were significantly changed in pmEpac1 versus wild type animals.

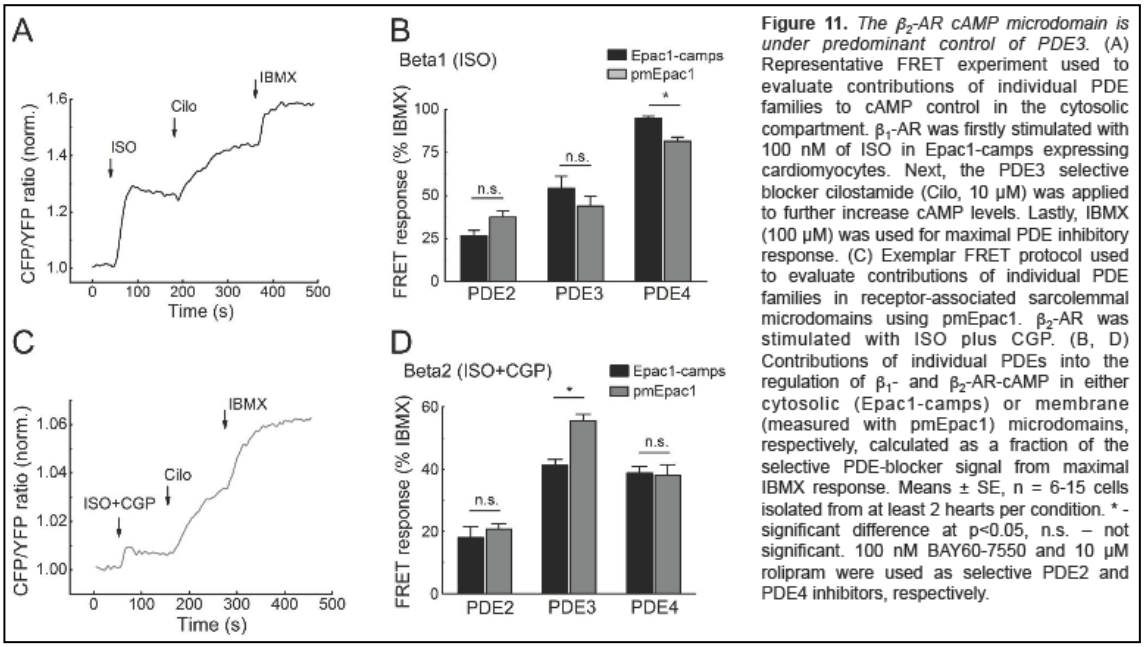

Figure 11. *The β_2-AR cAMP microdomain is under predominant control of PDE3.* (A) Representative FRET experiment used to evaluate contributions of individual PDE families to cAMP control in the cytosolic compartment. β_1-AR was firstly stimulated with 100 nM of ISO in Epac1-camps expressing cardiomyocytes. Next, the PDE3 selective blocker cilostamide (Cilo, 10 µM) was applied to further increase cAMP levels. Lastly, IBMX (100 µM) was used for maximal PDE inhibitory response. (C) Exemplar FRET protocol used to evaluate contributions of individual PDE families in receptor-associated sarcolemmal microdomains using pmEpac1. β_2-AR was stimulated with ISO plus CGP. (B, D) Contributions of individual PDEs into the regulation of β_1- and β_2-AR-cAMP in either cytosolic (Epac1-camps) or membrane (measured with pmEpac1) microdomains, respectively, calculated as a fraction of the selective PDE-blocker signal from maximal IBMX response. Means ± SE, n = 6-15 cells isolated from at least 2 hearts per condition. * - significant difference at $p<0.05$, n.s. – not significant. 100 nM BAY60-7550 and 10 µM rolipram were used as selective PDE2 and PDE4 inhibitors, respectively.

4.1.4 pmEpac1, compared to Epac1-camps, can particularly well resolve the β_2-AR/cAMP signals

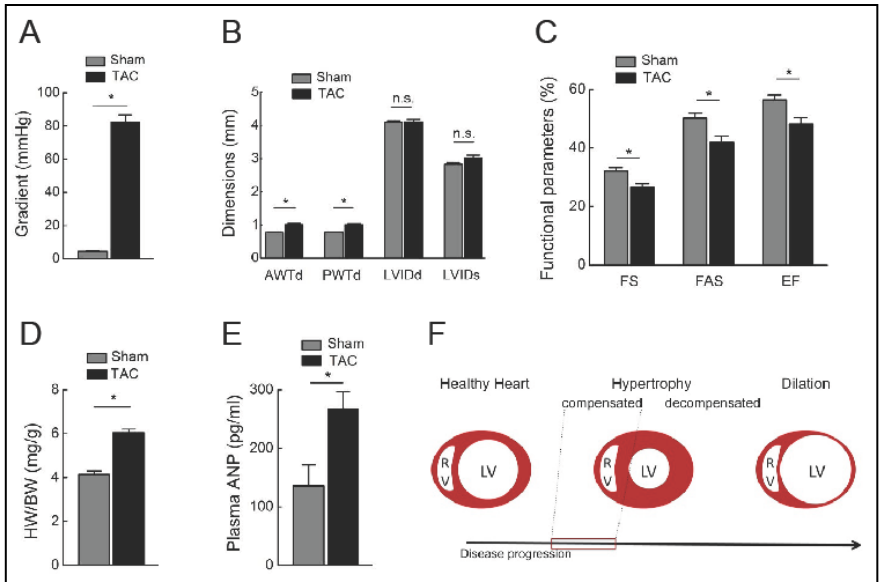

Figure 12. *Echocardiographic parameters of TAC compared to sham operated mice.* (A) Developed pressure gradients measured 3 days after aortic banding by Doppler-echocardiography, n=30-31 mice per group. Cardiac dimensions (B), functional parameters (C), and calculated HW/BW ratios (D) measured 7-8 weeks after surgery. Means ± SE, n=16-17 mice each. * - significant differences at $p<0.05$; n.s., not significant. AWTd, anterior wall thickness in diastole. (E), ANP plasma levels in representative TAC and sham mice measured by ELISA, n=4 each. * - significant difference at $p<0.05$. the morphology and functional values, were interpreted as a mild compensated hypertrophy phenotype, accounting for an early time point in progressive heart failure (F).

To analyze how sarcolemmal cAMP microdomains might differ from cytosolic cAMP pools in their real time dynamics, FRET data obtained from pmEpac1 expressing cardiomyocytes were compared side-by-side with those of the previously described cytosolic otherwise identical version of the same biosensor, Epac1-camps[36,46]. Concentration-response experiments with 8-Bromo-2'-O-methyladenosine-3',5'-cyclic monophosphate (8-Br-2'-O-Me-cAMP-AM), a membrane-permeable and non-PDE-hydrolyzable cAMP analog, revealed that targeted pmEpac1 showed slightly lower affinities to cAMP (Figure 10D). However, the membrane targeted sensor could more than two-fold better resolve local β_2-AR/cAMP signals (Figure 10B, C), which have previously been shown to be stringently compartmentalized close to T-tubular membranes[78]. In contrast, ISO and β_1-selective responses were not

significantly different when measured either in cardiomyocytes from pmEpac1 (sarcolemma) or from Epac1-camps (cytosol) transgenic mice, indicating that β_1-adrenergic stimulation is indeed coupled to a cAMP pool with far-reaching signal properties as previously described[31] (Figure10A, C). For calculations of β-AR cAMP signal proportions, β_1- and β_2-specific cAMP signals were set into relation to the maximal signal, achieved by addition of 10µM forskolin and 100µM IBMX.

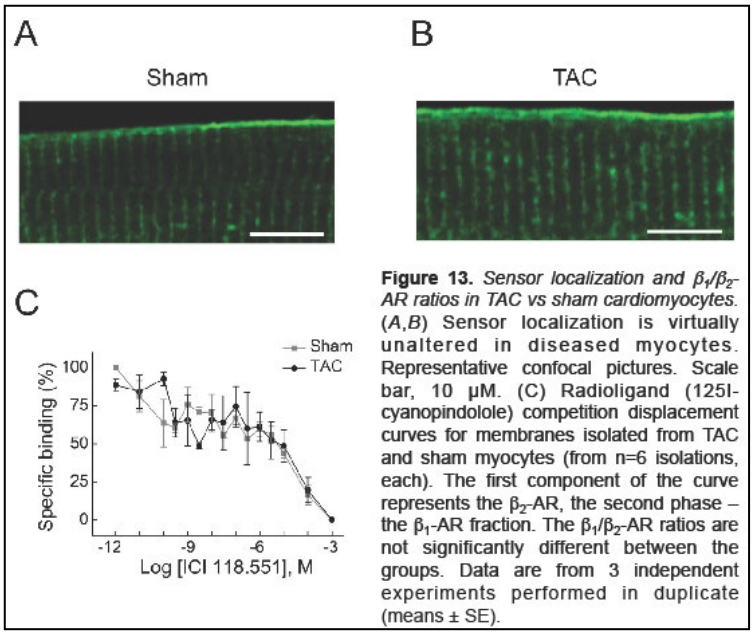

Figure 13. *Sensor localization and β_1/β_2-AR ratios in TAC vs sham cardiomyocytes.* (*A*,*B*) Sensor localization is virtually unaltered in diseased myocytes. Representative confocal pictures. Scale bar, 10 µM. (C) Radioligand (125I-cyanopindolole) competition displacement curves for membranes isolated from TAC and sham myocytes (from n=6 isolations, each). The first component of the curve represents the β_2-AR, the second phase – the β_1-AR fraction. The β_1/β_2-AR ratios are not significantly different between the groups. Data are from 3 independent experiments performed in duplicate (means ± SE).

To evaluate how receptor-subtype specific cAMP signals are controlled by PDEs in the cytosol vs. sarcolemmal receptor-associated cAMP microdomains, individual PDE profiles were measured in Epac1-camps1- and pmEpac1 expressing cardiomyocytes using selective PDE inhibitors applied after ISO stimulation with and without the β_1-AR-selective inhibitor CGP20712A. PDE-dependent regulation of the functionally relevant β_1-AR cAMP pool essentially showed the same hierarchical pattern of PDE4>>PDE3>PDE2 (Figure 11B), measured either in the cytosol (Epac1-camps) or at the sarcolemma (pmEpac1), further suggesting that the β_1-AR cAMP signals measured with pmEpac1-expressing cardiomyocytes were of the far-reaching nature. β_2-AR cAMP regulation, however, was much more different when monitored by the two differentially localized FRET probes, i.e. Epac1-camps and pmEpac1. Whereas a regulatory hierarchy of PDE4=PDE3>PDE2 was established when PDE contributions on β_2-AR cAMP were measured in Epac1-camps-expressing cardiomyocytes (cytosolic probe), in

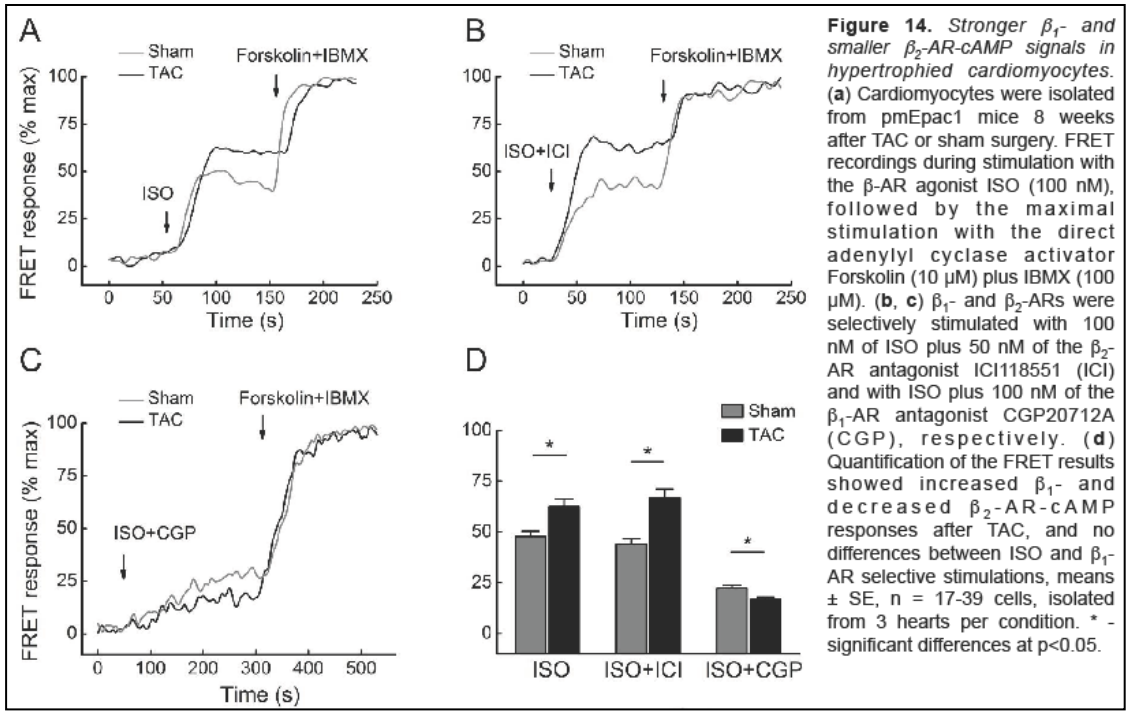

Figure 14. *Stronger β_1- and smaller β_2-AR-cAMP signals in hypertrophied cardiomyocytes.* (**a**) Cardiomyocytes were isolated from pmEpac1 mice 8 weeks after TAC or sham surgery. FRET recordings during stimulation with the β-AR agonist ISO (100 nM), followed by the maximal stimulation with the direct adenylyl cyclase activator Forskolin (10 µM) plus IBMX (100 µM). (**b**, **c**) β_1- and β_2-ARs were selectively stimulated with 100 nM of ISO plus 50 nM of the β_2-AR antagonist ICI118551 (ICI) and with ISO plus 100 nM of the β_1-AR antagonist CGP20712A (CGP), respectively. (**d**) Quantification of the FRET results showed increased β_1- and decreased β_2-AR-cAMP responses after TAC, and no differences between ISO and β_1-AR selective stimulations, means ± SE, n = 17-39 cells, isolated from 3 hearts per condition. * - significant differences at p<0.05.

pmEpac1-cardiomyocytes, PDE3 could be identified as the predominant regulator of the membrane-associated β_2-AR cAMP pool which can be expressed by the PDE regulation pattern PDE3>PDE4>PDE2 (Figure 11D).

4.1.5 FRET imaging reveals altered subtype-specific β-AR cAMP responses in diseased cardiomyocytes

In order to study local cAMP dynamics in early cardiac disease, TAC was performed in pmEpac1 mice to induce cardiac hypertrophy. 8 weeks post TAC, pmEpac1 mice showed substantially increased heart size and ventricular wall thickness with yet only a modest decline in cardiac output, indicative of a relatively mild, functionally still compensated phenotype of pathological hypertrophy, which was, however, accompanied by a two-fold increase of plasma ANP levels (Figure 12A-E). Importantly, in this relatively early pathological state, the localization of the FRET sensor in cardiomyocyte striation-associated T-tubular membranes and surface sarcolemma was virtually unchanged (Figure 13A, B). First, β_1- and β_2-AR specific responses were compared in cells isolated from TAC vs. sham-operated mice using analogous FRET protocols as shown in Figure

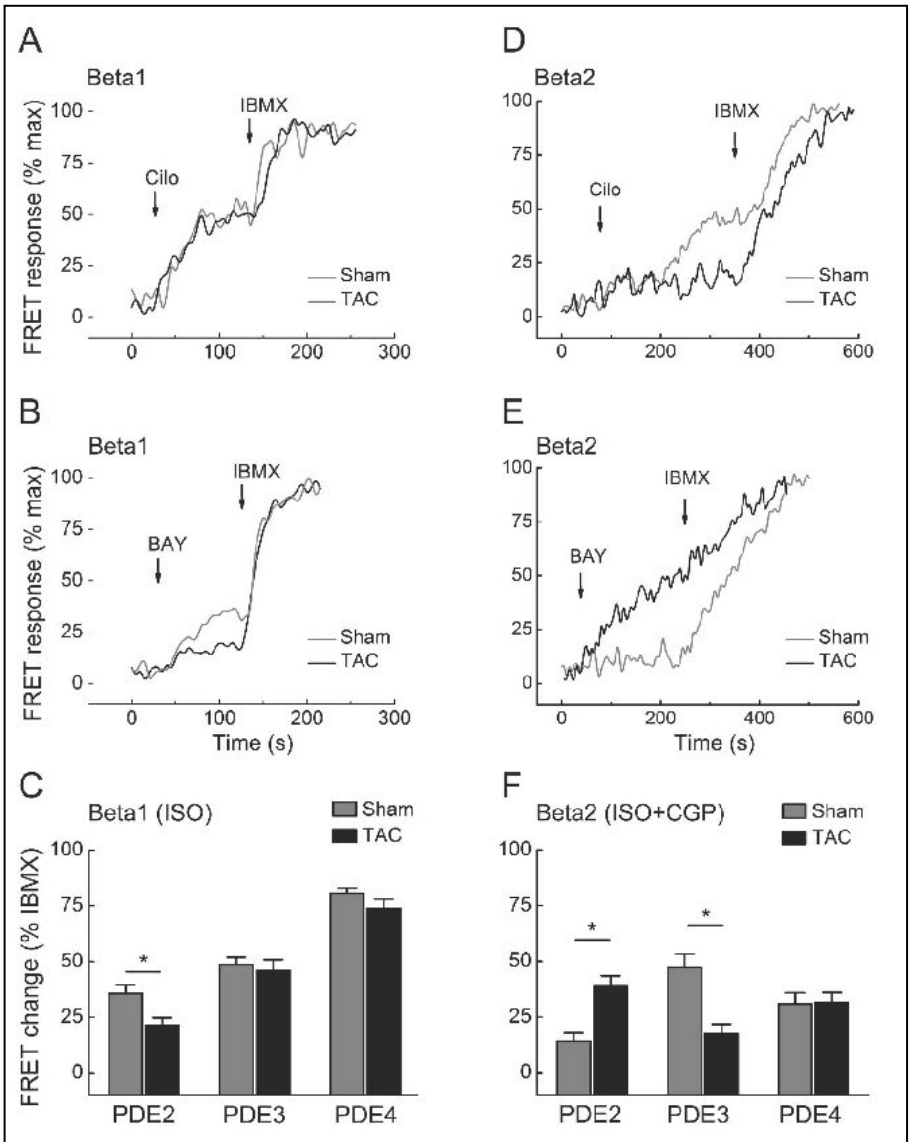

Figure 15. *PDE2 and PDE3 redistribute between β_1- and β_2-AR-associated cAMP microdomains in cardiac hypertrophy.* (A and B) Representative traces showing cilostamide (Cilo, 10 µM) and BAY60-7550 (BAY, 100 nM) effects in TAC and sham pmEpac1 cardiomyocytes after global ISO stimulation. (C) Quantifications of the PDE inhibitor signals (as % of the maximal response evoked by the unselective inhibitor IBMX) obtained after ISO stimulation in TAC and sham cardiomyocytes. (D) After selective β_2AR (ISO+CGP) prestimulation, PDE3 inhibitor effects are dramatically reduced while PDE2 inhibitor responses are markedly increased (E) in hypertrophied cells. (F) Quantifications of the PDE inhibitor signals after β_2-AR selective stimulation. Shown are means ± SE, n = 12-22 cells isolated from 3-4 hearts per condition. * - significant differences at $p<0.05$.

10A, B. Unexpectedly, much stronger ISO responses were detected in TAC compared to sham cardiomyocytes, which were apparently caused by stronger β_1-AR-selective cAMP signals (Figure 14A, B). Of note, ISO and β_1-AR-cAMP responses were indistinguishable, again suggesting that global ISO responses are predominantly mediated by β_1-AR. Therefore, ISO was used in all subsequent experiments to stimulate this global β_1-AR-associated pool of cAMP. In sharp contrast, β_2-AR/cAMP responses were significantly reduced in diseased cells (Figure 14 C, D). These changes of β-AR/cAMP signals were not due to altered β-AR densities (164 ± 16 vs. 128 ± 17 fmol/mg membrane protein in sham vs. TAC cells, not significant, p=0.1, n=3) or β_1-/β_2-AR ratio, as confirmed by radioligand binding studies (Figure13 C, performed by Christian Dees, University of Würzburg, Germany, Pharmacology Department). Therefore, the hypothesis arouse that shifted β_1/β_2-AR signal balance might be caused by changes in local, β-AR-associated PDE activities.

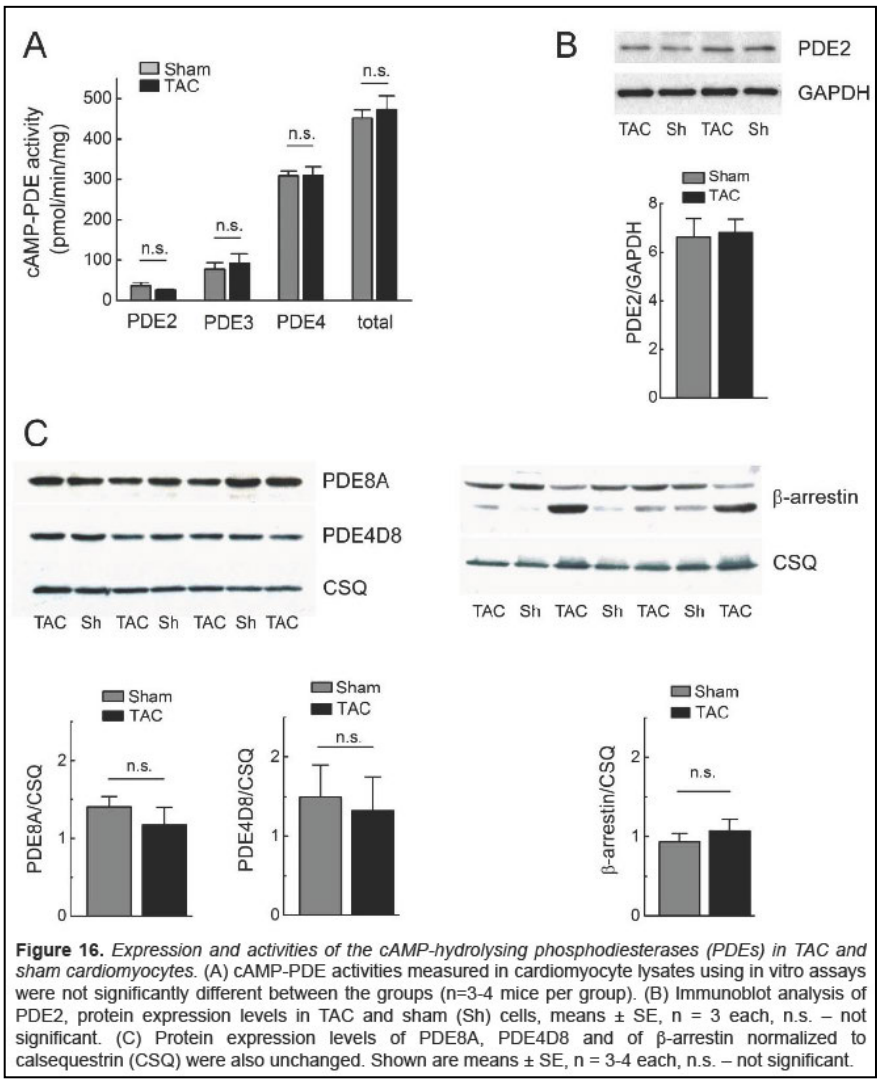

Figure 16. *Expression and activities of the cAMP-hydrolysing phosphodiesterases (PDEs) in TAC and sham cardiomyocytes.* (A) cAMP-PDE activities measured in cardiomyocyte lysates using in vitro assays were not significantly different between the groups (n=3-4 mice per group). (B) Immunoblot analysis of PDE2, protein expression levels in TAC and sham (Sh) cells, means ± SE, n = 3 each, n.s. – not significant. (C) Protein expression levels of PDE8A, PDE4D8 and of β-arrestin normalized to calsequestrin (CSQ) were also unchanged. Shown are means ± SE, n = 3-4 each, n.s. – not significant.

4.1.6 cGMP-regulated PDEs redistribute between β_1-AR and β_2-AR-associated microdomains in hypertrophy

When FRET-based PDE profiles on subtype-specific β-AR cAMP signals (for experimental settings, see Figure 11) were assayed in TAC vs. sham pmEpac1 cardiomyocytes, β_1-AR cAMP surprisingly was found to be mostly unaltered, with only decreased contributions of minor PDE2 (Figure 15A-C). The PDE subset regulating β_2-AR cAMP, however, turned out to be more severely changed. In fact, the pre-dominant PDE3 regulation observed under normal conditions was displaced by PDE2 in disease (Figure 15D-G). Importantly, these highly localized changes in PDE inhibitor responses, measured by FRET, were neither manifested in changed whole cell PDE activities, nor in altered expression levels of functionally relevant PDE isoforms (Figure 16A-C). Previously, βArr

has been established not only as a crucial negative regulator of the β-adrenergic signaling but, importantly, also as a scaffold which recruits in particular PDE4D isoforms to the stimulated β_2-AR[69]. However, βArr2 protein levels remained stable in mildly hypertrophied cardiomyocytes (Figure 16C, right panel), similar to PDEs. To prove the hypothesis of PDE redistribution, physical changes of PDE2 and 3 localizations were analyzed by co-immunostainings with α-actinin. Therefore, isolated adult wild type cardiomyocytes were stained with PDE family-specific antibodies to analyze the degree of their co-localization with α-actinin. Interestingly, in TAC cardiomyocytes, the subcellular PDE2 and 3 distributions were visibly altered, also reflected by a decreased Pearson's coefficient, which shows the degree of co-localization (Figure 17A, B).

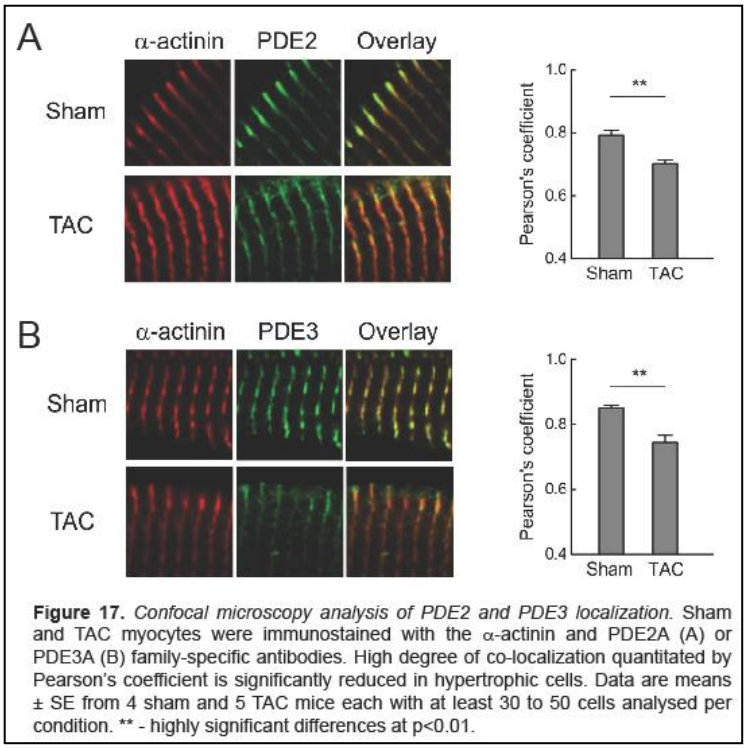

Figure 17. *Confocal microscopy analysis of PDE2 and PDE3 localization.* Sham and TAC myocytes were immunostained with the α-actinin and PDE2A (A) or PDE3A (B) family-specific antibodies. High degree of co-localization quantitated by Pearson's coefficient is significantly reduced in hypertrophic cells. Data are means ± SE from 4 sham and 5 TAC mice each with at least 30 to 50 cells analysed per condition. ** - highly significant differences at p<0.01.

4.1.7 PDE2 redistribution causes a shifting in ANP/cGMP-stimulatory effects from local (β_2-AR) to global (β_1-AR) cAMP, contractility and heart rates

Since cellular PDE protein levels were unaffected, the dramatic changes, especially of the PDE-dependent regulation of the β_2-AR/cAMP responses likely to arouse from subcellular redistribution of PDE2 and PDE3. Of note, these

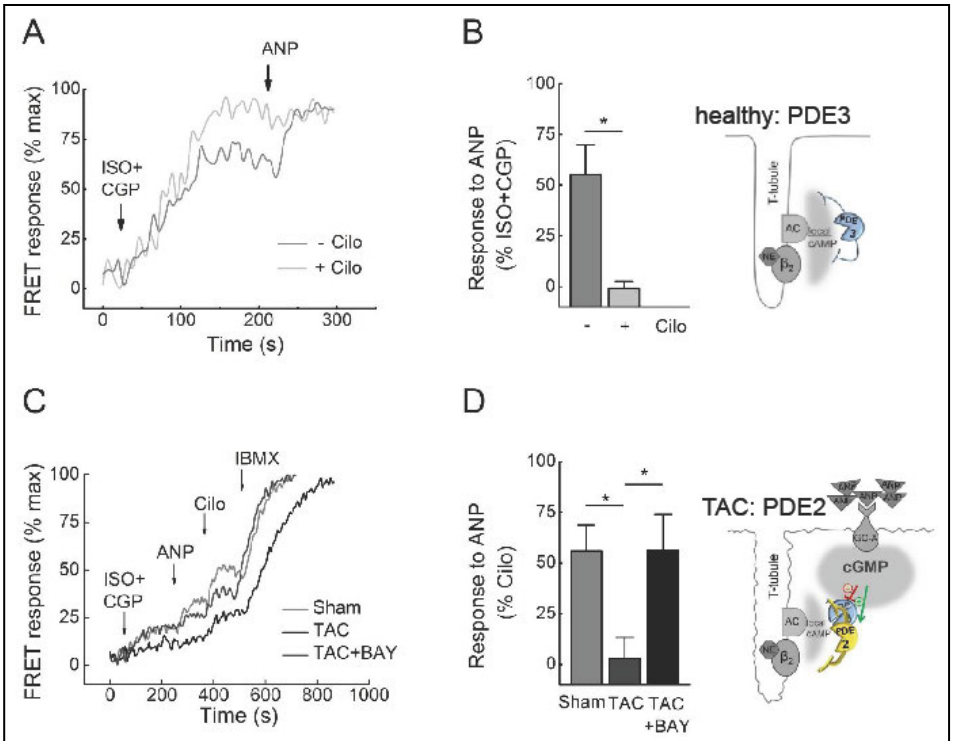

Figure 18. *Altered cGMP dependent regulation of membrane β_2-AR-cAMP levels in cardiac hypertrophy.* (A) Addition of atrial natriuretic peptide (ANP, 100 nM) after selective β_2-AR stimulation (ISO+CGP) leads to further significant increase in cAMP. Pretreatment of cells with 10 µM cilostamide (Cilo) prevents the effect of ANP, suggesting a PDE3-dependent effect. (B) Quantification of the ANP responses shown in % ISO + CGP, data are means ± SE, n = 7-8 cells isolated from 2 hearts each. (C) The effect of ANP is abolished in diseased myocytes but can be restored after preincubation with the PDE2 inhibitor BAY60-7550 (BAY, 100 nM). (D) Quantification of the ANP effect in TAC and sham cells as % of maximal PDE3 inhibition with cilostamide. Data are means ± SE, n = 9-11 cells isolated from 3 hearts per condition. * - significant differences at p<0.05.

two PDE families are oppositely regulated by cGMP. Whereas allosteric binding of cGMP stimulates PDE2 activity, it inhibits PDE3 cAMP-hydrolysis by substrate competition (*see Introduction, subsection 1.5*). Hence, since β_2-AR cAMP appeared to be at all times under the control of cGMP-regulated PDEs, the effects of cellular cGMP on β_2-AR cAMP were next studied. 2006 Castro et al.[92] reported the existence of two distinct cGMP pools in adult rat cardiomyocytes, each being stimulated by different ligands, e.g. natriuretic peptides such as ANP for the (sub-) sarcolemmal, but nitric oxide for the cytosolic cGMP pool. Therefore, in adult cardiomyocytes from untreated mice, it was first tested whether ANP would exert any effect on β_2-AR stimulated cAMP signals, considering that PDE3 (the cGMP-inhibited PDE) was the primary regulator in this cAMP microdomain, under normal conditions. Indeed, β_2-AR-triggered FRET signals could be further enhanced by the addition of ANP (Figure 18A). Importantly, this ANP effect was abrogated when cells were pre-treated with the PDE3-selective inhibitor cilostamide, strongly suggesting that that the ANP/cGMP-mediated inhibitory effect is PDE3 dependent (Figure 18A, B). However, when similar protocols were applied onto TAC-cardiomyocytes, the ANP effect was markedly reduced (even without cilostamide pretreatment) (Figure 18C, D).

Considering that in early disease, PDE2 displaces PDE3 as the predominant regulator of β_2-AR cAMP, as shown by the FRET-based β_2-AR PDE profile (see Figure 15F, G), cells were next pretreated with the PDE2-selective inhibitor, BAY 60-7550, which unmasked the ANP-mediated β_2-AR cAMP increase, suggesting increased PDE2 activity in this microdomain of diseased cells (Figure 18C, D). To clarify, to what extent the overall modest changes in regulation of fairly small β_2-AR cAMP signals could possibly translate into functional response, the same pharmacological protocols as described in Figures 11 and 15 were applied during single-cell contractility

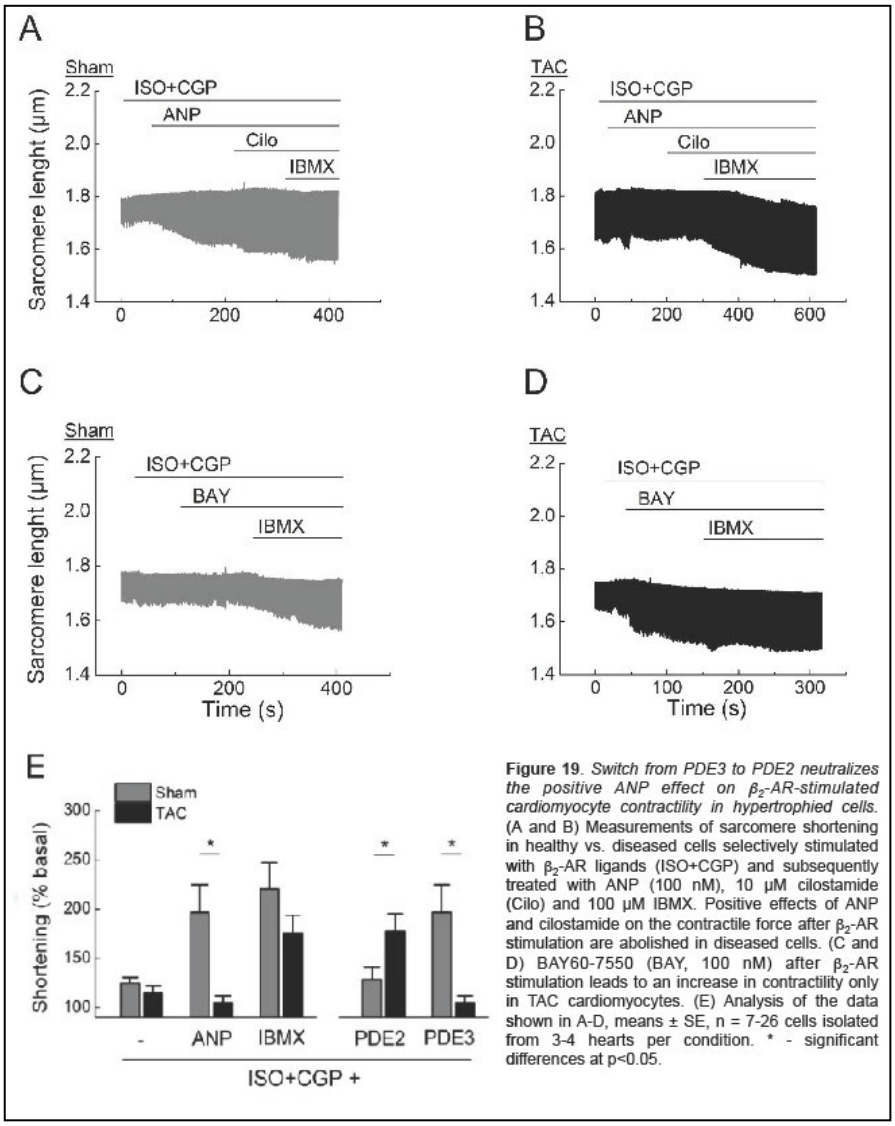

Figure 19. *Switch from PDE3 to PDE2 neutralizes the positive ANP effect on β_2-AR-stimulated cardiomyocyte contractility in hypertrophied cells.* (A and B) Measurements of sarcomere shortening in healthy vs. diseased cells selectively stimulated with β_2-AR ligands (ISO+CGP) and subsequently treated with ANP (100 nM), 10 µM cilostamide (Cilo) and 100 µM IBMX. Positive effects of ANP and cilostamide on the contractile force after β_2-AR stimulation are abolished in diseased cells. (C and D) BAY60-7550 (BAY, 100 nM) after β_2-AR stimulation leads to an increase in contractility only in TAC cardiomyocytes. (E) Analysis of the data shown in A-D, means ± SE, n = 7-26 cells isolated from 3-4 hearts per condition. * - significant differences at p<0.05.

measurements after β_2-AR-selective stimulation (Figure 19A-D). Importantly, contributions of PDE2 and PDE3 as well as the ANP-effect on β_2-AR cAMP in normal und diseased cardiomyocytes, directly translated into sarcomere shortening of single wild type cardiomyocytes (Figure 19E). Next, it was studied whether PDE redistribution may affect the physiologically more significant general contractile response stimulated by ISO for the global β_1-AR-dependent pool of cAMP. Strikingly, ANP showed completely opposite effects after global β-AR stimulation. Whereas ANP applied alone or after submaximal ISO stimulation did not exert any contractile

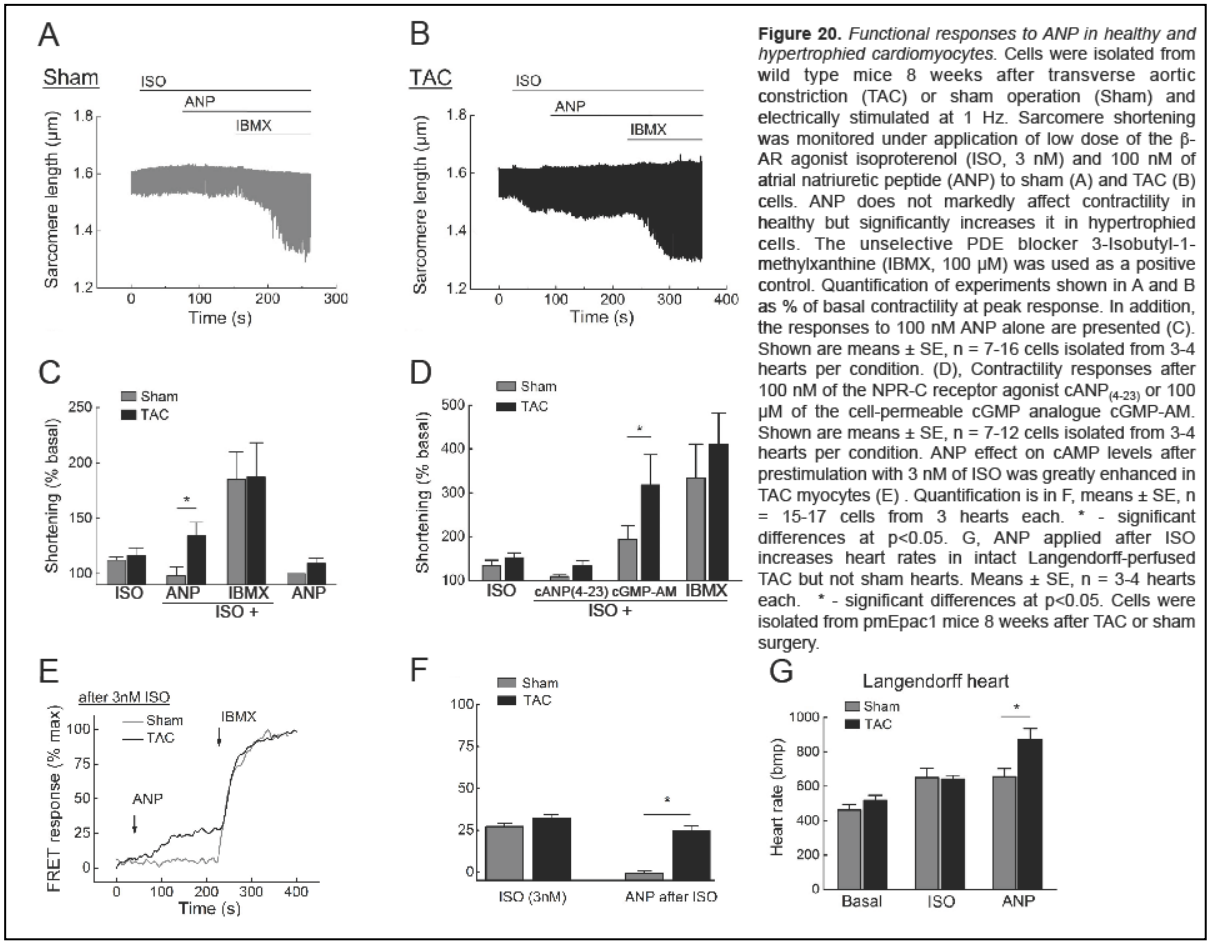

Figure 20. *Functional responses to ANP in healthy and hypertrophied cardiomyocytes.* Cells were isolated from wild type mice 8 weeks after transverse aortic constriction (TAC) or sham operation (Sham) and electrically stimulated at 1 Hz. Sarcomere shortening was monitored under application of low dose of the β-AR agonist isoproterenol (ISO, 3 nM) and 100 nM of atrial natriuretic peptide (ANP) to sham (A) and TAC (B) cells. ANP does not markedly affect contractility in healthy but significantly increases it in hypertrophied cells. The unselective PDE blocker 3-Isobutyl-1-methylxanthine (IBMX, 100 µM) was used as a positive control. Quantification of experiments shown in A and B as % of basal contractility at peak response. In addition, the responses to 100 nM ANP alone are presented (C). Shown are means ± SE, n = 7-16 cells isolated from 3-4 hearts per condition. (D), Contractility responses after 100 nM of the NPR-C receptor agonist $cANP_{(4-23)}$ or 100 µM of the cell-permeable cGMP analogue cGMP-AM. Shown are means ± SE, n = 7-12 cells isolated from 3-4 hearts per condition. ANP effect on cAMP levels after prestimulation with 3 nM of ISO was greatly enhanced in TAC myocytes (E) . Quantification is in F, means ± SE, n = 15-17 cells from 3 hearts each. * - significant differences at $p<0.05$. G, ANP applied after ISO increases heart rates in intact Langendorff-perfused TAC but not sham hearts. Means ± SE, n = 3-4 hearts each. * - significant differences at $p<0.05$. Cells were isolated from pmEpac1 mice 8 weeks after TAC or sham surgery.

response in healthy cells, it triggered a significant positive inotropic response in diseased cardiomyocytes (Figure 20A-C). Similar to β-AR/cAMP, also NPR-A/cGMP signaling has been shown to be downregulated in heart failure[159]. Besides NPR-A, ANP does also bind to the clearance receptor NPR-C. This receptor subtype not only eliminates ANP from the cell surface via internalization but, when bound to ANP, can also exert $G\alpha_i$-mediated AC inhibition and $G\beta\gamma$-dependent Ca^{2+} extrusion via membrane-bound transient receptor potential channels (TRPCs)[160]. To clarify whether the functional ANP effects on β_1- and β_2-AR signaling might be mediated by NPR-C pathways, $cANP_{4-23}$ was used to selectively activate NPR-C[161], but did not lead to such contractility effects, seen after ANP application. Conversely, application of the cell-permeable cGMP analogue cGMP-AM mimicked the ANP-mediated contractile responses, confirming that these functional responses were mediated by cGMP (Figure 20D). FRET experiments performed using the same stimulation protocols in TAC and sham pmEpac1 cardiomyocytes validated, that the differential effects of ANP on cardiomyocyte contractility were indeed caused by the same ANP effects on global cAMP (Figure 20E, F). Finally, the stimulatory effect of ANP

after ISO in diseased myocytes was also detected in heart rate measurements using intact perfused Langendorff hearts (Figure 20G), more closely reflecting the *in vivo* situation.

4.2 Atropine Modulates Phosphodiesterase Activity in the Heart

4.2.1 Atropine augments cAMP signaling in adult cardiomyocytes independently of muscarinic receptors

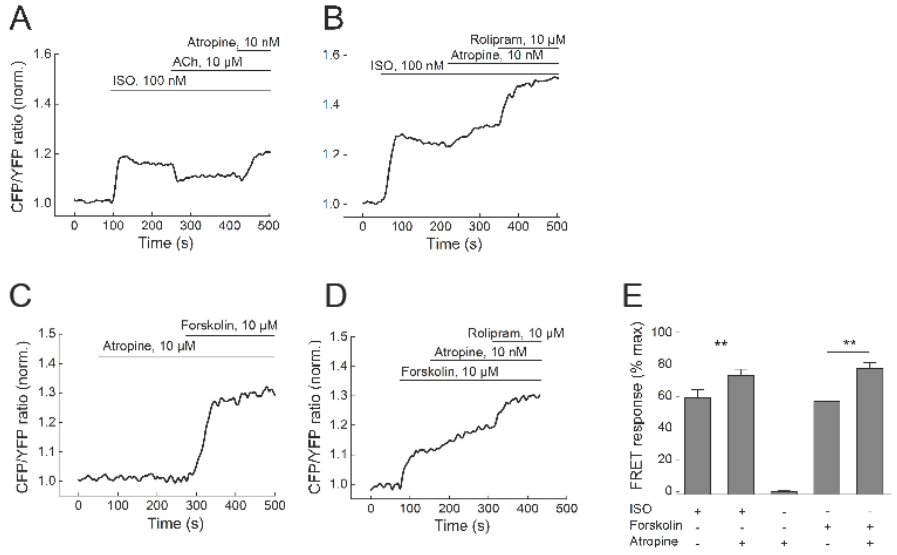

Figure 21. *Atropine stimulates cellular cAMP levels measured in adult mouse cardiomyocytes transgenically expressing the Epac1-camps sensor.* (A), the β-AR agonist isoprenaline (ISO) increases the CFP/YFP FRET ratio, and this response is partially reverted by acethylcholine (ACh). ACh effect is completely blocked by atropine. (B), atropine increases cAMP levels beyond the plateau reached after ISO stimulation. These can be further elevated by the selective PDE4 inhibitor rolipram. (C), atropine alone does not affect cAMP but (D) it potentiates forskolin-mediated increase in this second messenger. (E), quantification of the FRET ratio changes in response to ISO, forskolin and atropine from the experiments shown in A, B, D and E. The data are presented as a percent of the maximal FRET response reached after stimulation by 10nM ISO and 10µM rolipram or 10µM forskolin and 10µM rolipram respectively, means ± SE (n=5-6).

Atropine effects on cAMP dynamics were analyzed via FRET measurements in cardiomyocytes isolated from mice transgenically expressing Epac1-camps[36,46]. In these cells, stimulation with ISO classically leads to a substantial increase of intracellular cAMP, which can be partially (to ~50%) reversed by ACh, as this was previously also described in adult guinea pig cardiomyocytes infected with Epac2-camps adenovirus[162]. As expected, application of atropine after ACh fully blocked its effect. (Figure 21A). Unexpectedly, when applied after ISO and in the absence of ACh, atropine substantially potentiated the β-AR-induced cAMP response, which was also the case when cells were prestimulated with the general adenylyl cyclase activator forskolin (Figure 21B, D, E). However, when applied alone, atropine, even at very high concentrations, did not affect the FRET ratio (Figure 21C, E). Of all five known muscarinic receptor subtypes, cardiomyocytes predominantly, if not exclusively express the M_2-receptor which is coupled to inhibitory G-proteins[123]. However, treatment with PTX completely abolished the effect of ACh but strikingly did not affect the atropine-mediated increase in cardiomyocyte cAMP after ISO stimulation, suggesting its receptor-independent nature (Figure 22A-C). To further support this hypothesis, isolated cardiomyocytes from the M_2-receptor knockout mice were infected with Epac1-camps adenovirus. Even in these cells, the cAMP response to atropine could be clearly detected

(Fig22D, E). Analyzing the concentration-response dependency of this novel atropine effect in cardiomyocytes revealed biphasic kinetics with a saturation at ~10 nM (Figure 22F).

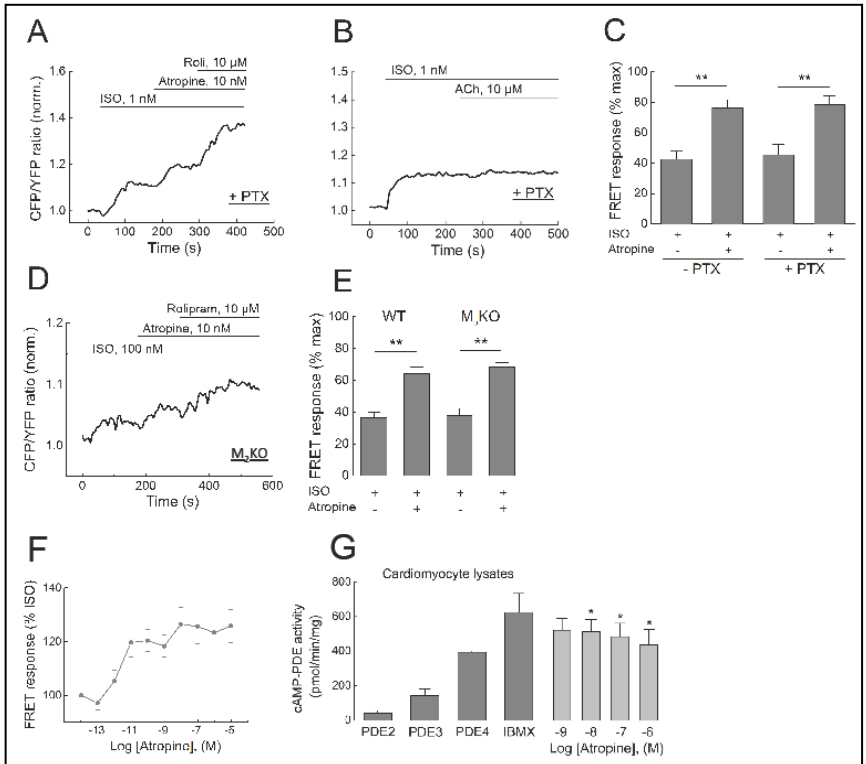

Figure 22. *Atropine increases cAMP$_i$ independently of muscarinic receptor blockade but via PDE inhibition.* (A) Inhibition of G_i-proteins with pertussis-toxin (1.5 µg/ml for 7-8 h) does not affect the atropine mediated stimulation of cAMP. Here, 1 nM ISO was used, since 100 nM lead to a complete saturation in PTX-treated cells. Representative experiment (n=5). Quantification of the FRET changes is shown in (C), means ± SE (n=5-6). Atropine, 10nM. (D), The atropine effect is conserved even in M_2KO mice, detected 48 hours post-infection with *Ad-Epac1-camps*. Representative experiment (n=4). Quantification of the FRET changes is shown in (E), means ± SE (n=3-4). (F), Concentration-response dependency of atropine on cAMP levels in cardiomyocytes after ISO (100nM) prestimulation, means ± SE (n=5-6). (G), Atropine inhibits PDE activity in cardiomyocyte whole cell lysates, means ± SE (n=4). Selective PDE inhibitors were used to assess single PDE family contributions. PDE2 = Bay 60-7550, 100nM; PDE3 = cilostamide; 10µM; PDE4 = rolipram, 10µM; all PDEs = 3-isobutyl-1-methylxanthine (IBMX), 100µM.

4.2.2 Atropine potently inhibits PDE4

The stimulatory effect of atropine on cAMP levels was reminiscent of the PDE inhibitor effects. For example, the PDE4 inhibitor rolipram similarly increased ISO-stimulated cardiomyocyte cAMP, however, with a higher efficacy. Previously, it has been shown that atropine potentiates PDE1 and PDE4 inhibitor effects in tracheal smooth muscle, even though the mechanism of this phenomenon was unclear[163]. Hence it was tested whether atropine could directly inhibit PDEs. Cardiomyocytes express at least five families of these enzymes, PDE1-5 and 8, which either selectively degrade cAMP (PDE4, PDE8), or both, cAMP and cGMP (PDE1, 2 and 3)[79,81,83,164]. PDE inhibitory potential of atropine was directly investigated using a classical *in vitro* activity assay. In heart lysates, atropine could clearly inhibit cAMP-hydrolysis in a concentration-dependent fashion, starting at low nanomolar concentrations (Figure 22G).

Using chimera sensors, comprising Epac1-camps fused to an active PDE1, PDE3, PDE4 or PDE5 isoform[146], atropine inhibitory potential on single PDE families was further analyzed. Atropine showed strong FRET responses at PDE4, while the activities of PDE1, PDE3 and PDE5 were not significantly affected, even at very high atropine concentrations (Figure 23A, B). The intracellular PDE4 inhibition responses by atropine reached their steady state within several minutes but the concentrations-response dependency in HEK293A cells was

clearly biphasic (Figure 23F, black trace). Importantly, atropine also inhibited recombinant PDE4D3 activities *in vitro*, though with a much lower efficacy than the PDE4 selective inhibitor rolipram (Figure 23C).

4.2.3 Atropine cell entry is facilitated by unselective organic cation transporters

At physiological conditions, atropine can cross cell membranes, at least to some extent, by free diffusion[165,166]. However, this way of transport is limited. In addition, organic cation transporters (OCTs) highly expressed in the heart and less abundantly found in HEK293 cells, can facilitate active cellular atropine uptake[167]. In line with this notion, the unselective OCT blocker MPP+ completely abolished the effect of atropine on cAMP levels in Epac1-camps cardiomyocytes (Figure 23D, E). Conversely, stable expression of OCT3 in HEK293 cells led to larger atropine responses causing a leftward shift of atropine concentration dependency (Figure 23F), suggesting that atropine can be actively imported into the cell where it inhibits PDE activity.

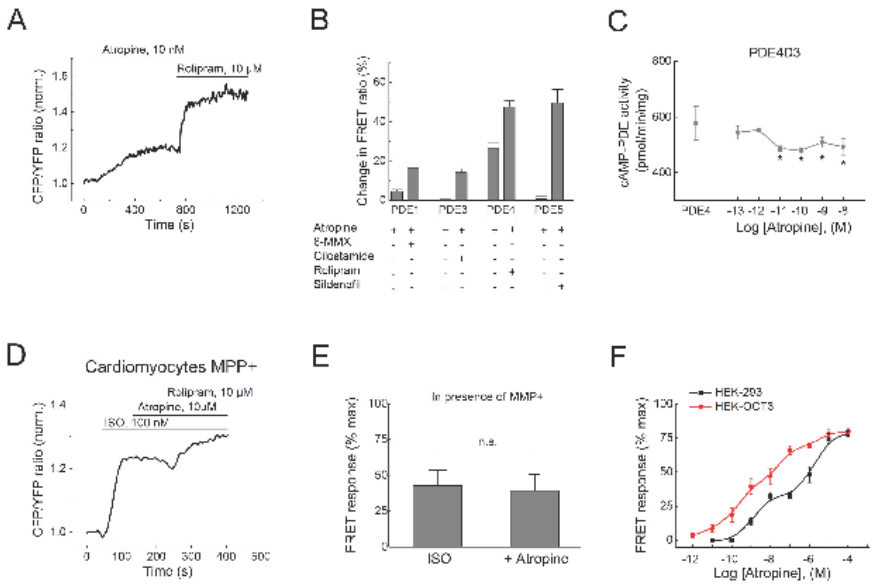

Figure 23. *Atropine inhibits PDE4 activity.* (A) Single-cell FRET analysis of PDE4 inhibition in 293A cells expressing the Epac1-camps-PDE4A sensor. Cells were prestimulated with 1 µM ISO for 3 min before adding atropine to pre-elevate intracellular cAMP levels. (B) Quantification of the data shown in A and further chimera sensors fused to PDE1, PDE3 and PDE5, as a % change of the FRET ratio in response to atropine for each individual PDE-sensor along with maximal effects measured by these sensors with respective inhibitors, means ± SE (n=6). 8-methoxymethyl-3-isobutyl-1-methylxanthine (8-MMX), 100µM; cilostamide, 10µM; rolipram, 10µM; sildenafil, 1µM (C) Concentration-response-dependencies for rolipram measured in an enzymatic *in vitro* assay using the recombinant PDE4D3 sensor in presence or absence of 10 nM atropine, means ± SE (n=3). The IC50-values were 29.9 ± 1.4 nM and 72.6 ± 5.7 nM with and without atropine, respectively. (D) Preincubation of cardiomyocytes with the OCT inhibitor MPP+ (100 µM) prevents the stimulatory effect of atropine measured as in Fig. 20B. Representative trace, n=5. (E) Amplitudes. (F) Overexpression of OCT3 in HEK293 cells enhances the stimulatory effect of atropine measured as in A, means ± SE (n=5).

4.2.4 Atropine augments cardiac function in adult mice

Next, atropine effects on heart rates in explanted perfused mouse hearts (Langendorff preparation), which lack any nervous innervation were analyzed. ISO increased the basal heart rate by ~20%, while atropine applied on top of ISO significantly augmented its response, which is indicative of the positive chronotropic effect of atropine after β-adrenergic stimulation. This effect was preserved in M_2-receptor knockout mouse hearts, further corroborating its receptor-independent nature (Figure 24A). cAMP increase in cardiomyocytes should lead not only to an increase in heart rate but also to an increase in beating force. Sarcomere shortening measurements in isolated ventricular cardiomyocytes showed that atropine also significantly enhanced the positive inotropic effect of ISO (Figure 24B, C).

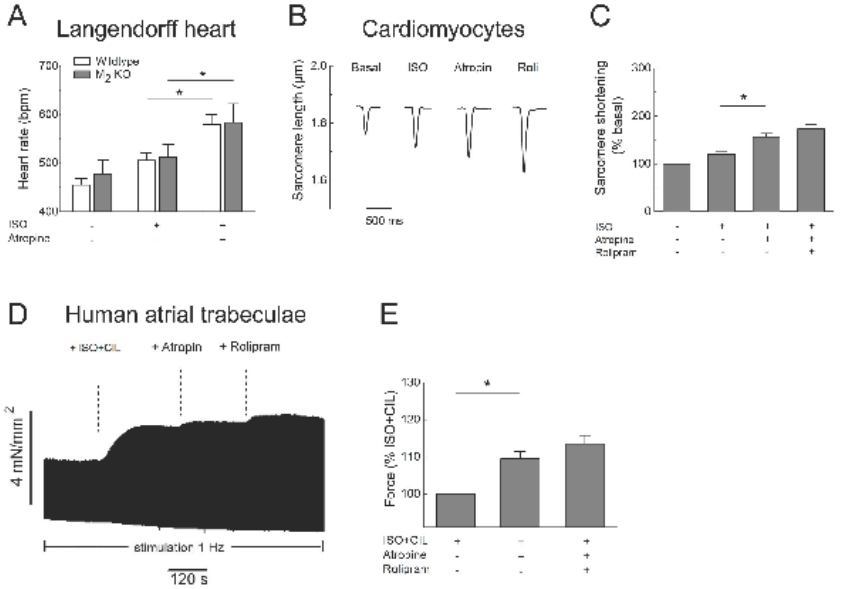

Figure 24. *Atropine stimulates cardiac function in mouse and human.* (A) Heart rate measurements in Langendorff-perfused hearts stimulated with ISO alone (10 nM), or with ISO plus atropine (10nM). Atropine significantly increases the beating frequency (n=5). Atropine increases the force of contraction in mouse cardiomyocytes and human atrial muscle trabeculae. (B) Representative traces from single cardiomyocyte contractility measurements by edge-detection show positive inotropic effect of atropine applied after ISO. Quantification is in (C), n=10-13. ISO, 3nM; atropine, 10nM; rolipam, 10µM (D) Effect of atropine (10nM) on the developed force of contraction in human right atrial trabeculae. Atropine increases the force of contraction in trabeculae which were prestimulated with 1 nM ISO and 10 µM cilostamide (CIL). Original representative trace. (E) Quantification of the contractility data. The data for each experiment were normalized to the force developed after prestimulation with 1 nM ISO plus 1 µM cilostamide (CIL). Shown are means ± SE (n=5). * - the difference is statistically significant (p=0.03, paired t-test). Force measurements were performed by Dr. Thomas Fischer, MD, Department of Cardiology and Pneumology, University Medical Centre Göttingen.

4.2.5 Atropine stimulatory effects on myocardial function are conserved in human

To link these novel findings from small animal models to the situation in human myocardium, force of contraction in heart muscle trabeculae isolated from human right atria was measured. While atropine alone or after sole ISO prestimulation did not affect the force of contraction, application of atropine to trabeculae pretreated with ISO and the PDE3 inhibitor cilostamide substantially increased contractility which was further augmented by rolipram (Figure 24D, E). Force measurements on human trabeculae were performed by Dr. Thomas Fischer, MD and Jonas Herting (University Medical Center Göttingen, Department of Cardiology).

5 Discussion

5.1 Local β-Adrenergic Signaling at the Sarcolemma of Adult Mouse Cardiomyocytes

This study describes the successful generation of a transgenic mouse model with heart-specific expression of the highly localized FRET-based cAMP sensor, pmEpac1. This sensor enables direct monitoring of cAMP dynamics exclusively in sarcolemmal microdomains. pmEpac1 was designed to associate predominantly with caveolar membrane structures to attain its high expression at the T-tubules (*see Figure 8*) with the aim to particularly well resolve and analyze the highly compartmentalized β_2-AR-cAMP signals.

5.1.1 pmEpac1 expressed in mice enables detailed analysis of subtype-specific β-AR-associated cAMP compartments, especially at β_2-AR

Indeed, β_2-AR-stimulated cAMP signal amplitudes in adult cardiomyocytes show to be two-fold larger when measured with pmEpac1 compared to the maternal cytosolic sensor, Epac1-camps (*see Figure 10B, C*). Considering a slight loss in sensor sensitivity of pmEpac1, when compared with Epac1-camps (*see Figure 10D*), the actual cAMP signals in this microdomain must be considered even greater. Likewise, this further marginalizes the possibility of pmEpac1 acting as a sarcolemmal cAMP sink, which could interfere with normal cardiac cAMP homeostasis. However, pmEpac1 mice do not develop any heart-specific or other phenotype (*see Figure 9*) per se, which makes this possibility rather unlikely.

Hence, the improved cAMP resolution of pmE1 enables real time analysis of subtype-specific β-AR- cAMP with high temporal and spatial resolution. Importantly, β_1-AR signals show virtually similar amplitudes and PDE-dependent regulation when measured either at the sarcolemma (pmEpac1) or in the cytosol (Epac1-camps) of adult cardiomyocytes (*see Figures 10A,C, 11B*). This likely reflects the far-reaching effects that have been attributed to β_1-AR signaling[37]. Interestingly, the presented data suggest that β_2-AR-cAMP signals are predominantly controlled by PDE3 (*see Figure 11D*), which has not been appreciated so far, most likely due to insufficient precision and spatial resolution of the experimental tools, used[37,168]. For example, one previous study with olfactory cyclic nucleotide gated (CNG) channels ectopically expressed in adult rat cardiomyocytes as reporters for subsarcolemmal cAMP showed that different membrane receptors evoke distinct submembrane cAMP signals due to their regulation by different PDE subsets[169]. However, the exact localization of these sensors is not thoroughly established, although it was demonstrated that CNG channels are predominantly associated with non-caveolar membrane microdomains[170], whereas β_2-ARs are almost exclusively localized in caveolin-rich membrane compartments[171-173]. Hence, when measured with either cytosolic FRET probes[37] (*see also Figure 11D*) or with CNG-channels[169] both, PDE3 and PDE4 show equal contributions to the control of β_2-AR-cAMP signals. Probably, due to insufficient proximity of the respective sensor to β_2-AR, its relative responses remained very small in both studies, preventing a more thorough analysis of such highly localized functionally important signals. In contrast to these previous observations, local

β_2-AR-cAMP signals measured with pmEpac1 reveal predominant control of PDE3, which is well in line with the strong augmenting effect of the selective PDE3 inhibitors, such as cilostamide on β_2-AR stimulated cardiomyocyte contractility (*see Figures 11D, 15F, 19A, E*). So far, cardiac cAMP regulation, especially of β_2-ARs was primarily attributed to the actions of different PDE4 isoforms[68-70]. In this regard, the pmEpac1 mouse has already proven to be a valuable new tool for investigations of cardiac cAMP signaling, especially regarding the highly localized β_2-AR-cAMP dynamics.

5.1.2 The FVB/N mouse strain shows certain resistance to experimentally induced cardiac disease

Transgenic expression of pmEpac1 in mice further allows combining pmEpac1 mice with experimental and genetic heart disease models.

For the present study, to investigate pathological changes in β-AR/cAMP signal compartmentation, transverse aortic constriction (TAC) was chosen to experimentally induce heart failure. Interestingly, regardless of a pronounced pressure gradient of 80 mmHg, eight weeks post TAC surgery pmEpac1 mice developed a very mild cardiac disease phenotype. As such, a yet pronounced gain in heart weight and wall thicknesses was accompanied by only mild reduction in contractile function, indicative of an early disease state, i.e. compensated hypertrophy (*see Figure 12A-D*). Since pmEpac1 transgenic mice do not show any developmental abnormalities per se (*see Figure 9*), the observed mild cardiac phenotype is most likely reasoned by the genetic background of those animals. This assumption is further corroborated by the fact, that wild type littermates of the heterozygous pmEpac1 transgenic mice, used for biochemical assays and functional studies (i.e. Langendorff ECGs and single cell contractility measurements) develop the same mild cardiac phenotype described above.

Several studies have reported that FVB/N mice indeed exhibit a certain resistance against different experimental disease models, such as parasite infection or type 2 diabetes[174,175]. Especially considering that FVB/N mice can even withstand the development of acquired systemic diseases such as type 2 diabetes, it can be presumed that the development of congestive heart failure is similarly slowed down. Therefore, the FVB/N mouse strain proves to be well suited to investigate especially early cardiac disease pathology.

5.1.3 ANP stimulates heart function at the onset of heart failure

However, in this early state of compensated hypertrophy, plasma ANP levels are already increased by two-fold. Considering ANP as a trigger of cardiomyocyte cGMP[92], changed cyclic nucleotide contents in diseased cardiomyocytes are very likely. Indeed, FRET measurements in pmEpac1 expressing TAC cardiomyocytes reveal ANP-stimulatory effects on global β-AR-cAMP signals (*see Figure 20E, F*). Importantly, this unexpected ANP effect on β-AR signaling in diseased cardiomyocytes readily translates into an augmentation of contractile function. Previously, ANP was reported to not affect catecholamine (ISO)-stimulated contractility in healthy cardiomyocytes[176], which is well in line with the unchanged sarcomere shortening in sham cardiomyocytes observed in the present study (*see Figure 20A, C*). In TAC cells, however, ANP shows robust contractile responses after β-AR stimulation (*see Figure 20B, C*). Furthermore, ISO-stimulated heart rates can be further increased by ANP only in hypertrophied hearts, indicating that this ANP effect, initially uncovered in single

isolated cardiomyocytes, is indeed applicable to the *in vivo* situation (Figure 20G). Hence, the novel localized FRET biosensor pmEpac1 transgenically expressed in adult mouse cardiomyocytes can truly report functionally relevant cAMP dynamics linked to myocardial function.

5.1.4 In early cardiac disease, local PDE redistribution precedes global molecular changes yet with functional effects on global β-AR signaling

Considering that FRET measurements reveal augmented β-AR responses as a result of a shifted balance in β_1-AR: β_2-AR signal ratio (i.e. increased β_1-AR-cAMP and decreased β_2-AR-cAMP), on first sight, these data seem to contradict the extensively investigated paradigm of β-AR and ANP receptor desensitization occurring in advanced chronic cardiac diseases such as heart failure[11,110]. However, it should be pointed out that the early pathology events addressed in the present study, are likely to display an adaptational process rather than the well described detrimental effects caused by excessively prolonged β-AR signaling. In support for this notion, sensor: sarcolemma integrity and β-AR densities are virtually unchanged in TAC myocytes (*see Figure 13*). How can this adaptive response be explained mechanistically?

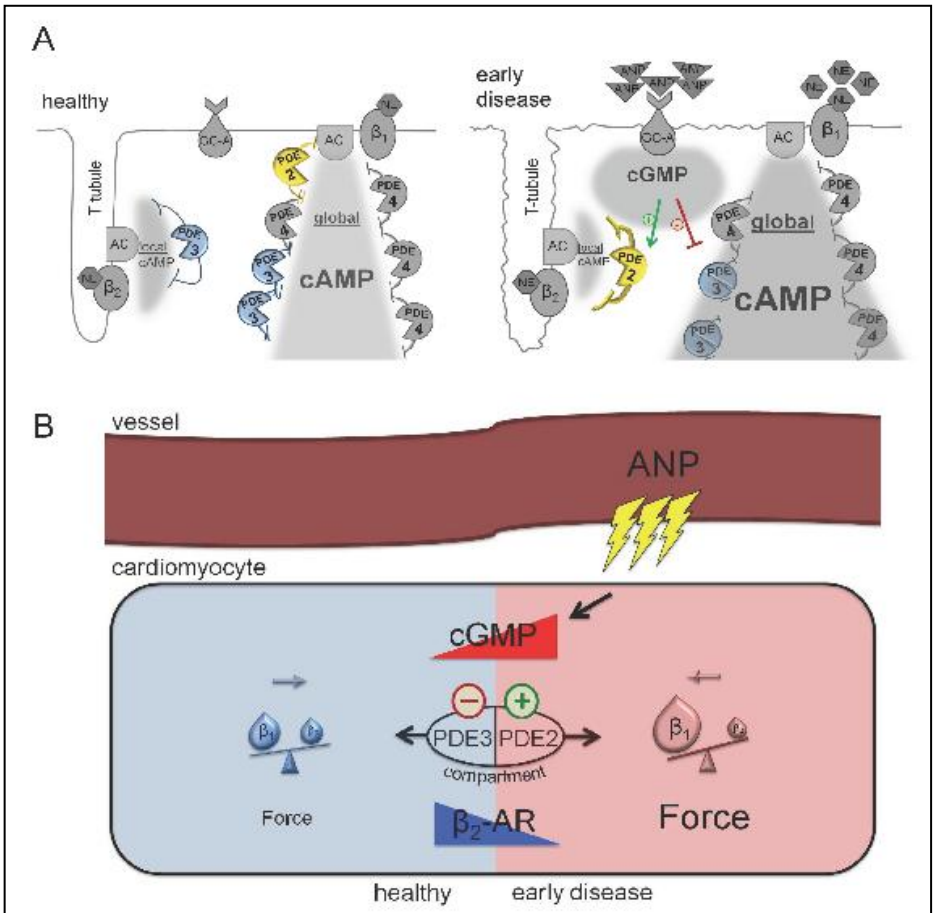

Figure 25. *Schematic representation of the proposed molecular switch mechanism occurring in early hypertrophy.* Redistribution of PDE2 from the β_1- to the β_2-AR-associated membrane microdomain leads to a decrease of the local β_2-AR-cAMP and to an increase of global β_1-AR-cAMP pool under elevated ANP and cGMP levels observed in hypertrophy. NE, norepinephrine, the physiological β-AR agonist (A). Switch of β_2-AR-associated PDE2 and 3 in early hypertrophy leads to a turnaround of cGMP/cAMP cross-talk between the β_2- and β_1-AR-associated microdomains, through which elevated ANP exerts a positive effect on b-adrenoceptor-stimulated contractility under shifted β_1-/β_2-AR-cAMP balance (B).

One key finding is that during early heart disease, locally detected PDE2 and PDE3 selective inhibitor effects (reflecting local PDE2/3 contributions) dramatically change, whereas whole-cell PDE amounts and activities remain stable (*see Figures 15D-G, 16*).

In order to explain this intriguing observation, it was hypothesized that changed local PDE inhibitor responses, especially at the β_2-AR, may possibly arise from a subcellular redistribution of PDE2 and 3 between the β_1-AR and β_2-AR-associated membrane microdomains. This scenario would eventually lead to a switching of cGMP/cAMP cross-talk from a formerly ANP-mediated cAMP increase (via PDE3) to an ANP-mediated cAMP decrease (via PDE2) at the β_2-AR (*see Figures 18, 25A*).

Physical proof of principle for this redistribution theory was approached by co-immunostaining of either PDE2 or PDE3 with the z-discs (α-actinin) of adult cardiomyocytes (*see Figure 17*); both PDEs showing decreased localization patterns with respect to α-actinin in early disease. However, more clear-cut evidence, i.e. co-localization of PDE2 and PDE3 with β_1- and β_2-ARs, currently remains technically difficult to accomplish. To bypass the lack of reliable subtype-specific β-AR antibodies, alternatively recombinant FLAG®-tagged β-ARs could be transiently expressed in normal and phenylephrine-treated neonatal cardiomyocytes to subsequently co-stain these with PDE2- and PDE3-specific antibodies. However this approach is highly artificial and it can be questioned whether functional cAMP microdomains are composed same in neonatal and adult cardiomyocytes.

Hence, in order to further corroborate the here claimed hypothesis of PDE-redistribution, one must rely mostly on indirect approaches. For instance, PDE2 and 3 could possibly be co-localized with particularly caveolin-3 enriched cell fractions. Here, shifted PDE2/3 expression patterns within subcellular fractions could serve as a further indication for PDE redistribution. However, the resolution of such an approach is clearly limited by the fact that both major β-AR subtypes reside in caveolar membrane compartments[177].

Nevertheless, regarding the functional relevance, it could be established that β_2-AR cAMP signaling well responds to ANP/cGMP stimulation in healthy cells (PDE3) as well as in early disease (PDE2) (*see Figure 18*). In untreated cells, ANP augments the β_2-stimulated cAMP levels. Importantly, this effect can be abolished by pre-incubating the cells with the PDE3-selective inhibitor cilostamide, confirming that the ANP-mediated effect on β_2-AR-cAMP is indeed caused by ANP/cGMP-dependent PDE3 inhibition (*see Figure 18A, B*). However, similar stimulation protocols in TAC cardiomyocytes reveal a dramatic reduction in the ANP-mediated β_2-AR-cAMP effect. In support of the PDE redistribution hypothesis, pre-incubation of diseased myocytes with the PDE2-selective inhibitor BAY 60-7550 partially unmasks the stimulatory effect of ANP on β_2-AR-cAMP levels (*see 18C, D*). This finding well contradicts possible NPR-A desensitization at this early stage of disease. Conversely, it further suggests that PDE3 is not fully displaced from the β_2-AR cAMP microdomain but its effect being covered by increased local PDE2 activity in disease, especially under conditions of elevated cellular cGMP levels.

5.1.5 Functional ANP responses in early cardiac disease are mediated by cGMP

Functionally, this observation correlates with the diminished ANP effect on selectively β_2-AR-stimulated cardiomyocyte contractility (*see Figure 19*). Most strikingly, not only does this lead to a change in physiologically less relevant β_2-AR-specific contractile effects, but importantly also to inversed ANP-effects on global contractile force after β-AR stimulation in hypertrophied myocytes (*see Figure 20B and C*). This effect is apparently caused by a shift in β_1/β_2-AR signal balance towards β_1-AR signaling in hypertrophied cells, despite unchanged β-AR densities. The elevated β-AR/ANP contractile response at this stage of disease is likely to be caused by the reorganization of microdomain-specific PDE activity patterns that cause the turnaround in cGMP/cAMP crosstalk. Unlike pronounced β_1-AR-cAMP and ANP/cGMP signal desensitization described for advanced heart failure, the present model of early cardiac hypertrophy provides insights into molecular changes, which take place during the onset of chronic cardiac disease. Although these changes appear rather neutral with regard to whole cell PDE activities, yet it could be shown that even slight changes in local PDE contributions can cause drastic changes in compartmentalized signaling patterns. These changes do directly

translate into opposite contractile effects of the same ligand such as ANP, which is present at higher levels in systemic circulation during hypertrophy (*see Figures 12E, 20A-C and 25B*). ANP has previously been reported to also act through the clearance receptor NPR-C that primarily removes bound ANP from the cell surface, but also exerts AC inhibitory properties via $G_{\alpha i}$-uncoupling. Furthermore, $G_{\beta\gamma}$ of NPR-Cs has been shown to activate transient receptor potential channels (TRPCs), in a phospholipase C-dependent manner[160,161]. So, in order to prove that the functional ANP effects are indeed triggered by NPR-A/cGMP, a cell-permeable cGMP analogue, cGMP-AM was used in analogous contractility experiments. Importantly, cGMP-AM induces contractile effects, highly similar to that evoked by ANP (*see Figure 20D*). Furthermore, a selective NPR-C agonist, $cANP_{(4-23)}$, was used to analyze possible involvement of the clearance receptor. However, $cANP_{(4-23)}$ did not exert any contractile responses as seen upon ANP application, making involvement of NPR-C in this mechanism unlikely.

5.1.6 PDE redistribution causes a turnaround of cGMP/cAMP crosstalk and mediates ANP stimulatory effects on contractility

Based on the current findings PDE2, which was thought to represent a minor fraction of total PDE activity under normal conditions, might serve as an important therapeutically interesting reservoir, which regulates and orchestrates β-AR/cAMP and ANP/cGMP signaling. When redistributed from the β_1- to the β_2-AR-associated compartment in early disease, this PDE facilitates the shift in β_1-/β_2-AR signal balance. Such shifting leads to a turnaround of the ANP/ cGMP-mediated control over β-AR-stimulated cAMP and contractility. The combined stimulatory effects by elevated ANP and catecholamines in cardiac hypertrophy can thereby further increase heart function. As mentioned above, concerning the pathophysiology, it is highly possible that this effect might represent a compensatory mechanism to meet the enhanced demand on cardiac output under pressure overload (Figure 25B). Strikingly, during early compensated cardiac hypertrophy, the β_2-AR, which generally plays a minor role in the catecholaminergic contractile response, seems to act as an important signaling module which can be regulated by either PDE2 or PDE3 to exert opposite effects on global β-AR-mediated cell function. Therefore, the previously postulated additive effects of both β-AR subtypes on myocardial force at healthy state (contractile response ~ β_1-AR- cAMP + β_2-AR-cAMP) might, in early heart disease transform into a relation of reciprocal interdependence (contractile response ~ β_1-AR-cAMP / β_2- AR-cAMP). Given that PDE3 generally dominates cAMP hydrolysis in human myocardium and that cardiac PDE2 amounts increase in late staged heart failure patients[120], such cGMP/cAMP crosstalk can be expected to have even more profound meaning for the human heart.

In summary, the presented data are indicative for a new cell adaptation mechanism, which involves subcellular redistribution of cGMP-sensitive PDEs. Such alterations well precede the abundantly documented more severe cellular changes which occur later during the decompensated cardiac phenotype and overt heart failure associated with changes of whole-cell PDE activities and the desensitization of the β_1-AR-cAMP and ANP/cGMP signaling cascades. In future, these findings might become clinically relevant in terms of novel therapeutic strategies acting on defined subcellular microdomains to prevent PDE redistribution and its detrimental effects. Since the PDE2/3-dependent cGMP/cAMP cross-talk is functionally important not only in cardiomyocytes but

also in many other cell types such as neurons [178], endothelial cells [179], platelets [180] and adrenal cells [181], this principle of cell function regulation can be expected to play an ubiquitous role in a wide variety of cells and disease conditions.

5.2 Atropine Modulates Phosphodiesterase Activity in the Heart

Atropine is widely used clinically as a non-selective antagonist of the muscarinic receptors to treat organophosphate intoxication as well as multiple other diseases such as acute bradycardia, heart block and chronic obstructive pulmonary disease. It binds all five muscarinic receptor subtypes with high affinity and prevents the ACh-mediated effects in target cells. In the heart, atropine abolishes the inhibitory effect of ACh on heart rate and contractility, often leading to tachycardia. These effects have been attributed exclusively to the antagonism at cardiac muscarinic M_2-receptors and inhibition of parasympathetic events.

5.2.1 Atropine modulates cardiomyocyte cAMP independently of muscarinic receptors

Atropine proves well to neutralize ACh-mediated reduction of ISO-induced cAMP (*see Figure 21A*). However, it increases cellular cAMP even without prior activation of muscarinic receptors, an effect that was observed only upon pre-stimulation with either ISO or forskolin (*see Figure 21B, C, D, E*). Previous studies have shown that M_2 receptors exert constitutive activity and, moreover, that G_i-$\beta\gamma$ subunits potentially stimulate AC subtypes[182-184]. Importantly, atropine-driven augmentation of cAMP is preserved even upon pertussis toxin (PTX) treatment (*see Figure 22A-C*), which prevents $G_{i\alpha}$ uncoupling by ADP-ribosylation, further indicating that this novel atropine effect is independent of M_2 receptor actions. Final proof is provided by analyzing cAMP dynamics in M_2-KO cells and hearts,[185] which behave virtually identical to those in either wild type or Epac1-camps transgenic mice. Therefore, it is very unlikely that the novel atropine effect on cardiomyocyte cAMP is linked to its properties as an inverse antagonist at muscarinic receptors[182,186]

5.2.2 cAMP effects are mediated via atropine-dependent PDE inhibition

However, exploring other directions, cardiomyocyte cAMP levels do increase with increasing atropine concentrations. The concentration-response dependency of this atropine effect in cardiomyocytes follows biphasic kinetics with a saturation at ~10 nM (*see Figure 22F*), which is in the therapeutically relevant concentration range of this drug. The stimulatory effect of atropine on cAMP levels observed here is consistent with the data from frog and rat ventricular myocytes where atropine stimulated L-type calcium channel currents when applied after ISO, presumably via a G-protein-dependent mechanism[186].

This and the observation that atropine only enhances pre-stimulated cAMP is reminiscent of the feedback actions of PDE4. In particular, of the long PDE4 isoforms the activities of which are stimulated upon PKA-dependent phosphorylation[187]. Using a classical biochemical assay, analysis of potential atropine effects on PDE activities in wild type cardiomyocyte lysates reveals a significant inhibition in a concentration-dependent manner.

Herget et al. previously established FRET biosensors, which can measure cAMP or cGMP in the vicinity of various PDEs, thereby directly reporting PDE inhibitor potential of various compounds in intact cells[146]. These sensors are comprised of a catalytically active PDE fused to Epac1-camps or to the cGMP sensor cGES-DE2[188] and respond to PDE inhibitors by a change of FRET. In addition to these previously described sensors for PDE3, 4 and 5, a new sensor construct was developed to measure PDE1 inhibition. Such chimeric sensors with Epac1-camps fused to PDE1A, PDE3A or PDE4A1 transiently expressed in HEK293A cells revealed pronounced atropine inhibitor effects exclusively on PDE4, with the concentration-response dependency being clearly biphasic (*see Figure 23 A, B, F*). Possible modulation of PDE5-dependent cellular cGMP pathways can be neglected since the cGMP-specific chimera cGES-DE2-PDE5A did not respond to atropine application.

Since this FRET approach pointed towards PDE4 as the intracellular target of atropine, its inhibitory potential was quantitated *in vitro* with recombinant PDE4D3, the pre-dominant PDE4 isoform expressed in mammalian myocardium. Importantly, the biphasic character of concentration-response dependence is also preserved here, although with a much lower overall efficacy than the selective well-established inhibitor rolipram (*see Figure 23 C*). This might indicate an unusual mechanism of action on PDE4, different from the classical inhibitors but sufficient to decrease the hydrolysis of cAMP and increase its intracellular levels in a functionally relevant range. In 1996, Jacobitz et al. established that PDE4s are present in two different conformations, with one showing higher susceptibility to rolipram-based inhibition than the other (high/low affinity rolipram binding states)[189]. Such findings leave room for speculations, such as that atropine could specifically bind to only one of those two PDE4 conformations, e.g. preferentially to the low affinity rolipram binding state. However, more efforts are required to fully understand the mechanisms behind atropine-dependent PDE4 inhibition.

Previously, PDE8A, a second cAMP-specific PDE in myocardial tissue which is insensitive to the unselective PDE inhibitor IBMX, has been reported to contribute to EC coupling regulation[105]. However, to date, a lack of appropriate PDE8 inhibitors has prevented further investigations of PDE8-mediated regulation of dynamic cAMP changes in cardiomyocyte. Hence, atropine inhibitory effects on PDE8 cannot be fully ruled out at that point. Conversely, PDE2, which likewise has not directly been addressed in this study, is rather unlikely to be side-targeted by atropine. Firstly, PDE2 is the minor contributor to cardiomyocyte cAMP-PDE activity due to relatively low expression levels. Secondly, atropine-mediated PDE inhibition, assessed in cardiomyocyte lysates (*see Figure 22 E*) clearly exceeded PDE2 activity, which was determined with the PDE2-specific inhibitor BAY 60-7550.

5.2.3 Organic cation transporters facilitate cellular atropine uptake

Another critical issue to address was how atropine actually enters the cell. Under physiological pH, the membrane is permeable to atropine to a certain extent[165,166]. In addition, organic cation transporters can facilitate active atropine uptake into cells. Incubating adult Epac1-camps cardiomyocytes with the unselective OCT blocker MPP+ abolished atropine-mediated FRET responses (*see Figure 23D, E*). Thus, it can be assumed that atropine is actively transported into the cells by OCTs. Especially OCT3 is expressed in the heart[190] but is

barely detectable in HEK cells, which could explain why the FRET kinetics assessed by Epac1-camps (cardiomyocytes) and by Epac1-camps-PDE4A1 (HEK293 cells) are remarkably different. The left-shifted concentration dependencies of atropine FRET responses obtained from HEK293 cells stably overexpressing OCT3 is indicative of an accelerated cellular atropine uptake upon enhanced OCT expression (*see Figure 23F*).

5.2.4 Atropine-mediated PDE4 inhibition may trigger arrhythmias

Which functional implications does atropine-mediated PDE4 inhibition have on the heart? It is well accepted that atropine induces tachycardia as a frequent and prominent side effect *in vivo*, which has been mainly attributed to a decreased parasympathetic stimulation. Atropine clearly potentiates ISO-simulated heart rates in perfused Langendorff hearts. An experimental advantage of this approach in contrast to *in vivo* ECG measurements is the exclusion of any nervous tone. Therefore, concerns such as that atropine-driven positive chronotropy as a result from the blockade of a basal vagal tone can be excluded. Likewise, basal activity of M_2 receptor on which atropine might act as an inverse agonist is not relevant, since atropine-mediated augmentation of heart rates is preserved even in M_2-KO mice (*see Figure 24A*). If atropine truly increased cAMP via PDE4 inhibition, this should be also manifested in an enhanced contractile force. Importantly, measurements of sarcomere shortening in isolated adult ventricular cardiomyocytes show that atropine also significantly augments the positive inotropic effect of ISO (*see Figure 24 B, C*).

Unlike in rodent hearts, PDE4 is not the predominant contributor to cAMP hydrolysis in human myocardium. In human atria for instance, PDE4 accounts for only ~15% of the cAMP-specific PDE activity, whereas PDE3 represents the major PDE family[191]. Nevertheless, PDE4 plays an important protective role against atrial arrhythmias, and its effects on cAMP levels can be unmasked by PDE3 inhibition[44]. When measuring contractile forces of trabeculae isolated from human right atria, atropine alone or after sole ISO prestimulation does not affect the force of contraction, but trabeculae pretreated with ISO and cilostamide (PDE3-selective inhibitor) substantially increase contractility upon atropine addition, which can be further augmented by rolipram (PDE4-selective inhibitor) (*see Figure 24 D, E*). This confirms that the stimulatory effect of atropine is also relevant for the human heart and results from PDE4 inhibition. Interestingly, during these experiments, it was noticed that the trabeculae often became arrhythmic after atropine administration.

In summary, it is now evident that atropine, a clinically relevant drug, does not modulate myocardial cAMP solely by preventing Vagus-mediated effects on the heart via muscarinic receptor inhibition. It can furthermore exert PDE4 inhibitor properties. This new mechanism accounts for sustained cAMP signals, especially in situations of missing negative regulation via the parasympathetic nerve drive. Therefore, it can be assumed that this novel effect might play a crucial role in mediating various side effects of atropine, especially arrhythmogenesis. PDE4 inhibition by atropine promotes an increase in intracellular cAMP, heart contractility and contributes to tachycardia. This might be especially important under adrenergic stress which occurs either due to increased endogenous catecholamine levels in heart failure[192] or during diagnostic procedures such as the dobutamine atropine stress echocardiography[129]. One must expect that the effect of atropine inhibiting PDE4 in various other tissues can also account for the pharmacological actions of this drug.

Addressing the hypotension-bradycardia paradox occurring during vasovagal syncope, characterized by a sudden drop in blood pressure and concurrent reflexive fall in heart rate, atropine has been reported to counteract bradycardia but not hypotension. Atropine can be assumed to exert similar effects on both cardiac and vascular PDE4s, though with very diverse functional outcomes. While atropine increases function of the stressed heart by PDE4 inhibition and subsequent cAMP elevation, that same mechanism in vascular smooth muscle can rather stabilize the peripheral vascular resistance or even favor vasodilatation[193,194]

6 Conclusions

6.1 PDE2 is important for myocardial adaptation to long-term stress

Phosphodiesterases are indispensable enzymes in any cell type that reacts to external stimuli via cyclic nucleotide signaling pathways. Especially myocardial tissue possesses a plethora of different cAMP-hydrolyzing PDEs, suggesting that these enzymes do not solely contribute to cAMP signal termination, but do also modulate cyclic nucleotide signals at the subcellular level. But what are the exact roles of these PDE families? The current work exemplifies how cGMP-regulated PDEs such as PDE2 and 3 can act as potential cyclic nucleotide crosstalk hubs. Moreover, by replacing a cGMP-inhibited (PDE3) by the cGMP-stimulated PDE (PDE2) inside the β_2-AR microdomain, the cell can readily shift cAMP microdomains inside single cardiomyocytes in order to adapt to changed environmental conditions (e.g. increased demand on cardiac function in hypertrophy). These observations indicate that cGMP-sensitive PDEs, especially PDE2, which is normally only a minor contributor to myocardial cAMP handling, can serve as an adaptation module used by cardiomyocyte to meet increased demand on functional output. Following this assumption, the cell might respond to long-term stress conditioning by differential expression of PDE2 and 3, thereby causing generally altered cyclic nucleotide signaling (cross-talk) patterns, thus changing cellular perception and physiology. Indications for this phenomenon have also been provided by the recent findings of Mehel et al.[120], which show that PDE2 is upregulated in the failing, heart of rodents and dogs but also in congestive heart failure patients. In contrast, the here presented findings about subcellular PDE2 redistribution despite unchanged cellular PDE2 amounts, occur during an early phase of disease progression. As such, this rather dynamic adaptive molecular response might be readily reversible when early diagnosed. Therefore, preventing PDE2/3 redistribution leading to ANP-stimulatory cardiac responses, could be interesting with regard to clinical intervention, perhaps even to disease prevention strategies.

6.2 PDE4 firstly processes normal short-termed cAMP increases in adult myocardium

In contrast to the findings about cGMP-regulated PDEs 2 and 3, PDE4 has previously been shown to regulate normal cAMP handling in order to prevent arrhythmogenesis, especially in mice[43,102], but importantly even in human[44]. Especially the long PDE4 isoforms possess PKA-dependent phosphorylation motifs for feed-forward regulation[187]. Furthermore, at least for the murine model, different PDE4 families, partly even single PDE4 isoforms have been identified in several functionally crucial cAMP microdomains, especially at EC coupling hubs[43,70,101,102,195]. Such stress-induced negative cAMP regulation represents a perhaps simpler mechanism of enzyme activity modulation, compared to the flexible ANP/cGMP-mediated regulation of PDE2 and PDE3. Therefore, PDE4s, which at least in rodent cardiac tissue contribute the largest fraction of cAMP-PDE activity, are well suited to process and sequester prestimulated cAMP levels during normal beat-to-beat events. As such they are likely being especially important in regulating increased cAMP during short-termed stress, i.e. the fight or flight response. The here presented findings about atropine-mediated PDE4 inhibition well fit into this

context and suggest that this previously unappreciated action of atropine is likely to promote tachyarrhythmias as the most prominent side effect of this drug. Reasoned by this and other frequent side effects, such as nausea or emesis, atropine has been withdrawn from most systemic clinical applications. However, it is still used during organophosphate poisoning or intensive cardiac care. In light of the new findings, even in emergency scenarios, it should be reconsidered to replace atropine by muscarinic receptor antagonists without PDE inhibitor potential in order to avoid unwanted side effects.

7 References

1. Morgado, M., Cairrao, E., Santos-Silva, A.J. & Verde, I. Cyclic nucleotide-dependent relaxation pathways in vascular smooth muscle. *Cellular and molecular life sciences : CMLS* **69**, 247-266 (2012).
2. Altarejos, J.Y. & Montminy, M. CREB and the CRTC co-activators: sensors for hormonal and metabolic signals. *Nature reviews* **12**, 141-151 (2011).
3. Leech, C.A., Chepurny, O.G. & Holz, G.G. Epac2-dependent rap1 activation and the control of islet insulin secretion by glucagon-like peptide-1. *Vitamins and hormones* **84**, 279-302 (2010).
4. Tengholm, A. & Gylfe, E. Oscillatory control of insulin secretion. *Molecular and cellular endocrinology* **297**, 58-72 (2009).
5. Bodor, J.*, et al.* Cyclic AMP underpins suppression by regulatory T cells. *European journal of immunology* **42**, 1375-1384 (2012).
6. Brudvik, K.W. & Tasken, K. Modulation of T cell immune functions by the prostaglandin E(2) - cAMP pathway in chronic inflammatory states. *British journal of pharmacology* **166**, 411-419 (2012).
7. Kandel, E.R. The molecular biology of memory storage: a dialogue between genes and synapses. *Science (New York, N.Y* **294**, 1030-1038 (2001).
8. Lompre, A.M.*, et al.* Ca2+ cycling and new therapeutic approaches for heart failure. *Circulation* **121**, 822-830.
9. Strang, K.T., Sweitzer, N.K., Greaser, M.L. & Moss, R.L. Beta-adrenergic receptor stimulation increases unloaded shortening velocity of skinned single ventricular myocytes from rats. *Circulation research* **74**, 542-549 (1994).
10. Engelhardt, S., Hein, L., Wiesmann, F. & Lohse, M.J. Progressive hypertrophy and heart failure in beta1-adrenergic receptor transgenic mice. *Proceedings of the National Academy of Sciences of the United States of America* **96**, 7059-7064 (1999).
11. Lohse, M.J., Engelhardt, S. & Eschenhagen, T. What is the role of beta-adrenergic signaling in heart failure? *Circulation research* **93**, 896-906 (2003).
12. Michel, M.C., Maisel, A.S. & Brodde, O.E. Mitigation of beta 1- and/or beta 2-adrenoceptor function in human heart failure. *British journal of clinical pharmacology* **30 Suppl 1**, 37S-42S (1990).
13. Narula, J.*, et al.* Apoptosis in myocytes in end-stage heart failure. *The New England journal of medicine* **335**, 1182-1189 (1996).
14. Shizukuda, Y.*, et al.* beta-adrenergic stimulation causes cardiocyte apoptosis: influence of tachycardia and hypertrophy. *The American journal of physiology* **275**, H961-968 (1998).
15. Communal, C., Singh, K., Sawyer, D.B. & Colucci, W.S. Opposing effects of beta(1)- and beta(2)-adrenergic receptors on cardiac myocyte apoptosis : role of a pertussis toxin-sensitive G protein. *Circulation* **100**, 2210-2212 (1999).
16. Milano, C.A.*, et al.* Enhanced myocardial function in transgenic mice overexpressing the beta 2-adrenergic receptor. *Science (New York, N.Y* **264**, 582-586 (1994).
17. Dorn, G.W., 2nd, Tepe, N.M., Lorenz, J.N., Koch, W.J. & Liggett, S.B. Low- and high-level transgenic expression of beta2-adrenergic receptors differentially affect cardiac hypertrophy and function in Galphaq-overexpressing mice. *Proceedings of the National Academy of Sciences of the United States of America* **96**, 6400-6405 (1999).
18. Buxton, I.L. & Brunton, L.L. Compartments of cyclic AMP and protein kinase in mammalian cardiomyocytes. *The Journal of biological chemistry* **258**, 10233-10239 (1983).
19. Di Benedetto, G.*, et al.* Protein kinase A type I and type II define distinct intracellular signaling compartments. *Circulation research* **103**, 836-844 (2008).
20. Vila Petroff, M.G., Egan, J.M., Wang, X. & Sollott, S.J. Glucagon-like peptide-1 increases cAMP but fails to augment contraction in adult rat cardiac myocytes. *Circulation research* **89**, 445-452 (2001).
21. Gloerich, M. & Bos, J.L. Epac: defining a new mechanism for cAMP action. *Annual review of pharmacology and toxicology* **50**, 355-375 (2010).
22. Kawasaki, H.*, et al.* A family of cAMP-binding proteins that directly activate Rap1. *Science (New York, N.Y* **282**, 2275-2279 (1998).
23. Ruiz-Hurtado, G.*, et al.* Epac in cardiac calcium signaling. *Journal of molecular and cellular cardiology* **58**, 162-171 (2013).
24. Berthouze, M., Laurent, A.C., Breckler, M. & Lezoualc'h, F. New perspectives in cAMP-signaling modulation. *Current heart failure reports* **8**, 159-167.
25. Metrich, M.*, et al.* Epac mediates beta-adrenergic receptor-induced cardiomyocyte hypertrophy. *Circulation research* **102**, 959-965 (2008).

26. Zhang, X.*, et al.* Cardiotoxic and cardioprotective features of chronic beta-adrenergic signaling. *Circulation research* **112**, 498-509 (2013).
27. Mangmool, S., Shukla, A.K. & Rockman, H.A. beta-Arrestin-dependent activation of Ca(2+)/calmodulin kinase II after beta(1)-adrenergic receptor stimulation. *The Journal of cell biology* **189**, 573-587 (2010).
28. Soltis, A.R. & Saucerman, J.J. Synergy between CaMKII substrates and beta-adrenergic signaling in regulation of cardiac myocyte Ca(2+) handling. *Biophysical journal* **99**, 2038-2047 (2010).
29. Brooker, G., Harper, J.F., Terasaki, W.L. & Moylan, R.D. Radioimmunoassay of cyclic AMP and cyclic GMP. *Advances in cyclic nucleotide research* **10**, 1-33 (1979).
30. Williams, C. cAMP detection methods in HTS: selecting the best from the rest. *Nature reviews. Drug discovery* **3**, 125-135 (2004).
31. Nikolaev, V.O. & Lohse, M.J. Monitoring of cAMP synthesis and degradation in living cells. *Physiology* **21**, 86-92 (2006).
32. Willoughby, D. & Cooper, D.M. Live-cell imaging of cAMP dynamics. *Nature methods* **5**, 29-36 (2008).
33. Förster, T. Zwischenmolekulare Energiewanderung. *Annalen der Physik* **437**, 55-75 (1948).
34. Adams, S.R., Harootunian, A.T., Buechler, Y.J., Taylor, S.S. & Tsien, R.Y. Fluorescence ratio imaging of cyclic AMP in single cells. *Nature* **349**, 694-697 (1991).
35. DiPilato, L.M., Cheng, X. & Zhang, J. Fluorescent indicators of cAMP and Epac activation reveal differential dynamics of cAMP signaling within discrete subcellular compartments. *Proceedings of the National Academy of Sciences of the United States of America* **101**, 16513-16518 (2004).
36. Nikolaev, V.O., Bunemann, M., Hein, L., Hannawacker, A. & Lohse, M.J. Novel single chain cAMP sensors for receptor-induced signal propagation. *The Journal of biological chemistry* **279**, 37215-37218 (2004).
37. Nikolaev, V.O., Bunemann, M., Schmitteckert, E., Lohse, M.J. & Engelhardt, S. Cyclic AMP imaging in adult cardiac myocytes reveals far-reaching beta1-adrenergic but locally confined beta2-adrenergic receptor-mediated signaling. *Circulation research* **99**, 1084-1091 (2006).
38. Ponsioen, B.*, et al.* Detecting cAMP-induced Epac activation by fluorescence resonance energy transfer: Epac as a novel cAMP indicator. *EMBO reports* **5**, 1176-1180 (2004).
39. Zaccolo, M. & Pozzan, T. Discrete microdomains with high concentration of cAMP in stimulated rat neonatal cardiac myocytes. *Science (New York, N.Y* **295**, 1711-1715 (2002).
40. Kirshenbaum, L.A., MacLellan, W.R., Mazur, W., French, B.A. & Schneider, M.D. Highly efficient gene transfer into adult ventricular myocytes by recombinant adenovirus. *The Journal of clinical investigation* **92**, 381-387 (1993).
41. Chakir, K.*, et al.* RGS2 is a primary terminator of beta(2)-adrenergic receptor-mediated G(i) signaling. *Journal of molecular and cellular cardiology* **50**, 1000-1007.
42. Kabaeva, Z., Zhao, M. & Michele, D.E. Blebbistatin extends culture life of adult mouse cardiac myocytes and allows efficient and stable transgene expression. *American journal of physiology* **294**, H1667-1674 (2008).
43. Lehnart, S.E.*, et al.* Phosphodiesterase 4D deficiency in the ryanodine-receptor complex promotes heart failure and arrhythmias. *Cell* **123**, 25-35 (2005).
44. Molina, C.E.*, et al.* Cyclic adenosine monophosphate phosphodiesterase type 4 protects against atrial arrhythmias. *Journal of the American College of Cardiology* **59**, 2182-2190 (2012).
45. Horackova, M. & Byczko, Z. Differences in the structural characteristics of adult guinea pig and rat cardiomyocytes during their adaptation and maintenance in long-term cultures: confocal microscopy study. *Experimental cell research* **237**, 158-175 (1997).
46. Calebiro, D.*, et al.* Persistent cAMP-signals triggered by internalized G-protein-coupled receptors. *PLoS biology* **7**, e1000172 (2009).
47. Sin, Y.Y.*, et al.* Disruption of the cyclic AMP phosphodiesterase-4 (PDE4)-HSP20 complex attenuates the beta-agonist induced hypertrophic response in cardiac myocytes. *Journal of molecular and cellular cardiology* **50**, 872-883 (2011).
48. Stangherlin, A.*, et al.* cGMP signals modulate cAMP levels in a compartment-specific manner to regulate catecholamine-dependent signaling in cardiac myocytes. *Circulation research* **108**, 929-939 (2011).
49. Jiang, L.I.*, et al.* Use of a cAMP BRET sensor to characterize a novel regulation of cAMP by the sphingosine 1-phosphate/G13 pathway. *The Journal of biological chemistry* **282**, 10576-10584 (2007).
50. Brunton, L.L., Hayes, J.S. & Mayer, S.E. Functional compartmentation of cyclic AMP and protein kinase in heart. *Advances in cyclic nucleotide research* **14**, 391-397 (1981).

51. Jurevicius, J. & Fischmeister, R. cAMP compartmentation is responsible for a local activation of cardiac Ca2+ channels by beta-adrenergic agonists. *Proceedings of the National Academy of Sciences of the United States of America* **93**, 295-299 (1996).
52. Perera, R.K. & Nikolaev, V.O. Compartmentation of cAMP signalling in cardiomyocytes in health and disease. *Acta physiologica* **207**, 650-662 (2013).
53. Diviani, D., Dodge-Kafka, K.L., Li, J. & Kapiloff, M.S. A-kinase anchoring proteins: scaffolding proteins in the heart. *American journal of physiology* **301**, H1742-1753 (2011).
54. Perino, A., Ghigo, A., Scott, J.D. & Hirsch, E. Anchoring proteins as regulators of signaling pathways. *Circulation research* **111**, 482-492 (2012).
55. Scott, J.D., Dessauer, C.W. & Tasken, K. Creating order from chaos: cellular regulation by kinase anchoring. *Annual review of pharmacology and toxicology* **53**, 187-210 (2013).
56. Scott, J.D. & Santana, L.F. A-kinase anchoring proteins: getting to the heart of the matter. *Circulation* **121**, 1264-1271 (2010).
57. Troger, J., Moutty, M.C., Skroblin, P. & Klussmann, E. A-kinase anchoring proteins as potential drug targets. *British journal of pharmacology* **166**, 420-433 (2012).
58. Mauban, J.R., O'Donnell, M., Warrier, S., Manni, S. & Bond, M. AKAP-scaffolding proteins and regulation of cardiac physiology. *Physiology* **24**, 78-87 (2009).
59. Dodge-Kafka, K.L., Langeberg, L. & Scott, J.D. Compartmentation of cyclic nucleotide signaling in the heart: the role of A-kinase anchoring proteins. *Circulation research* **98**, 993-1001 (2006).
60. Dodge, K.L*., et al.* mAKAP assembles a protein kinase A/PDE4 phosphodiesterase cAMP signaling module. *The EMBO journal* **20**, 1921-1930 (2001).
61. Marx, S.O*., et al.* PKA phosphorylation dissociates FKBP12.6 from the calcium release channel (ryanodine receptor): defective regulation in failing hearts. *Cell* **101**, 365-376 (2000).
62. Nichols, C.B*., et al.* Sympathetic stimulation of adult cardiomyocytes requires association of AKAP5 with a subpopulation of L-type calcium channels. *Circulation research* **107**, 747-756 (2010).
63. Hulme, J.T., Lin, T.W., Westenbroek, R.E., Scheuer, T. & Catterall, W.A. Beta-adrenergic regulation requires direct anchoring of PKA to cardiac CaV1.2 channels via a leucine zipper interaction with A kinase-anchoring protein 15. *Proceedings of the National Academy of Sciences of the United States of America* **100**, 13093-13098 (2003).
64. Lefkowitz, R.J. & Shenoy, S.K. Transduction of receptor signals by beta-arrestins. *Science (New York, N.Y* **308**, 512-517 (2005).
65. Luttrell, L.M. & Lefkowitz, R.J. The role of beta-arrestins in the termination and transduction of G-protein-coupled receptor signals. *Journal of cell science* **115**, 455-465 (2002).
66. Ungerer, M*., et al.* Expression of beta-arrestins and beta-adrenergic receptor kinases in the failing human heart. *Circulation research* **74**, 206-213 (1994).
67. Baillie, G.S. & Houslay, M.D. Arrestin times for compartmentalised cAMP signalling and phosphodiesterase-4 enzymes. *Current opinion in cell biology* **17**, 129-134 (2005).
68. Baillie, G.S*., et al.* beta-Arrestin-mediated PDE4 cAMP phosphodiesterase recruitment regulates beta-adrenoceptor switching from Gs to Gi. *Proceedings of the National Academy of Sciences of the United States of America* **100**, 940-945 (2003).
69. Perry, S.J*., et al.* Targeting of cyclic AMP degradation to beta 2-adrenergic receptors by beta-arrestins. *Science (New York, N.Y* **298**, 834-836 (2002).
70. Richter, W*., et al.* Signaling from beta1- and beta2-adrenergic receptors is defined by differential interactions with PDE4. *The EMBO journal* **27**, 384-393 (2008).
71. Ghigo, A*., et al.* Phosphoinositide 3-kinase gamma protects against catecholamine-induced ventricular arrhythmia through protein kinase A-mediated regulation of distinct phosphodiesterases. *Circulation* **126**, 2073-2083 (2012).
72. Kuschel, M*., et al.* beta2-adrenergic cAMP signaling is uncoupled from phosphorylation of cytoplasmic proteins in canine heart. *Circulation* **99**, 2458-2465 (1999).
73. Liu, Q.H*., et al.* Membrane depolarization causes a direct activation of G protein-coupled receptors leading to local Ca2+ release in smooth muscle. *Proceedings of the National Academy of Sciences of the United States of America* **106**, 11418-11423 (2009).
74. Xiao, R.P. Beta-adrenergic signaling in the heart: dual coupling of the beta2-adrenergic receptor to G(s) and G(i) proteins. *Sci STKE* **2001**, re15 (2001).
75. Bernstein, D*., et al.* Differential cardioprotective/cardiotoxic effects mediated by beta-adrenergic receptor subtypes. *American journal of physiology* **289**, H2441-2449 (2005).
76. Patterson, A.J*., et al.* Protecting the myocardium: a role for the beta2 adrenergic receptor in the heart. *Critical care medicine* **32**, 1041-1048 (2004).

77. Novak, P.*, et al.* Nanoscale live-cell imaging using hopping probe ion conductance microscopy. *Nature methods* **6**, 279-281 (2009).
78. Nikolaev, V.O.*, et al.* Beta2-adrenergic receptor redistribution in heart failure changes cAMP compartmentation. *Science (New York, N.Y* **327**, 1653-1657 (2010).
79. Conti, M. & Beavo, J. Biochemistry and physiology of cyclic nucleotide phosphodiesterases: essential components in cyclic nucleotide signaling. *Annual review of biochemistry* **76**, 481-511 (2007).
80. Fischmeister, R.*, et al.* Compartmentation of cyclic nucleotide signaling in the heart: the role of cyclic nucleotide phosphodiesterases. *Circulation research* **99**, 816-828 (2006).
81. Houslay, M.D., Baillie, G.S. & Maurice, D.H. cAMP-Specific phosphodiesterase-4 enzymes in the cardiovascular system: a molecular toolbox for generating compartmentalized cAMP signaling. *Circulation research* **100**, 950-966 (2007).
82. Osadchii, O.E. Myocardial phosphodiesterases and regulation of cardiac contractility in health and cardiac disease. *Cardiovasc Drugs Ther* **21**, 171-194 (2007).
83. Zaccolo, M. & Movsesian, M.A. cAMP and cGMP signaling cross-talk: role of phosphodiesterases and implications for cardiac pathophysiology. *Circulation research* **100**, 1569-1578 (2007).
84. Sonnenburg, W.K., Seger, D. & Beavo, J.A. Molecular cloning of a cDNA encoding the "61-kDa" calmodulin-stimulated cyclic nucleotide phosphodiesterase. Tissue-specific expression of structurally related isoforms. *The Journal of biological chemistry* **268**, 645-652 (1993).
85. Miller, C.L. & Yan, C. Targeting cyclic nucleotide phosphodiesterase in the heart: therapeutic implications. *Journal of cardiovascular translational research* **3**, 507-515 (2010).
86. Dunkern, T.R. & Hatzelmann, A. Characterization of inhibitors of phosphodiesterase 1C on a human cellular system. *The FEBS journal* **274**, 4812-4824 (2007).
87. Han, P., Werber, J., Surana, M., Fleischer, N. & Michaeli, T. The calcium/calmodulin-dependent phosphodiesterase PDE1C down-regulates glucose-induced insulin secretion. *The Journal of biological chemistry* **274**, 22337-22344 (1999).
88. Miller, C.L.*, et al.* Role of Ca2+/calmodulin-stimulated cyclic nucleotide phosphodiesterase 1 in mediating cardiomyocyte hypertrophy. *Circulation research* **105**, 956-964 (2009).
89. Nagel, D.J.*, et al.* Role of nuclear Ca2+/calmodulin-stimulated phosphodiesterase 1A in vascular smooth muscle cell growth and survival. *Circulation research* **98**, 777-784 (2006).
90. Rybalkin, S.D., Rybalkina, I., Beavo, J.A. & Bornfeldt, K.E. Cyclic nucleotide phosphodiesterase 1C promotes human arterial smooth muscle cell proliferation. *Circulation research* **90**, 151-157 (2002).
91. Martinez, S.E.*, et al.* The two GAF domains in phosphodiesterase 2A have distinct roles in dimerization and in cGMP binding. *Proceedings of the National Academy of Sciences of the United States of America* **99**, 13260-13265 (2002).
92. Castro, L.R., Verde, I., Cooper, D.M. & Fischmeister, R. Cyclic guanosine monophosphate compartmentation in rat cardiac myocytes. *Circulation* **113**, 2221-2228 (2006).
93. Mongillo, M.*, et al.* Compartmentalized phosphodiesterase-2 activity blunts beta-adrenergic cardiac inotropy via an NO/cGMP-dependent pathway. *Circulation research* **98**, 226-234 (2006).
94. Patrucco, E.*, et al.* PI3Kgamma modulates the cardiac response to chronic pressure overload by distinct kinase-dependent and -independent effects. *Cell* **118**, 375-387 (2004).
95. Abi-Gerges, A.*, et al.* Decreased expression and activity of cAMP phosphodiesterases in cardiac hypertrophy and its impact on beta-adrenergic cAMP signals. *Circulation research* **105**, 784-792 (2009).
96. Wechsler, J.*, et al.* Isoforms of cyclic nucleotide phosphodiesterase PDE3A in cardiac myocytes. *The Journal of biological chemistry* **277**, 38072-38078 (2002).
97. Weishaar, R.E., Kobylarz-Singer, D.C. & Kaplan, H.R. Subclasses of cyclic AMP phosphodiesterase in cardiac muscle. *Journal of molecular and cellular cardiology* **19**, 1025-1036 (1987).
98. Houslay, M.D. & Adams, D.R. PDE4 cAMP phosphodiesterases: modular enzymes that orchestrate signalling cross-talk, desensitization and compartmentalization. *The Biochemical journal* **370**, 1-18 (2003).
99. Kostic, M.M.*, et al.* Altered expression of PDE1 and PDE4 cyclic nucleotide phosphodiesterase isoforms in 7-oxo-prostacyclin-preconditioned rat heart. *Journal of molecular and cellular cardiology* **29**, 3135-3146 (1997).
100. Richter, W.*, et al.* Conserved expression and functions of PDE4 in rodent and human heart. *Basic research in cardiology* **106**, 249-262 (2011).
101. Leroy, J.*, et al.* Phosphodiesterase 4B in the cardiac L-type Ca(2)(+) channel complex regulates Ca(2)(+) current and protects against ventricular arrhythmias in mice. *The Journal of clinical investigation* **121**, 2651-2661 (2011).

102. Beca, S.*, et al.* Phosphodiesterase 4D regulates baseline sarcoplasmic reticulum Ca2+ release and cardiac contractility, independently of L-type Ca2+ current. *Circulation research* **109**, 1024-1030 (2011).
103. Kerfant, B.G.*, et al.* PI3Kgamma is required for PDE4, not PDE3, activity in subcellular microdomains containing the sarcoplasmic reticular calcium ATPase in cardiomyocytes. *Circulation research* **101**, 400-408 (2007).
104. Soderling, S.H., Bayuga, S.J. & Beavo, J.A. Cloning and characterization of a cAMP-specific cyclic nucleotide phosphodiesterase. *Proceedings of the National Academy of Sciences of the United States of America* **95**, 8991-8996 (1998).
105. Patrucco, E., Albergine, M.S., Santana, L.F. & Beavo, J.A. Phosphodiesterase 8A (PDE8A) regulates excitation-contraction coupling in ventricular myocytes. *Journal of molecular and cellular cardiology* **49**, 330-333 (2010).
106. Brown, K.M., Lee, L.C., Findlay, J.E., Day, J.P. & Baillie, G.S. Cyclic AMP-specific phosphodiesterase, PDE8A1, is activated by protein kinase A-mediated phosphorylation. *FEBS letters* **586**, 1631-1637 (2012).
107. Ganau, A.*, et al.* Patterns of left ventricular hypertrophy and geometric remodeling in essential hypertension. *Journal of the American College of Cardiology* **19**, 1550-1558 (1992).
108. Bristow, M.R.*, et al.* Decreased catecholamine sensitivity and beta-adrenergic-receptor density in failing human hearts. *The New England journal of medicine* **307**, 205-211 (1982).
109. Ungerer, M., Bohm, M., Elce, J.S., Erdmann, E. & Lohse, M.J. Altered expression of beta-adrenergic receptor kinase and beta 1-adrenergic receptors in the failing human heart. *Circulation* **87**, 454-463 (1993).
110. Kuhn, M. Structure, regulation, and function of mammalian membrane guanylyl cyclase receptors, with a focus on guanylyl cyclase-A. *Circulation research* **93**, 700-709 (2003).
111. Potter, L.R. Guanylyl cyclase structure, function and regulation. *Cellular signalling* **23**, 1921-1926 (2011).
112. Zakhary, D.R., Moravec, C.S. & Bond, M. Regulation of PKA binding to AKAPs in the heart: alterations in human heart failure. *Circulation* **101**, 1459-1464 (2000).
113. Shan, J.*, et al.* Role of chronic ryanodine receptor phosphorylation in heart failure and beta-adrenergic receptor blockade in mice. *The Journal of clinical investigation* **120**, 4375-4387 (2010).
114. Shan, J.*, et al.* Phosphorylation of the ryanodine receptor mediates the cardiac fight or flight response in mice. *The Journal of clinical investigation* **120**, 4388-4398 (2010).
115. Wehrens, X.H.*, et al.* FKBP12.6 deficiency and defective calcium release channel (ryanodine receptor) function linked to exercise-induced sudden cardiac death. *Cell* **113**, 829-840 (2003).
116. Bittar, G. & Friedman, H.S. The arrhythmogenicity of theophylline. A multivariate analysis of clinical determinants. *Chest* **99**, 1415-1420 (1991).
117. Maier, L.S., Bers, D.M. & Brown, J.H. Calmodulin and Ca2+/calmodulin kinases in the heart - physiology and pathophysiology. *Cardiovascular research* **73**, 629-630 (2007).
118. Neef, S.*, et al.* CaMKII-dependent diastolic SR Ca2+ leak and elevated diastolic Ca2+ levels in right atrial myocardium of patients with atrial fibrillation. *Circulation research* **106**, 1134-1144 (2010).
119. Kashimura, T.*, et al.* In the RyR2(R4496C) mouse model of CPVT, beta-adrenergic stimulation induces Ca waves by increasing SR Ca content and not by decreasing the threshold for Ca waves. *Circulation research* **107**, 1483-1489 (2010).
120. Mehel, H.*, et al.* Phosphodiesterase-2 is up-regulated in human failing hearts and blunts beta-adrenergic responses in cardiomyocytes. *Journal of the American College of Cardiology* **62**, 1596-1606 (2013).
121. Zakharov, S.I., Wagner, R.A. & Harvey, R.D. Muscarinic regulation of the cardiac CFTR Cl- current by quaternary ammonium compounds. *The Journal of pharmacology and experimental therapeutics* **273**, 470-481 (1995).
122. Hulme, E.C., Birdsall, N.J. & Buckley, N.J. Muscarinic receptor subtypes. *Annual review of pharmacology and toxicology* **30**, 633-673 (1990).
123. Brodde, O.E. & Michel, M.C. Adrenergic and muscarinic receptors in the human heart. *Pharmacological reviews* **51**, 651-690 (1999).
124. Chapman, K.R.*, et al.* Epidemiology and costs of chronic obstructive pulmonary disease. *The European respiratory journal* **27**, 188-207 (2006).
125. Lee, M.R. Solanaceae IV: Atropa belladonna, deadly nightshade. *The journal of the Royal College of Physicians of Edinburgh* **37**, 77-84 (2007).

126. Scullion, J.E. The development of anticholinergics in the management of COPD. *International journal of chronic obstructive pulmonary disease* **2**, 33-40 (2007).
127. Oba, Y. Cost-effectiveness of long-acting bronchodilators for chronic obstructive pulmonary disease. *Mayo Clinic proceedings* **82**, 575-582 (2007).
128. Restrepo, R.D. Use of inhaled anticholinergic agents in obstructive airway disease. *Respiratory care* **52**, 833-851 (2007).
129. Geleijnse, M.L*., et al.* Incidence, pathophysiology, and treatment of complications during dobutamine-atropine stress echocardiography. *Circulation* **121**, 1756-1767 (2010).
130. Ecc Committee, S. & Task Forces of the American Heart, A. 2005 American Heart Association Guidelines for Cardiopulmonary Resuscitation and Emergency Cardiovascular Care. *Circulation* **112**, IV1-203 (2005).
131. Dauchot, P. & Gravenstein, J.S. Effects of atropine on the electrocardiogram in different age groups. *Clinical pharmacology and therapeutics* **12**, 274-280 (1971).
132. Wellstein, A. & Pitschner, H.F. Complex dose-response curves of atropine in man explained by different functions of M1- and M2-cholinoceptors. *Naunyn-Schmiedeberg's archives of pharmacology* **338**, 19-27 (1988).
133. Epstein, A.E*., et al.* Evidence for a central site of action to explain the negative chronotropic effect of atropine: studies on the human transplanted heart. *Journal of the American College of Cardiology* **15**, 1610-1617 (1990).
134. Montano, N*., et al.* Central vagotonic effects of atropine modulate spectral oscillations of sympathetic nerve activity. *Circulation* **98**, 1394-1399 (1998).
135. Brown, W.M. Treating COPD with PDE 4 inhibitors. *International journal of chronic obstructive pulmonary disease* **2**, 517-533 (2007).
136. Dyke, H.J. & Montana, J.G. Update on the therapeutic potential of PDE4 inhibitors. *Expert opinion on investigational drugs* **11**, 1-13 (2002).
137. Kaiho, Y*., et al.* The effects of a type 4 phosphodiesterase inhibitor and the muscarinic cholinergic antagonist tolterodine tartrate on detrusor overactivity in female rats with bladder outlet obstruction. *BJU international* **101**, 615-620 (2008).
138. Yougbare, I*., et al.* NCS 613, a potent and specific PDE4 inhibitor, displays anti-inflammatory effects on human lung tissues. *American journal of physiology. Lung cellular and molecular physiology* **301**, L441-450 (2011).
139. Lagente, V., Martin-Chouly, C., Boichot, E., Martins, M.A. & Silva, P.M. Selective PDE4 inhibitors as potent anti-inflammatory drugs for the treatment of airway diseases. *Memorias do Instituto Oswaldo Cruz* **100 Suppl 1**, 131-136 (2005).
140. Rolan, P., Hutchinson, M. & Johnson, K. Ibudilast: a review of its pharmacology, efficacy and safety in respiratory and neurological disease. *Expert opinion on pharmacotherapy* **10**, 2897-2904 (2009).
141. Nishiguchi, J*., et al.* Suppression of detrusor overactivity in rats with bladder outlet obstruction by a type 4 phosphodiesterase inhibitor. *BJU international* **99**, 680-686 (2007).
142. Ribeiro, A.S*., et al.* Powerful relaxation of phosphodiesterase type 4 inhibitor rolipram in the pig and human bladder neck. *The journal of sexual medicine* **11**, 930-941 (2014).
143. Galindo-Tovar, A. & Kaumann, A.J. Phosphodiesterase-4 blunts inotropism and arrhythmias but not sinoatrial tachycardia of (-)-adrenaline mediated through mouse cardiac beta(1)-adrenoceptors. *British journal of pharmacology* **153**, 710-720 (2008).
144. Ding, B*., et al.* Functional role of phosphodiesterase 3 in cardiomyocyte apoptosis: implication in heart failure. *Circulation* **111**, 2469-2476 (2005).
145. Wachten, S*., et al.* Distinct pools of cAMP centre on different isoforms of adenylyl cyclase in pituitary-derived GH3B6 cells. *Journal of cell science* **123**, 95-106 (2010).
146. Herget, S., Lohse, M.J. & Nikolaev, V.O. Real-time monitoring of phosphodiesterase inhibition in intact cells. *Cellular signalling* **20**, 1423-1431 (2008).
147. Buitrago, M*., et al.* The transcriptional repressor Nab1 is a specific regulator of pathological cardiac hypertrophy. *Nature medicine* **11**, 837-844 (2005).
148. Sprenger, J.U., Perera, R.K., Gotz, K.R. & Nikolaev, V.O. FRET microscopy for real-time monitoring of signaling events in live cells using unimolecular biosensors. *Journal of visualized experiments : JoVE*, e4081 (2012).
149. Gorelik, J*., et al.* A novel Z-groove index characterizing myocardial surface structure. *Cardiovasc Res* **72**, 422-429 (2006).

150. Hu, P.*, et al.* Minimally invasive aortic banding in mice: effects of altered cardiomyocyte insulin signaling during pressure overload. *American journal of physiology. Heart and circulatory physiology* **285**, H1261-1269 (2003).
151. Wagner, E.*, et al.* Stimulated emission depletion live-cell super-resolution imaging shows proliferative remodeling of T-tubule membrane structures after myocardial infarction. *Circulation research* **111**, 402-414 (2012).
152. Simpson, I.A. & Sahn, D.J. Comparative imaging techniques and models. *Current opinion in cardiology* **8**, 1021-1026 (1993).
153. Paur, H.*, et al.* High levels of circulating epinephrine trigger apical cardiodepression in a beta2-adrenergic receptor/Gi-dependent manner: a new model of Takotsubo cardiomyopathy. *Circulation* **126**, 697-706 (2012).
154. Thompson, W.J. & Appleman, M.M. Multiple cyclic nucleotide phosphodiesterase activities from rat brain. *Biochemistry* **10**, 311-316 (1971).
155. Richter, W. & Conti, M. Dimerization of the type 4 cAMP-specific phosphodiesterases is mediated by the upstream conserved regions (UCRs). *The Journal of biological chemistry* **277**, 40212-40221 (2002).
156. Laemmli, U.K. Cleavage of structural proteins during the assembly of the head of bacteriophage T4. *Nature* **227**, 680-685 (1970).
157. Towbin, H., Staehelin, T. & Gordon, J. Electrophoretic transfer of proteins from polyacrylamide gels to nitrocellulose sheets: procedure and some applications. *Proceedings of the National Academy of Sciences of the United States of America* **76**, 4350-4354 (1979).
158. Zacharias, D.A., Violin, J.D., Newton, A.C. & Tsien, R.Y. Partitioning of lipid-modified monomeric GFPs into membrane microdomains of live cells. *Science (New York, N.Y* **296**, 913-916 (2002).
159. Klaiber, M.*, et al.* A cardiac pathway of cyclic GMP-independent signaling of guanylyl cyclase A, the receptor for atrial natriuretic peptide. *Proceedings of the National Academy of Sciences of the United States of America* **108**, 18500-18505 (2011).
160. Rose, R.A. & Giles, W.R. Natriuretic peptide C receptor signalling in the heart and vasculature. *The Journal of physiology* **586**, 353-366 (2008).
161. Maack, T.*, et al.* Physiological role of silent receptors of atrial natriuretic factor. *Science (New York, N.Y* **238**, 675-678 (1987).
162. Iancu, R.V.*, et al.* Cytoplasmic cAMP concentrations in intact cardiac myocytes. *American journal of physiology. Cell physiology* **295**, C414-422 (2008).
163. Guerra de Gonzalez, L., Gonzalez de Alfonzo, R., Lippo de Becemberg, I. & Alfonzo, M.J. Cyclic nucleotide-dependent phosphodiesterases (PDEI) inhibition by muscarinic antagonists in bovine tracheal smooth muscle. *Biochem Pharmacol* **68**, 651-658 (2004).
164. Francis, S.H., Blount, M.A. & Corbin, J.D. Mammalian cyclic nucleotide phosphodiesterases: molecular mechanisms and physiological functions. *Physiol Rev* **91**, 651-690 (2011).
165. Sawyer, G.W., Ehlert, F.J. & Shults, C.A. A conserved motif in the membrane proximal C-terminal tail of human muscarinic m1 acetylcholine receptors affects plasma membrane expression. *J Pharmacol Exp Ther* **332**, 76-86 (2010).
166. Ward, S.D., Hamdan, F.F., Bloodworth, L.M. & Wess, J. Conformational changes that occur during M3 muscarinic acetylcholine receptor activation probed by the use of an in situ disulfide cross-linking strategy. *The Journal of biological chemistry* **277**, 2247-2257 (2002).
167. Muller, J.*, et al.* Drug specificity and intestinal membrane localization of human organic cation transporters (OCT). *Biochemical pharmacology* **70**, 1851-1860 (2005).
168. Leroy, J.*, et al.* Spatiotemporal dynamics of beta-adrenergic cAMP signals and L-type Ca2+ channel regulation in adult rat ventricular myocytes: role of phosphodiesterases. *Circulation research* **102**, 1091-1100 (2008).
169. Rochais, F.*, et al.* A specific pattern of phosphodiesterases controls the cAMP signals generated by different Gs-coupled receptors in adult rat ventricular myocytes. *Circulation research* **98**, 1081-1088 (2006).
170. Brady, J.D.*, et al.* Functional role of lipid raft microdomains in cyclic nucleotide-gated channel activation. *Molecular pharmacology* **65**, 503-511 (2004).
171. Head, B.P.*, et al.* G-protein-coupled receptor signaling components localize in both sarcolemmal and intracellular caveolin-3-associated microdomains in adult cardiac myocytes. *The Journal of biological chemistry* **280**, 31036-31044 (2005).
172. Macdougall, D.A.*, et al.* Caveolae compartmentalise beta2-adrenoceptor signals by curtailing cAMP production and maintaining phosphatase activity in the sarcoplasmic reticulum of the adult ventricular myocyte. *Journal of molecular and cellular cardiology* **52**, 388-400.

173. Steinberg, S.F. beta(2)-Adrenergic receptor signaling complexes in cardiomyocyte caveolae/lipid rafts. *Journal of molecular and cellular cardiology* **37**, 407-415 (2004).
174. Haluzik, M.*, et al.* Genetic background (C57BL/6J versus FVB/N) strongly influences the severity of diabetes and insulin resistance in ob/ob mice. *Endocrinology* **145**, 3258-3264 (2004).
175. Knott, M.L., Hogan, S.P., Wang, H., Matthaei, K.I. & Dent, L.A. FVB/N mice are highly resistant to primary infection with Nippostrongylus brasiliensis. *Parasitology* **136**, 93-106 (2009).
176. Takimoto, E.*, et al.* Compartmentalization of cardiac beta-adrenergic inotropy modulation by phosphodiesterase type 5. *Circulation* **115**, 2159-2167 (2007).
177. Steinberg, S.F. & Brunton, L.L. Compartmentation of G protein-coupled signaling pathways in cardiac myocytes. *Annual review of pharmacology and toxicology* **41**, 751-773 (2001).
178. Hu, F., Ren, J., Zhang, J.E., Zhong, W. & Luo, M. Natriuretic peptides block synaptic transmission by activating phosphodiesterase 2A and reducing presynaptic PKA activity. *Proceedings of the National Academy of Sciences of the United States of America* **109**, 17681-17686 (2012).
179. Surapisitchat, J., Jeon, K.I., Yan, C. & Beavo, J.A. Differential regulation of endothelial cell permeability by cGMP via phosphodiesterases 2 and 3. *Circulation research* **101**, 811-818 (2007).
180. Dunkern, T.R. & Hatzelmann, A. The effect of Sildenafil on human platelet secretory function is controlled by a complex interplay between phosphodiesterases 2, 3 and 5. *Cellular signalling* **17**, 331-339 (2005).
181. Nikolaev, V.O., Gambaryan, S., Engelhardt, S., Walter, U. & Lohse, M.J. Real-time monitoring of the PDE2 activity of live cells: hormone-stimulated cAMP hydrolysis is faster than hormone-stimulated cAMP synthesis. *The Journal of biological chemistry* **280**, 1716-1719 (2005).
182. Hilf, G. & Jakobs, K.H. Agonist-independent inhibition of G protein activation by muscarinic acetylcholine receptor antagonists in cardiac membranes. *European journal of pharmacology* **225**, 245-252 (1992).
183. Federman, A.D., Conklin, B.R., Schrader, K.A., Reed, R.R. & Bourne, H.R. Hormonal stimulation of adenylyl cyclase through Gi-protein beta gamma subunits. *Nature* **356**, 159-161 (1992).
184. Tang, W.J. & Gilman, A.G. Type-specific regulation of adenylyl cyclase by G protein beta gamma subunits. *Science (New York, N.Y* **254**, 1500-1503 (1991).
185. Gomeza, J.*, et al.* Pronounced pharmacologic deficits in M2 muscarinic acetylcholine receptor knockout mice. *Proceedings of the National Academy of Sciences of the United States of America* **96**, 1692-1697 (1999).
186. Hanf, R., Li, Y., Szabo, G. & Fischmeister, R. Agonist-independent effects of muscarinic antagonists on Ca2+ and K+ currents in frog and rat cardiac cells. *The Journal of physiology* **461**, 743-765 (1993).
187. Sette, C. & Conti, M. Phosphorylation and activation of a cAMP-specific phosphodiesterase by the cAMP-dependent protein kinase. Involvement of serine 54 in the enzyme activation. *The Journal of biological chemistry* **271**, 16526-16534 (1996).
188. Nikolaev, V.O., Gambaryan, S. & Lohse, M.J. Fluorescent sensors for rapid monitoring of intracellular cGMP. *Nature methods* **3**, 23-25 (2006).
189. Jacobitz, S., McLaughlin, M.M., Livi, G.P., Burman, M. & Torphy, T.J. Mapping the functional domains of human recombinant phosphodiesterase 4A: structural requirements for catalytic activity and rolipram binding. *Molecular pharmacology* **50**, 891-899 (1996).
190. Klaassen, C.D. & Aleksunes, L.M. Xenobiotic, bile acid, and cholesterol transporters: function and regulation. *Pharmacological reviews* **62**, 1-96 (2010).
191. Christ, T., Engel, A., Ravens, U. & Kaumann, A.J. Cilostamide potentiates more the positive inotropic effects of (-)-adrenaline through beta(2)-adrenoceptors than the effects of (-)-noradrenaline through beta (1)-adrenoceptors in human atrial myocardium. *Naunyn-Schmiedeberg's archives of pharmacology* **374**, 249-253 (2006).
192. Olshansky, B., Sabbah, H.N., Hauptman, P.J. & Colucci, W.S. Parasympathetic nervous system and heart failure: pathophysiology and potential implications for therapy. *Circulation* **118**, 863-871 (2008).
193. Lewis, T. A Lecture on VASOVAGAL SYNCOPE AND THE CAROTID SINUS MECHANISM. *British medical journal* **1**, 873-876 (1932).
194. Prakash, E.S. & Madanmohan. When the heart is stopped for good: hypotension-bradycardia paradox revisited. *Advances in physiology education* **29**, 15-20 (2005).
195. Mika, D., Richter, W., Westenbroek, R.E., Catterall, W.A. & Conti, M. PDE4B mediates local feedback regulation of beta1-adrenergic cAMP signaling in a sarcolemmal compartment of cardiac myocytes. *Journal of cell science* **127**, 1033-1042 (2014).

Acknowledgements

The presented PhD thesis was performed at the Heart Research Center Göttingen, in the research work group “Molecular imaging of the heart” under supervision of Dr. Viacheslav O. Nikolaev.
I address my sincere gratitude to the members of my thesis committee, Prof. Dr. Blanche Schwappach, Prof. Dr. Stefan Luther, Prof. Dr. Dörthe Katschinski and Prof. Dr. Ali-El-Armouche for their challenging and encouraging feedback and vivid discussions throughout all committee meetings, with the intention of putting up the best strategies possible to conquer the topics of this thesis.
In this regard I likewise thank Prof. Dr. Stephan Lehnart, whose thorough review of especially the first part, “Local β-Adrenergic Signaling at the Sarcolemma of Adult Mouse Cardiomyocytes” markedly increased its quality.

Next, I would like to address special thanks to several people, who contributed with their specialized skills, which for me to learn would have exceeded the scope of this thesis:
Dipl. Biol. Julia H. Steinbrecher and Dr. Daniela Hübscher for mouse surgeries,
Dr. Ursula Fünfschilling and co-workers for transgenic mouse generation,
Kirsten Koschel, Sabrina Wollborn, Beate Knocke, Roland Blume and Marcel Zoremba for echocardiography and analysis,
Dr. Thomas Fischer and Jonas Herting for human trabeculae force measurements,
Christian Dees for radio-ligand binding assays.
Further, I thank Dr. Mei-Ling Chang Liao and Dr. Jan-Hendrik Streich for their technical advice on the IonOptix and Langendorff setups, respectively.

Much appreciation shall be addressed to my fellow co-workers, explicitly to mention Karina Zimmermann for her excellent and thoughtful assistance.
I am especially grateful to Dr. Viacheslav Nikolaev for his excellent counsel and guidance throughout the deployment of this PhD thesis. Especially his open-mindedness regarding the exploration of new avenues gave great distinction.

At the end I express my sincere gratitude to my parents for their support with good advice when needed and always open ears to my concerns, at all times.
Julia, thank you for you sheer infinite patients with me, always reassuring me when I am in serious doubt. It is you who reads me best.

Conference contributions

Oral Presentations:

Perera R.K., Steinbrecher J.H., Hübscher D., Lehnart S.E., Nikolaev V.O.
Microdomain switch of PDE2 and 3 modulates cGMP-mediated control on β-adrenergic cAMP signaling in early cardiac disease
Cyclic Nucleotide Phosphodiesterases Gordon Research Conference, 2014

Perera R.K., Nikolaev V.O.
FRET measurements of local cAMP signaling in the sarcolemmal / T- tubular compartment of cardiomyocytes
Heart Failure Congress 2013

Posters:

Perera R.K., Steinbrecher J.H., Hübscher D., Lehnart S.E., Nikolaev V.O.
ANP potentiates catecholaminergic stress in early cardiac disease
Frontiers in Cardiovascular Biology Conference, July 2014

Perera R.K., Steinbrecher J.H., Hübscher D., Lehnart S.E., Nikolaev V.O.
Microdomain switch of PDE2 and 3 modulates cGMP-mediated control on β-adrenergic cAMP signaling in early cardiac disease
Cyclic Nucleotide Phosphodiesterases Gordon Research Conference, 2014

Perera R.K., Steinbrecher J.H., Lehnart S.E., Nikolaev V.O.
β_1- and β_2-AR signals show reciprocal interdependence which is severely altered by ANP/cGMP in compensated hypertrophy
Heart Failure Association Winter Meeting 2014

Perera R.K., Nikolaev V.O.
Cardiac remodeling involves redistribution of cGMP-sensitive PDEs between β_1- and β_2-adrenergic receptor-associated microdomains and leads to altered cAMP signaling patterns
German Cardiac Society Fall Meeting 2013

Perera R.K., Nikolaev V.O.
Roles of phosphodiesterases 2 and 3 at the T-tubules of adult mouse cardiomyocytes
American Heart Association Basic Science Conference 2013

Perera R.K., Nikolaev V.O.
FRET measurements of local cAMP signaling in the sarcolemmal / T- tubular compartment of cardiomyocytes
Heart Failure Congress 2013

Perera R.K., Nikolaev V.O.
Local cAMP signaling at the sarcolemma and the T-tubules of adult mouse cardiomyocytes
Heart Failure Association Winter Meeting 2013

Perera R.K., Nikolaev V.O.
Atropine increases cardiomyocyte cAMP and contractility by allosteric inhibition of PDE 1 and 4
Cyclic Nucleotide Phosphodiesterases Gordon Research Conference 2012

Perera R.K., Nikolaev V.O.
Local cAMP signaling at the T-Tubules of adult cardiomyocytes
Dutch-German Joint Meeting of the Molecular Cardiology Groups 2011

Awards:

Young Investigator Award, Heart Failure Association Winter Meeting 2014

First Contact Initiative Grant 2013 Award of the European Society of Cardiology

Hans-Jürgen-Brettschneider Basic Science Award, German Cardiac Society Fall Meeting 2013